The Role of the IgSF9 Transmembrane Protein Borderless in Regulating Axonal Transport of Presynaptic Components in *Drosophila*

By

Hunter Stefan Shaw

Department of Biology

McGill University

Montreal, Quebec, Canada

August 2019

A thesis submitted to McGill University in partial fulfillment of the requirements of the degree of Doctor of Philosophy

Abstract

Normal brain function requires proper targeting of synaptic vesicle (SV) and active zone (AZ) components for presynaptic assembly and function. Whether and how synaptogenic signals (e.g. adhesion) at axo-dendritic contact sites promote axonal transport of presynaptic components for synapse formation, however, remain unclear. The first section of my thesis work reveals that Borderless (Bdl), a member of the conserved IgSF9-family of trans-synaptic cell adhesion molecules, plays a novel and specific role in regulating axonal transport of SV components. Loss of *bdl* disrupts axonal transport of SV components in photoreceptor R8 axons. Genetic mosaic analysis, transgene rescue and cell-type-specific knockdown indicate that Bdl is required both pre- and postsynaptically for delivering SV components in R8 axons. Consistent with a role for Bdl in R8 axons, loss of *bdl* causes a failure of R8-dependent phototaxis response to green light. *bdl* interacts genetically with *imac* encoding for a member of the Unc-104/Imac/KIF1A-family motor proteins, and is required for proper localization of Imac in R8 presynaptic terminals. In the second part of my thesis, I show that loss of Neuroligin-2 (Dnlg2), another trans-synaptic adhesion molecule, induces a *bdl*-like SV phenotype in R8 axons. The results from biochemical and cell biology experiments suggest that Bdl and Dnlg2 physically interact in *cis* through the Bdl extracellular domain. Consistent with this observation, expression of a truncated Bdl protein lacking the cytoplasmic domain is sufficient to rescue the R8 SV mislocalization phenotype. Like *bdl*, *dnlg2* interacts genetically with *imac*, suggesting a role for Dnlg2 in the Bdl-dependent pathway to mediate Imac activation. My thesis work supports a model in which Bdl and Dnlg2 function together in mediating specific axo-dendritic interactions, which up-regulates the Imac motor in promoting axonal transport of SV components for R8 presynaptic assembly and function.

Résumé

Les fonctions cérébrales requièrent le ciblage approprié des composants des vésicules synaptiques (VS) et des zones actives pour l'assemblage et la fonction des éléments pré-synaptiques des neurones. Cependant, on ignore encore si les signaux synaptogéniques (*e.g.* l'adhésion) survenant au niveau des sites de contact axono-dendritiques favorisent le transport axonal des composants pré-synaptiques nécessaires à la formation des synapses. La première partie de ma thèse met en évidence que Borderless (Bdl), un membre de la famille des molécules d'adhésion trans-synaptiques IgSF9 , joue un rôle dans la régulation du transport axonal des composants de VS. La perte de *bdl* compromet le transport axonal des composants de VS dans les axones des photorécepteurs R8. Des expériences d'analyse mosaïque , de sauvetage de mutants par expression de transgènes et d''inactivation dans un type cellulaire spécifique indiquent que Bdl est requis au niveau pré- et post-synaptique pour apporter les composants des VS aux axones R8. En accord avec un rôle de Bdl dans les axones R8, la perte de *bdl* bloque la phototaxie en réponse à la lumière verte, dépendante des R8. Nos expériences révèlent que *bdl* interagit génétiquement avec *imac*, un membre de la famille des protéines motrices Unc-104/Imac/KIF1A, et est requis pour la localisation de Imac dans les terminaisons pré-synaptiques des R8. Dans la seconde partie de ma thèse, je montre que la perte de Neuroligin-2 (Dnlg2), une autre molécule d'adhésion trans-synaptique, induit au niveau des VS un phénotype similaire à celui induit par la perte de *bdl* dans les axones R8. Les résultats d'expériences de biochimie et de biologie cellulaire suggèrent que Bdl et Dnlg2 interagissent physiquement en *cis,* via le domaine extracellulaire de Bdl. En accord avec cette observation, l'expression d'une forme tronquée de la protéine Bdl dépourvue de son domaine cytoplasmique, est suffisante pour sauver le phénotype de localisation des VS dans les R8. Comme *bdl*, *dnlg2* interagit génétiquement avec *imac,* suggérant un rôle pour Dnlg2 dans la voie d'activation de Imac dépendante de Bdl. Mon travail de thèse est en faveur d'un modèle dans lequel Bdl et Dnlg2 fonctionnent ensemble pour contrôler les interactions axono-dendritiques spécifiques, et réguler positivement le moteur Imac favorisant le transport axonal des composants des VS pour l'assemblage et la fonction des éléments pré-synaptiques des photorécepteurs R8.

Acknowledgements

Here I would like to acknowledge all the individuals who have helped me throughout the progress of this work. There are so many people to thank and limited space, so I apologize in advance for those I have omitted.

First and foremost, I would like to thank my supervisor, Dr. Yong Rao, for giving me the opportunity to work on these projects in his lab and his guidance throughout my doctoral studies. His mentorship and approach to science allowed me to hone my research and critical thinking abilities, while his intellect, patience, and understanding set an example all educators should strive for.

I would like to thank the members of my advisory committee: Dr. Tim Kennedy and Dr. Nam-Sung Moon. Their advice and critical evaluation of my work during the progress of my graduate degree is sincerely appreciated.

I would like to thank current and former members of the Rao Lab. Ms. Wen-Tzu Chang for exceptional technical support with this work and throughout my graduate degree. In addition, she provided me with plenty of tasty goodies and delicious recipe ideas. Dr. Scott Cameron and Dr. Mahmoudreza Ramin for being exceptional mentors and teaching me many of the research techniques I employed in this thesis. Dr. Hsiao-Han Hsieh and Dr. Yixu Chen for insightful input and discussion during the early stages of my project. Mr. Austin Zhang for insightful input on my work and the beautiful red hat he got me from the 1000th F1 Grand Prix in China. Ms. Camille Couture, who worked with me as an undergrad. And to any other members I missed, for insightful discussion and input on my work.

I would like to thank all members of the CRN in the Rao, van Meyel, Murai, and Chen lab for engaging and useful discussion about this work. I especially appreciated the Thursday morning

breakfasts with Dr. Ibrahim Kays, the noon-hour coffee breaks with the members of the CRN Coffee Club, Dr. Emilie Peco, Ms. Diedre Hatton, and Ms. Camille Couture, and the Friday night CRN Journal Clubs with Dr. Scott Cameron, Dr. Andrew Greenhalgh, Dr. Christopher Salmon, and Dr. David Stellwagen. I would also like to thank Dr. Tiago Ferreira for insightful advice on using the FIJI ImageJ software.

I would like to thank other members of the scientific community who helped me along the way. Dr. Marie-Julie Allard and Dr. Emilie Peco for the translation and editing of my abstract into French. Thank you to Ms. Deirdre Hatton, Dr. Scott Cameron, Dr. Ibrahim Kays, and Dr. Christopher Salmon for reviewing this manuscript. Dr. Ian Meinertzhagen and members of his lab for allowing me to visit their lab and gain insights on EM and IHC techniques in the fly visual system. Mr. Joe Larkin for building the T-Maze apparatus.

I would like to thank Mr. Martin “Senior” Patterson for all the post-hockey steak frites and warm words of encouragement.

Finally and most importantly, I would like to thank my Mother and Father, Kim Kurylo and Harry Shaw (back home in British Columbia), and my two younger sisters, Jahnnie Shaw and Starr Strommen, for their unwavering love and support. I would not be here without the work ethic and commitment they instilled into me growing up.

Preface

Whether and how synaptogenic adhesion at axo-dendritic contact sites regulates axonal transport of presynaptic components remain unknown. My thesis work demonstrates for the first time that trans-synaptic adhesion molecules (i.e. Borderless and Neuroligin-2) mediate specific interactions at axo-dendritic contact sites, and that this is required for up-regulating the Unc-104/Imac/KIF1A motor in promoting axonal transport of synaptic vesicle components and active zone proteins for presynaptic assembly and function in the adult fly visual system.

This is a manuscript-based thesis that consists of four chapters and is partially based on a published manuscript. Chapter 1 contains a literature review of relevant fields and objectives of this study. Chapters 2 and 3 contain the results of my research. Chapter 2 includes published material. Chapter 3 includes unpublished material in preparation. Both chapters are comprised of Abstract, Introduction, Materials and Methods, Results, and Discussion sections. Chapter 4 contains discussion and future directions.

Contribution of Co-authors

Chapter 2 has been published in the journal paper: *Shaw HS, Cameron SA, Chang W-T, Rao Y (2019) The conserved IgSF9 protein Borderless regulates axonal transport of presynaptic components and color vision in Drosophila. J Neurosci:0075–19*. My supervisor Dr. Yong Rao and I developed the rationale, designed experiments and wrote the paper. Dr. Scott Cameron performed *bdl* mosaic analysis experiments, R7 synaptic vesicle localization experiments, and R8 synaptic vesicle localization in bdl^{ex1}/bdl^{ex2} transheterozygotes experiments. Ms. Wen-Tzu Chang performed co-immunoprecipitation experiments, coaggregation and aggregation experiments in S2 cells, and generated the *bdl* rescue constructs. I performed and analyzed all other experiments. In this thesis, Dr. Scott Cameron contributed Figures 2.1E-F and 2.2A-D. Ms. Wen-Tzu Chang contributed Figures 3.4, 3.5, 3.6. and 3.7. Dr. Yong Rao provided suggestions for writing and revising the thesis.

Table of Contents

List of Figures and Tables

Chapter 1

Chapter 2

Chapter 3

List of Abbreviations Used

APF	After puparium formation
Arl	ADP ribosylation factor-like
AZ	Active zone
Bdl	Borderless
Brp	Bruchpilot
Ca^{2+}	Calcium ion
Cac	Cacophony
CadN	N-Cadherin
CAM	Cell adhesion molecule
CASK	Calcium/calmodulin-dependent serine protein kinase
CAST	Cytomatrix at the active zone-associated structural protein
CAZ	Cytomatrix at the active zone
CNS	Central Nervous System
Co-IP	Co-immunoprecipitation
Dasm	Dendrite arborization and synapse maturation
DCV	Dense Core Vesicle
DGC	Dystroglycan complex
DHC	Dynein heavy chain
Dm	Distal medulla
Dnlg	*Drosophila* Neuroligin
Dnrx	*Drosophila* Neurexin
Dscam	Down syndrome cell adhesion molecule
EM	Electron microscopy
ERG	Electroretinogram
Ey	Eyeless
Fmi	Flamingo

FN(III)	Fibronectin (type III)
GABA	gamma-Aminobutyric acid
GFP	Green fluorescent protein
GKAP	Guanylate-kinase-associated protein
GMR	Glass multiple reporter
Gogo	Golden Goal
hNL	Human Neuroligin
Ig	Immunoglobulin
IgSF	Immunoglobulin superfamily
IHC	Immunohistochemistry
Imac	Immaculate Connections
JNK MAP	c-Jun N-terminal kinases mitogen-activated protein
KIF	Kinesin superfamily proteins
KLC	Kinesin light chain
LAR	Leukocyte-antigen-related-like
MAb	Monoclonal antibody
Magi	Membrane-associated guanylate kinase inverted
MAGUK	Membrane-associated guanylate kinase
MAP	Microtubule-associated protein
MDGA	MAM domain-containing glycosylphosphatidylinositol anchor
MINT	Munc-18-interacting protein
Munc	Mammalian uncoordinated
Nlg	Neuroligin
NMJ	Neuromuscular Junction
Nrx	Neurexin
nSyb	Neuronal Synaptobrevin
p	Pale
PDZ	Combined first letters of the first three proteins discovered to share the domain: PSD-95, Dlg1, and Zo-1.

PI	Preference Index
PLV	Presynaptic lysosome-related vesicles
Prd	Pruning defect
PSD	Postsynaptic density
PSD-95	Postsynaptic density protein
PTP	Phosphotyrosine phosphatase
PTV	Piccolo-bassoon Transport Vesicle
RBP	Rab3-interacting molecule binding protein
R-cell	Retinula cell (*Drosophila* photoreceptor cell)
RFP	Red fluorescent protein
Rh	Rhodopsin
RIM	Rab3-interacting molecule
RNAi	Ribonucleic acid interference
RPTP	Receptor phosphotyrosine phosphatase
SEM	Standard error of the mean
SM	Sec1/Munc18-like
SNAP	Synaptosomal nerve-associated protein
SNARE	Synaptosomal nerve-associated protein receptor
S-SCAM	Synaptic scaffolding molecule
SV	Synaptic vesicle
SVP	Synaptic vesicle precursors
Syb	Synaptobrevin
Syd	Sunday driver
Syt	Synaptotagmin
TEM	Transmission electron microscopy
Tm	Transmedulla
TRiP	Transgenic RNAi Project
Tutl	Turtle

UAS	Upstream activation sequence
Unc	Uncoordinated
UV	Ultraviolet
VAMP	Vesicle-associated membrane protein
VIAAT	Vesicular inhibitory amino acid transporter
y	Yellow

Chapter 1: Introduction and Literature Review

1.1 Presynaptic Formation and Maintenance

1.1.1 The Make-up of a Chemical Synapse

Synapses are the intercellular junctions between a presynaptic neuron and a postsynaptic target. In most cases, the target is another neuron but can also include non-neuronal cells such as muscles, glia, and endocrine or secretory cells. The morphology of the synapse from an electron micrograph resembles two precisely apposed pre- and postsynaptic specializations that contain electron-dense, dark staining material on their plasma membranes (Gray, 1963). Information arrives at the presynaptic terminal in the form of an action potential and is transmitted to the postsynaptic cell via chemical neurotransmitters. These neurotransmitters are packaged into synaptic vesicles which are localized and recruited to the presynaptic terminal for release into the synaptic cleft.

A series of well-characterized docking and priming steps are required for synaptic vesicle exocytosis to occur (Südhof, 2004). The arrival of an action potential induces the opening of presynaptic voltage-gated Ca^{2+} channels. This influx of Ca^{2+} triggers the synaptic vesicle to dock and release their neurotransmitter contents into the synaptic cleft, where it can bind and activate postsynaptic receptors. Neurotransmitter binding with the receptor induces the opening of postsynaptic ion channels, resulting in either an increase or decrease in membrane potential, depending on if the synapse is excitatory or inhibitory, respectively. At excitatory synapses, an influx of positively-charged ions into the postsynaptic membrane raises the resting membrane potential (depolarizes), bringing the membrane potential closer to action potential threshold. Conversely, at inhibitory synapses, an influx of negatively-charged ions into the postsynaptic membrane drops the resting membrane potential (hyperpolarizes) and decreases the ability of the postsynaptic membrane to reach the threshold required to generate an action potential.

Exocytosis of synaptic vesicles is restricted to the "active zone" (AZ), the small electron-dense section of the presynaptic plasma membrane (Südhof, 2012). The AZ is the interface between the presynaptic terminal and the synaptic cleft, where the presynaptic action potential signal is transformed into a released neurotransmitter signal. Directly opposite to the AZ (across the synaptic cleft) lies the "postsynaptic density" (PSD), an electron-dense segment of the postsynaptic membrane (Sheng and Kim, 2011). The PSD is the interface between synaptic cleft and dendritic shaft, transforming the neurotransmitter received into a change in membrane potential. There are many different synapse types that differ in not only the neurotransmitter they release but also in terms of basic synaptic parameters such as neurotransmitter release probability and postsynaptic receptor composition.

1.1.2 Molecular Organization of the Presynaptic Active Zone

The presynaptic AZ is a key component in defining a synapse. The evolutionarily conversed function of the AZ is to organize and trigger Ca^{2+} dependent neurotransmitter secretion and restrict that release to a small patch opposite clusters of postsynaptic receptors. In neurotransmitter release, the presynaptic AZ performs four principal functions (Südhof, 2012). First, they dock and prime synaptic vesicles for release into the synaptic cleft. Second, AZs recruit voltage-gated Ca^{2+} channels to the presynaptic membrane, thereby allowing fast synchronous excitation and release coupling. Third, trans-synaptic cell-adhesion molecules expressed in the AZ allows for the precise localization of pre- and postsynaptic specializations exactly opposite each other. Finally, much of the short- and long-term presynaptic plasticity observed in synapses is mediated by the active zone. All these functions aim to organize neurotransmitter release such that presynaptic vesicle exocytosis occurs with the appropriate speed and plasticity required to maintain information transfer and computational function at the synapse.

The core of the AZ is made up of five evolutionarily conserved proteins: RIM, Munc13, RBP, Liprin-α, and ELKS (Fig. 1.1). RIM, Munc13, and RBP are multidomain proteins made up of a series of identifiable modules, while Liprin-α and ELKS are much simpler in structure (Südhof, 2012). These proteins are often encoded by single genes in invertebrates, and by multiple genes in vertebrates, often with several splice variants. These five core AZ proteins form a single large protein complex that is required for basic functionalities of the AZ including docking and priming of synaptic vesicles, recruiting calcium channels to the docked and primed vesicles, tethering the vesicles and Ca^{2+} channels to synaptic cell-adhesion molecules, and mediating synaptic plasticity (Südhof, 2012).

RIMs (Rab3-interacting molecules) are central organizers of the AZ and have been shown to be essential for synaptic vesicle docking and priming (Koushika et al., 2001; Schoch et al., 2002; Gracheva et al., 2008; Deng et al., 2011; Han et al., 2011), for recruiting Ca^{2+} channels to active zones (Kaeser et al., 2011), and for short-term plasticity of neurotransmitter release (Castillo et al., 2002; Schoch et al., 2002). RIMs have many domains that interact with many of the other AZ molecules. Importantly, RIMs play a role in synaptic vesicle (SV) docking by linking synaptic vesicles (through binding of the SV membrane protein, Rab3) in close proximity to the SV priming factor, Munc13 (Gracheva et al., 2008; Kaeser et al., 2011). The central PDZ-domain of RIMs bind ELKS and N- and P/Q-type but not L-type Ca2+ channels, which is critical in recruiting Ca^{2+} channels to active zone (Ohtsuka et al., 2002; Schoch et al., 2002; Han et al., 2011; Kaeser et al., 2011). RIM mediates this through interactions with RBP (RIM binding protein). RBPs are large multidomain proteins that link Ca^{2+} channels to RIMs. Synaptic N- and P/Q-type Ca^{2+} channels are recruited to active zones by binding simultaneously to both RIM and RBP (Kaeser et al., 2011; Liu et al., 2011).

Unc-13 was originally identified in *C. elegans* when its mutation caused an "uncoordinated" phenotype (Maruyama and Brenner, 1991). Its mammalian homolog, Munc-13, was shown to localize to the active zone and mediate synaptic vesicle priming (Brose et al., 1995; Augustin et al., 1999). Munc-13 proteins have two principal functions at the active zone: render synaptic vesicles competent for exocytosis by priming the SNARE/SM protein fusion machinery and mediating short-term plasticity by regulating this priming activity (Südhof, 2012). Munc13s mediate their priming function via the MUN domain (Basu et al., 2005; Stevens et al., 2005), which "opens" the SNARE protein Syntaxin-1, enabling it to form SNARE complexes (Koushika et al., 2001; Gerber et al., 2008; Ma et al., 2011).

Liprin-α was first linked to presynaptic active zones when *liprin*-α loss-of-function mutants in *C. elegans* and *Drosophila* were found to have increased active zone size and disrupted synaptic vesicle accumulation at the AZ (Zhen and Jin, 1999; Kaufmann et al., 2002; Dai et al., 2006). Interestingly, Liprin-α links trans-synaptic cell adhesion and presynaptic AZ assembly via its interactions with a LAR-type receptor phosphotyrosine phosphatase (RPTP). Deleting the synaptic isoform of the LAR-type RPTP, PTP-3, caused the mis-localization of Liprin-α, while deletions of *liprin*-α caused a mis-localization of the synaptic isoform of PTP-3 (Ackley et al., 2005). In addition, Liprin-α binding to Syd-1 and ELKS is important for synapse assembly in invertebrates. These observations suggest that AZ formation with the recruitment of synaptic vesicles and of LAR-type RPTP requires Liprin-α, possibly by simultaneous binding of Liprin-α to the RPTP, RIM, ELKS, Syd-1, and others. Furthermore, Liprin-α links synaptic cell adhesion to the RIM/Munc13/RBP core complex that recruits vesicles and calcium channels to active zones.

Other proteins that have been shown to be important at the AZ include the two large homologous proteins, Piccolo and Bassoon (tom Dieck et al., 1998; Wang et al., 1999; Fenster et

al., 2000; Limbach et al., 2011). Piccolo and Bassoon are large proteins specific to vertebrates whose major function appears to be to guide synaptic vesicles from the backfield of the synapse to the AZ (Hallermann et al., 2010a; Mukherjee et al., 2010). Partial knockout of *bassoon* causes partial lethality and impairs neurotransmitter release (Altrock et al., 2003), while synapses with a partial loss of both *piccolo* and *bassoon*, have impairments in vesicle clustering (Mukherjee et al., 2010).

1.1.3 Molecular Organization of the Postsynaptic Density

The postsynaptic density (PSD) is the compartment beneath the postsynaptic membrane that lies opposite to the presynaptic AZ and is specialized to receive neurotransmitter signal released from the presynaptic terminal. The PSD is comprised of several hundred proteins that include neurotransmitter receptors, ion channels, adhesion molecules, signalling enzymes, and cytoskeletal elements, all held together by an abundance of scaffolding molecules (Sheng and Kim, 2011). The primary role for the PSD is to cluster postsynaptic receptors and couple the activation of these receptors to biochemical signalling events in the postsynaptic neuron. The PSD of excitatory and inhibitory synapses are quite different in their morphology, molecular composition, and organization. Excitatory postsynaptic sites in the mammalian brain occur mainly on tiny protrusions called dendritic spines (Bourne and Harris, 2008), while most inhibitory synapses are formed on the shaft of dendrites, cell bodies, or axon initial segments.

The membrane proteins at the excitatory PSD are the best understood and include the ionotropic AMPA and NMDA glutamate receptors, metabotropic glutamate receptors, as well as other ion channels and adhesion molecules (Missler et al., 2012; Smart and Paoletti, 2012). The ionotropic and metabotropic ion channels are critical for the primary function of the postsynaptic terminal. Activation of these channels by neurotransmitter received from the presynaptic terminal

will lead to changes in membrane potential from the flow of charged ions through the cell membrane. The adhesion molecules on the PSD span across the synaptic cleft and bind to their corresponding presynaptic partner. Binding of these molecules is critical for mediating synaptic contact, formation, specialization, and modulation. The role of adhesion and scaffolding molecules at the synapses will be discussed in-depth in another part of this chapter.

The composition of neurotransmitter receptors and associated proteins at the postsynaptic membrane of inhibitory synapses are substantially different from that of excitatory synapses. However, many of the organizing principles such as scaffold-based assembly of receptors and signalling proteins, adhesion-mediated differentiation, and activity-regulated trafficking of neurotransmitter receptors are for the most part conserved. Because of its lesser electron-dense postsynaptic membrane, the PSD at inhibitory synapses was assumed to be less elaborate than that of excitatory synapses (Gray, 1959), although some of its components have been well characterized. The chloride permeable $GABA_A$ and glycine receptors are the major neurotransmitter receptors at central inhibitory synapses. Activation of these receptors leads to a decrease in membrane potential due to the influx of negatively charged chloride anions. Both receptors interact directly with Gephyrin, the major postsynaptic scaffold protein at inhibitory synapses (Prior et al., 1992; Lüscher and Keller, 2004; Fritschy et al., 2008; Jacob et al., 2008). Trans-synaptic adhesion also has a critical role in inhibitory synapses development. Neuroligin-2 is specifically localized to inhibitory synapses and couples with the homophilic transmembrane protein IgSF9b and S-SCAM (Varoqueaux et al., 2004; Sumita et al., 2007; Woo et al., 2013). Neuroligin 2 is thought to be critical for the development and functionality of inhibitory synapses and will be discussed in greater detail in the following section.

1.1.4 Synaptic Vesicle Proteins

Neurotransmitter release relies on a series of synaptic vesicle trafficking reactions (Kittel and Heckmann, 2016). Classic work by Bernard Katz and colleagues established that quanta (the content within a single synaptic vesicle) of neurotransmitters are released from presynaptic terminals (Fatt and Katz, 1952; del Castillo and Katz, 1954; Palay, 1956; Couteaux and Pécot-Dechavassine, 1970). Further work showed how the localized opening of Ca^{2+} channels leads to the exocytotic discharge of the neurotransmitters stored within synaptic vesicles (Heuser et al., 1979; Augustine et al., 1987). Following the priming and docking steps of neurotransmitter release, vesicular components are recycled into new vesicles (Heuser and Reese, 1973). Therefore, the release of neurotransmitter is a local cycle of presynaptic vesicle trafficking with the primary objective of SV fusion. This process is mediated by SV membrane proteins, AZ proteins, and Ca^{2+} ions.

Rab3 is a small synaptic vesicle-associated GTPase that interacts with RIM and Munc-13 and is involved in vesicle cycling, docking and exocytosis (Südhof, 2004). In *Drosophila*, Rab3 also controls the protein composition of AZs. At the NMJ of *rab3* mutant flies, the number of AZs positive for Brp (CAST/ ELKS homolog and AZ marker) drops dramatically while individual AZs containing Brp are substantially enlarged (Graf et al., 2009).

The vesicular protein Synaptotagmin-1 (Syt1) plays a decisive role as a calcium sensor by triggering neurotransmitter secretion by regulating the SNARE zipping mechanism, a critical step in SV docking (Sutton et al., 1995; Fernandez et al., 2001). The SNARE complex is composed of the synaptic vesicle-associated membrane protein Synaptobrevin (also known as VAMP) on the synaptic vesicle, and Syntaxin-1 and SNAP-25 on the presynaptic plasma membrane (Trimble et al., 1988; Oyler et al., 1989; Südhof et al., 1989; Bennett et al., 1992). All three proteins bind

together to form the core SNARE complex. Once bound, the SNARE proteins zipper up into an α-helical bundle called the "trans-SNARE-complex" that pulls the two membranes tightly together, exerting the force required for vesicle fusion (Sutton et al., 1998). The SM (Sec1/Munc18-like) proteins are also required in this process (Hata et al., 1993). Shaped like clasps (Misura et al., 2000), SM proteins bind to trans-SNARE complexes and spatially and temporarily organizes their fusion. SNARE and SM proteins are considered the two universally required components of the intracellular membrane fusion machinery (Sudhof and Rothman, 2009).

1.1.5 The *Drosophila* Synapse as a Model

Exact descriptions of synapses and their ability to be manipulated genetically in the *Drosophila melanogaster* (fruit fly) make them an exceptional model to explore the mechanisms and principles underlying synapse formation and function. More precisely, there are two major strengths of using *Drosophila* as a model organism to give us insights into the synapse in both vertebrates and invertebrates alike (Fig. 1.2) (Prokop and Meinertzhagen, 2006). Firstly, the amenability of *Drosophila* to genetic analysis and unbiased studies on likely translatable or conserved developmental mechanisms in other animals (St Johnston, 2002; Matthews et al., 2005). Secondly, *Drosophila* have individually identifiable brain cells that undergo stereotyped developmental events, allowing researchers to perform highly detailed cellular assays of gene function (Prokop, 1999). The larval neuromuscular junction (NMJ) and adult photoreceptor synapses are the two most highly studied synapses in the fly (Prokop and Meinertzhagen, 2006; Ehmann et al., 2018). Both have benefits of being accessible with electrophysiological, histological, and genetic approaches. Electroretinogram (ERG) screens in the fly eye have been critical in identifying many of the earliest-known molecular players in synaptic function and development (Hotta and Benzer, 1970; Pak et al., 1970; Dolph et al., 2011). In addition, the

accessibility of the larval NMJ for electrophysiology has made it a critical player in the understanding of the genetic contributions to synaptic development, function, and plasticity (Bykhovskaia and Vasin, 2017).

The *Drosophila* nervous system has many chemically and physiologically distinct types of synapses as reflected in its broad repertoire of neurotransmitters, neuropeptides, and ionotropic and metabotropic neurotransmitter receptors. Central synapses, interneurons, and sensory neurons are predominantly cholinergic, but other neurotransmitters in the fly brain include GABA, glutamate, taurine, aspartate, dopamine, histamine, octopamine, and serotonin (Monastirioti et al., 1995; Yasuyama et al., 2002; Landgraf et al., 2003; Strausfeld et al., 2003; Nässel and Winther, 2010). The NMJ is surprisingly glutamatergic and executes low out-put neurotransmitter release by presynaptic spikes (Broadie and Bate, 1993; Rohrbough et al., 2003). Conversely, high out-put adult photoreceptors are histaminergic and execute tonic neurotransmitter release by small, light-evoked, graded depolarizations (Juusola et al., 1996).

Drosophila synapses are quite easily distinguishable with transmission electron microscopy (TEM). They usually possess diameters of less than 1 µm and have noticeably darker pre- and postsynaptic membranes (Prokop and Meinertzhagen, 2006). Morphologically, the AZs are characterized by an electron-dense cytomatrix (CAZ, cytomatrix at the AZ), which is made up of specialized proteins required for the speed and precision necessary for synaptic transmission (Zhai and Bellen, 2004; Ehmann et al., 2018). On the PSD, the electron-dense postsynaptic membrane is made up of signalling molecules, scaffolding proteins, neurotransmitter receptors, ion channels, and adhesion molecules (Sheng and Kim, 2011).

One of the most noticeable features at NMJ and photoreceptor synapses is the T-bar ribbon (Fig. 1.2), a common “flat mushroom-shaped (⊤)” presynaptic organelle with a pronounced dense

body comprised of a base or pedestal surmounted by a platform (appearing to be in the shape of a capital “T”) (Prokop and Meinertzhagen, 2006). The T-bar ribbons protrude approximately 100–200 nm from the AZ membrane into the cytoplasm and are normally surrounded by or attached to vesicles (Jiao et al., 2010; Wichmann and Sigrist, 2010). These filamentous protrusions made up of the CAST/ELKS homolog Bruchpilot (Brp), tether synaptic vesicles to the AZ and are specialized for the delivery of synaptic vesicles at high rates to the presynaptic membrane (Hallermann et al., 2010a, 2010b). In support of this, T-bars are closely associated with calcium channels and exocytosis of synaptic vesicles occurs at the presynaptic plasma membrane directly below the T-bar (Koenig and Ikeda, 1996).

NMJs are monadic, where one presynaptic site creates a continuous junction (composed of several boutons) onto a single postsynaptic site on the muscle (Prokop and Meinertzhagen, 2006). Conversely, photoreceptor synapses (and most central synapses in flies) possess multiple postsynaptic cells innervated by a single presynaptic release site. These constellations of two, three or four (sometimes more) postsynaptic elements receiving neurotransmitter from a single T-bar ribbon are referred to as dyads, triads, and tetrads. The tetrad synapses generated by R1-R6 photoreceptors in the lamina of the fly visual system have been studied extensively (Fröhlich and Meinertzhagen, 1983; Meinertzhagen and O’Neil, 1991; Millard et al., 2010; Rivera-Alba et al., 2011; Lah et al., 2014; Schwabe et al., 2014; Kerwin et al., 2018; Millard and Pecot, 2018). The four cells that make up the postsynaptic partners at these tetrad synapses range from projection neurons, local amacrine cells and/or glia.

Three potential explanations have been suggested for why such a synapse with one presynaptic terminal onto multiple postsynaptic targets would benefit the fly nervous system (Millard and Pecot, 2018). Firstly, it is more energy-efficient. Due to the energy requirements for

presynaptic release at a single synapse, a tetrad synapse allows the energy to be "cost-shared" amongst the postsynaptic targets (Laughlin et al., 1998). For example, you can achieve the same amount of information transfer with a single presynaptic terminal, as opposed to four presynaptic terminals. Secondly, target neurons would receive evenly-balanced inputs at a shared synapse. This is important in fly motion vision, where L1 and L2 neurons that receive equal inputs from the same R-cell through a tetrad synapse are part of functionally distinct motion detection circuits (Borst, 2014; Silies et al., 2014). Finally, this could be a method to increase the compositional complexity of each neuron's synapses. With the limited size of the fly brain compared to that of vertebrates, this would be a straightforward way to achieve synaptic divergence and circuit complexity. Such an increase in network complexity in vertebrates with monadic synapses can be simply achieved by increasing the number of neurons.

1.1.6 Molecular Composition of the Fly Active Zone

Similar to vertebrates, in *Drosophila* the arrival of an action potential elicits calcium (Ca^{2+}) influx through voltage-gated ion channels, which in turn triggers neurotransmitter release from SVs. Most of the current understanding of the molecular mechanisms controlling the development and function of AZ physiology in *Drosophila* has been uncovered from work done at the glutamatergic synapses of the larval NMJ. Nearly all AZ proteins identified at invertebrate synapses are also present at mammalian synapses, suggesting significant conservation of function throughout evolution. Those include proteins that regulate exocytosis with SNARE (soluble NSF-attachment protein receptor) and SM (Sec1/Munc18-like) proteins of the core fusion complex; AZ-specific proteins important for scaffolding or synaptic vesicle release including Liprin-α (Kaufmann et al., 2002; Fouquet et al., 2009), Syd-1 (Owald et al., 2010, 2012), Unc13 (Aravamudan et al., 1999; Böhme et al., 2016), RIM (Graf et al., 2012; Müller et al., 2012), and

its family member Fife [related to mammalian Piccolo; (Bruckner et al., 2012)], RBP (Liu et al., 2011) and the CAST/ELKS homolog Brp (Kittel et al., 2006).

AZ assembly at the NMJ is a step-wise process with the molecular complexity increasing as the synapse matures (Ehmann et al., 2018). Initial assembly is mediated by the interactions of Syd-1 and Liprin-α, generating a scaffolding complex composed of the two molecules (Owald et al., 2010). This complex positions the Unc-13B isoform at a distance of 120 nm from AZ Ca^{2+} channels (Fouquet et al., 2009; Liu et al., 2011). Further maturation of the AZ involves recruitment of Brp and RBP which in turn generate their own protein complex that positions the Unc-13A isoform nearer to the Ca^{2+} channels than Unc-13B, at 70 nm (Böhme et al., 2016). Both isoforms have discrete roles in SV docking and priming, as well as regulation of release probability. It is suggested that the precise spatiotemporal placement of Unc13A and Unc13B is critical for AZ maturation and synaptic vesicle exocytosis.

As mentioned previously, the protein Brp is a central component of the AZ and a key component for the formation of the T-bar (Wagh et al., 2006; Ackermann et al., 2015). This ELKS fusion protein garnered the name *bruchpilot* from the German word "crash pilot", due to the flies showing unstable flight patterns. Brp is a large molecule, weighing roughly 200 kDa and consisting of an N-terminal ELKS-related domain and a C-terminal plectin-related domain (Wagh et al., 2006). In *brp* null mutant *Drosophila*, the presence of the T-bar is abolished and calcium channels are declustered at the AZ (Kittel et al., 2006). Super-resolution microscopy further revealed that a single Brp molecule adopts an elongated conformation which stretches from the AZ membrane into the cytoplasm. The addition of multiple Brp threads at a single AZ creates a tuft, thereby forming the T-bar structure (Fig. 1.2). Brp is also required for clustering Ca^{2+} channels in close proximity to the fusion machinery, directly beneath the T-bar (Fouquet et al., 2009). Interestingly,

this clustering is mediated by the alternate patterning of two Brp isoforms, in a circular array around the T-bar, creating discrete adjacent slots for the Ca^{2+} channels and SV docking sites (Matkovic et al., 2013). It is thought that Brp performs a double function at the *Drosophila* synapse, with the N-terminal ELKS component acting as a standard ELKS protein, and the C-terminal plectin-homology region involved in vesicle recruitment in a manner analogous to Piccolo and Bassoon in mammalian synapses (Kittel et al., 2006; Hallermann et al., 2010a; Südhof, 2012)

The other major constituents of the T-bar include Rab3-interacting protein (RIM), Dunc-13 (*Drosophila* homolog of Unc-13), RIM-binding protein (RBP), and Fife (*Drosophila* homolog of Piccolo). RIM has a critical role in synaptic transmission, as it works together with Dunc-13 to promote SV priming and docking (Graf et al., 2012). *RIM* mutants show a dramatic decrease in synaptic transmission due to a reduction in the neurotransmitter release probability. The reduced release probability at synapses in *RIM* loss-of-function can partially be explained by the reduced localization of the voltage-gated Ca^{2+} channel, *cacophony (cac)*, to the AZ. This localization of voltage-gated Ca^{2+} channels to AZs is also mediated by RBP. Similar to *RIM*, *RBP* loss-of-function impairs synaptic transmission at the *Drosophila* NMJ and leads to the mis-localization of Cac (Wang et al., 2000; Liu et al., 2011) The role of RBP appears to be in stabilizing and maintaining voltage-gated Ca^{2+} channels beneath T-bars. Consistent with this, super-resolution microscopy identified that RBP surrounds calcium channels at T-bars and in the absence of RBP, calcium channel clustering is impaired (Liu et al., 2011).

As of yet, no *Drosophila* homolog for Bassoon has been identified, however the homolog of Piccolo, aptly named Fife (all three are woodwind musical instruments) has been recently characterized (Bruckner et al., 2012). Fife is selectively localized at *Drosophila* AZs and structurally is a hybrid molecule with features from both Piccolo and RIM. At the larval NMJ, *Fife*

loss-of-function dramatically affects AZ organization and synaptic transmission, as made evident by a decrease in excitatory junctional potential amplitude and quantal content. Additionally, in the absence of Fife, in the number of SVs associated with T-bars is reduced (Ackermann et al., 2015).

1.2 Synaptic Adhesion and Scaffolding Molecules

1.2.1 Synaptic Adhesion Molecules in Synapse Formation and Maintenance

For effective neurotransmission, the pre- and postsynaptic specializations must be precisely apposed to one another across the synaptic cleft, as well as be at an appropriate distance from each other for the neurotransmitters to reach the receptor. The precise apposition of pre- and postsynaptic specializations additionally suggests that interactions across the cleft delineate their mutual boundaries (Schikorski and Stevens, 1997). Direct linkage via transmembrane cell adhesion molecules (CAMs) are thought to play a prominent role in achieving this, as well as many other important functions throughout the lifetime of a synapse (Yamagata et al., 2003; Missler et al., 2012). Adhesion molecules are membrane-anchored molecules, with extracellular domains that directly interact with their counterparts on an opposing membrane, thereby holding the membranes of the two cells together (Fig. 1.3). Adhesion molecules may also have cytoplasmic tails with important signalling roles. Therefore, the primary role of the ligand-receptor interactions may not solely be that of adhesion, in fact adhesion may even be a later-evolved byproduct of the originally intended function.

Synaptic cell adhesion molecules are thought to be required for four distinct, but interrelated roles. These roles correspond with the stages of synapse formation including the initial establishment of synaptic contacts, assembly of the pre- and postsynaptic molecular machinery,

functional maturation of the emerging synapses, and finally synaptic maintenance and plasticity (Missler et al., 2012).

Firstly, CAMs provide mechanical stability to synapses and maintain the integrity of the junction by physically linking the pre- and postsynaptic membranes to each other (Yamagata et al., 2003). CAM-mediated linkage of the pre- and postsynaptic membranes to each other could facilitate interactions among other trans-synaptic signalling CAMs. Additionally, binding of synaptic scaffolding molecules through a CAMs cytoplasmic tail maybe be important for the recruitment and stabilization of pre- and postsynaptic intracellular proteins.

Secondly, CAMs play an essential role in target recognition, guiding the presynaptic axon to the proper postsynaptic neuron at the site of a future synapse. During synaptogenesis, axonal growth cones and their dendritic targets extend filopodia to form initial contacts (Cooper and Smith, 1992). As the axon reaches the target region, it has already interacted with many guidance cues and target recognition molecules and must choose the appropriate synaptic partner in the face of many possibilities (Sperry, 1963; Mueller, 1999; Sanes and Yamagata, 1999; Benson et al., 2001). Additionally, it may need to choose the specific location on the surface of the neuron such as the spine, shaft, or soma (Yamagata et al., 2003). Such specificity can be achieved by the appropriate pre- and postsynaptic expression of many different families and subtypes of CAMs with their corresponding binding partners. Furthermore, CAMs may require minor changes in adhesive properties generated by specific isoform expression or alternative splicing within certain adhesive domains, adding to the specificity and complexity of neural circuit development.

Thirdly, synaptic adhesion molecules promote differentiation of the pre- and postsynaptic terminals. An instructive role for synaptic cell adhesion in synapse development is consistent with the spatially and temporally coordinated assembly of pre- and postsynaptic membranes. This

molecular assembly stage involves the recruitment of synaptic vesicles, AZ proteins, and postsynaptic density structures to a developing synaptic contact (Vaughn, 1989; Garner et al., 2002; Munno and Syed, 2003). Although not a functional synapse at this stage, anatomically the features of an identifiable synapse begin to emerge. As the axonal growth cone transforms into a nerve terminal, shortly after contact with its postsynaptic target, it begins recruiting the necessary proteins for synaptic vesicle release. Synaptic membrane specializations assemble at these contacts and are ultrastructurally defined by synaptic vesicles, electron-dense cleft material, and thickened postsynaptic membranes (Rees et al., 1976). Conversely, the postsynaptic side simultaneously begins recruiting the corresponding receptors and postsynaptic proteins to be competent in receiving the signal sent by the presynaptic terminal. Trans-synaptic interactions and signalling via CAMs are strong candidates to be the mediators of such reciprocal interactions.

Finally, adhesion molecules may have a role in the structure, function, and maintenance of the mature synapse. Such involvement would be important in the maturation of the synapse after initial synaptogenesis, as well as maintaining the overall integrity of synaptic functionality over time. Organization of the pre- and postsynaptic molecular components during maturation renders the synapse functional, and also confers specific properties to it. In addition, mature synapses are remodelled by activity-dependent structural and functional plasticity mechanisms that may be regulated by synaptic CAMs (Toni et al., 1999; Knott et al., 2002).

1.2.2 IgSF9 Family of Molecules at the Synapse

Members of the Ig superfamily (IgSF) of transmembrane adhesion molecules have extracellular domains composed of multiple Ig-domains that normally bind to other Ig-domains either as homo- or heterophilic complexes (Hansen and Walmod, 2013). Ig-domains are comprised of a β-sandwich that is stabilized by a disulphide bond. Most IgSF molecules also contain

fibronectin III (FNIII) modules with a similar β-sandwich fold in the extracellular domain (Missler et al., 2012). Two molecules in this family of interest include IgSF9a/Dasm1/Turtle and IgSF9b/Borderless. Mammalian *IgSF9a* and *IgSF9b* are part of the evolutionarily ancient family of IgSF9 molecules (Hansen and Walmod, 2013). Extracellularly, both IgSF9 proteins contain five Ig and two FNIII subunits and have homophilic and heterophilic binding capabilities (Fig. 1.5). The extracellular segment is followed by a single short transmembrane domain and a cytoplasmic tail with PDZ binding abilities (Shi et al., 2004; Woo et al., 2013).

In rodents, *IgSF9a* is expressed in pyramidal cells and subsets of interneurons in the CA1 region of the hippocampus (Mishra et al., 2014). Initial reports suggested that IgSF9a was important in the regulation of hippocampal neuron differentiation and excitatory synaptic maturation (Shi et al., 2004). It was also found that the cytoplasmic tail of IgSF9a interacts with the postsynaptic scaffolding proteins Shank and S-SCAM. Their findings suggested that IgSF9a controls excitatory synapse maturation by bridging extracellular signals and intracellular signalling complexes. However, the interpretation of these results was difficult as they were obtained in organotypic hippocampal cultures using RNA interference and an IgSF9a dominant-negative (with a truncated cytoplasmic tail). A decade later, Mishra et al., (2014) generated *IgSF9a*$^{-/-}$ mice and discovered that IgSF9a is dispensable for excitatory synapse development and function, but necessary for normal inhibitory synapse number. Surprisingly, *IgSF9a* knock-in mice expressing IgSF9a protein with a truncated cytoplasmic domain (*IgSF9a*$^{\Delta C/\Delta C}$ mice) had no defects in inhibitory synapse development, suggesting that IgSF9a regulates synapse development via ectodomain interactions rather than acting itself as a signaling receptor. In addition, they found that although IgSF9 possessed homophilic binding abilities, it failed to induce synapse formation

on its own, supporting that the primary role of IgSF9a is to maintain inhibitory synapses through its adhesive properties.

IgSF9b has been linked to major depressive disorder and the negative symptoms of schizophrenia (Shyn et al., 2011; Fabbri and Serretti, 2017). It was identified as a novel homophilic adhesion molecule, strongly expressed in GABAergic interneurons that preferably localized to inhibitory synapses (Woo et al., 2013). Interestingly, IgSF9b was shown to be linked to the inhibitory synapse-specific Neuroligin-2 (Nlg-2) via the multi-PDZ protein S-SCAM. IgSF9b and Nlg-2 could reciprocally cluster each other in the forming of inhibitory synapses in culture. This data suggests that Nlg-2 and IgSF9b function together in inhibitory synapse formation. However, a recent study *in vivo* suggests that they may be able to function independently of each other (Babaev et al., 2018). Babaev et al., 2018 found that the removal of *IgSF9b* is anxiolytic and normalizes the anxiety-related behaviours and neural processing defects observed in *nlg2* null mice. They went on to show that IgSF9b and Nlg2 are required in different inhibitory neuron populations to regulate the amygdala anxiety circuitry.

The *Drosophila* homologs for IgSF9a and IgSF9b are Turtle and Borderless (note that Borderless has four Ig-domains, one fewer than IgSF9a, IgSF9b, and Turtle; Fig. 1.4) (Bodily et al., 2001; Cameron et al., 2013). Although studied extensively in dendritic self-avoidance and axon layer selection and tiling (Bodily et al., 2001; Ferguson et al., 2009; Long et al., 2009; Cameron et al., 2013, 2016; Chen et al., 2017), no one has yet looked at the role of either of these molecules in synaptogenesis.

1.2.3 Neuroligins/Neurexins

The role of trans-synaptic interactions between presynaptic neurexins (Nrx) and the postsynaptic neuroligins (Nlg) in synaptogenesis is one of most extensively studied trans-synaptic

adhesion interactions (Yamagata et al., 2003; Araç et al., 2007; Craig and Kang, 2007; Shapiro et al., 2007; Südhof, 2008; Missler et al., 2012). Presynaptic neurexins have large extracellular sequences, that can differ depending on whether it is alternatively spliced into the longer α or shorter β isoform (Both isoforms bind to all four neuroligins) (Ushkaryov et al., 1992). The extracellular sequence of neuroligins is largely composed of a single esterase-like domain, which forms homodimers with another neuroligin molecule (Ichtchenko et al., 1995). Both neurexins and neuroligins contain an intracellular PDZ binding domain that mediates synaptic scaffolding protein interactions (Hata et al., 1996; Irie et al., 1997). In vertebrates, there are three *neurexin* genes and four *neuroligin* genes. Neurexins are present at both excitatory and inhibitory synapses while neuroligins are specifically localized to particular synapses with Nlg-1 present at excitatory synapses, Nlg-2 and Nlg-4 at inhibitory synapses, and Nlg-3 at both (Budreck and Scheiffele, 2007; Chanda et al., 2017).

Early experiments showed that contact of non-neuronal cells expressing neuroligin or neurexin lead to the recruitment of presynaptic or postsynaptic markers, respectively (Scheiffele et al., 2000; Graf et al., 2004; Nam and Chen, 2005). Knockdown and overexpression experiments *in vitro* suggested that Nlg-1 and Nlg-2 are necessary and sufficient for excitatory and inhibitory synapse formation, respectively (Chih et al., 2005). However, in a study using *Nlg-123* triple knock-out mice, Varoqueaux et al. (2006) showed that neuroligins were not required for the initial formation of synapses in the brainstem but were essential for the maturation of synaptic currents (Varoqueaux et al., 2006). Likewise, although overexpression and knockdown of neurexins result in an increase and decrease respectively in synapse number, synapse formation still occurred in the absence of all three α-Neurexins *in vivo* (Missler et al., 2003). Increasing lines of evidence

suggest that neurexins and neuroligins are not completely required for synapse formation but could play important roles in synapse maturation and function.

In the *Drosophila* nervous system, four *neuroligins* (Dnlg1-4) and two *neurexins* (Dnrx-1 and Dnrx-IV) are expressed. Only Dnrx-1 has been shown to bind the Dnlgs and to have a critical role in synaptic development and functionality (Li et al., 2007; Sun et al., 2011). Interestingly, a neuron-specific isoform of Dnrx-IV interacts with the glial Ig-domain protein Wrapper to mediate glial wrapping of axons at the CNS midline (Stork et al., 2009; Wheeler et al., 2009). All four Dnlgs have been studied extensively at the *Drosophila* larval glutamatergic NMJ and have been shown to contribute to NMJ development, synaptic differentiation, and function (Banovic et al., 2010; Sun et al., 2011; Chen et al., 2012; Xing et al., 2014; Zhang et al., 2017b). In addition, Dnlg4 has been shown to have a role in regulating *Drosophila* sleeping behaviour by regulating GABA transmission (Li et al., 2013). Until this point, contributions of neuroligins and neurexins to synaptic function in the *Drosophila* visual system have not been looked at. However, recent work has shown that interactions between Dnrx-1 and Dnlg4 are important for L4 neuron columnar restriction in the medulla during development (Liu et al., 2017).

1.2.4 Synaptic Scaffolding Molecules

Critical to almost all intercellular contacts are intracellular scaffold proteins with multiple protein-protein interaction sites. Synaptic scaffolding molecules ensure the accurate accumulation of neurotransmitter receptors in precise apposition to presynaptic release sites, as well as interact with cytoskeletal anchoring elements (Sheng and Kim, 2011). They provide a physical platform to maintain receptors at synapses and regulate downstream signalling pathways. Many different synaptic scaffold proteins are known, typically containing multiple PDZ domains and other dedicated protein-binding modules. These domains function together to coordinate synapse

organization by physically linking protein components involved in cell adhesion, receptor recruitment, cytoskeletal anchoring, and downstream intracellular signalling (Fig. 1.3).

1.2.5 Excitatory Synaptic Scaffolding Molecules

Scaffolding molecules are highly abundant at the excitatory PSD and include molecules such as PSD-95, GKAP, Shank, and Homer (Sheng and Kim, 2011). A common feature of PSD scaffold proteins is the PDZ domain, a roughly 90 amino acid-long module that normally interacts with the C-terminus of binding partners (Kim and Sheng, 2004; Funke et al., 2005; Feng and Zhang, 2009). One of the best characterized of these scaffolding molecules is one of the earliest identified proteins in the PSD, PSD-95 (Cho et al., 1992). PSD-95 belongs to the membrane-associated guanylate kinase (MAGUK) protein family. The function of PSD-95 is to bind, tether and stabilize the various membrane proteins and signalling molecules within the PSD (Kim and Sheng, 2004). RNAi knockdown of PSD-95 in rat hippocampal cultures leads to the loss of entire patches of PSD material (Chen et al., 2011). The list of molecules that PSD-95 potentially binds to includes glutamate receptors, signalling proteins, adhesion molecules (including the neuroligins), and other scaffolding proteins. The diversity of molecules in the PSD dependent on PSD-95 suggests it plays a critical role in the function of the synapse. By interacting simultaneously with these important components of the excitatory synapse, PSD-95 family proteins play a central role in the morphological and functional maturation of synapses at sites of axo-dendrite contacts (Han and Kim, 2008).

Mutations in Shank family proteins are correlated in neurological disorders, such as autism and schizophrenia (Kursula, 2019). Shanks are major contributors to the PSD and interact directly with GKAP and Homer and indirectly with PSD-95 through GKAP (Kim et al., 1997; Naisbitt et al., 1999; Tu et al., 1999). Although it is known that Shanks are large modular scaffolding

molecules, with long flexible regions between domains, an understanding of the structural conformation and function of full-length Shank remains largely unknown.

Presynaptic scaffolding molecules include CASK, another member of the MAGUKs, and MINT. CASK and MINT interact with each other to organize the presynaptic AZ. Mint binds to Munc18-1, a protein essential for synaptic vesicle exocytosis, while CASK has been shown to interact with β-Neurexin (Hata et al., 1996; Zhang et al., 2001). A possible function of CASK/MINT interactions is to localize the vesicle fusion protein Munc18 to the areas of the AZ as defined by neurexins (Biederer and Südhof, 2000).

1.2.6 Inhibitory Scaffolding Molecules

Gephyrin is the predominant scaffolding protein at inhibitory synapses and is a key player in the formation, stabilization, and maintenance of glycinergic and GABAergic postsynapses (Krueger-Burg et al., 2017). Gephyrin is a central element that anchors, clusters and stabilizes glycine and γ-aminobutyric acid type A ($GABA_A$) receptors at inhibitory synapses of the mammalian brain. Gephyrin organizes into hexagonal lattices which allows $GABA_A$/glycine receptors to functionally interact with other gephyrin-associated proteins. Roughly a dozen Gephyrin-interacting proteins (including Nlg-2) have been identified with varying roles in inhibitory synapse functionality, differentiation, and maturation (Choii and Ko, 2015).

A less prominent yet important scaffolding protein at both excitatory and inhibitory synapses is S-SCAM (synaptic scaffolding molecule), also known as MAGI-2 (membrane-associated guanylate kinase inverted-2) (Sumita et al., 2007). S-SCAM interacts with inhibitory synapse-specific proteins such as Nlg-2, the dystroglycan complex (DGC), and IgSF9b. The function of S-SCAM appears to be to bridge trans-synaptic adhesion complexes at inhibitory synapses. For example, although Nlg-2 and IgSF9b do not directly interact with each other, they

are linked together by S-SCAM, potentially allowing them to synergistically coordinate their roles in inhibitory synaptogenesis and function (Woo et al., 2013).

1.3 Neuronal Transport of Synaptic Components

Neurons are highly polarized cells, comprised of a cell body or soma, several branch-like dendritic processes, and a long, thin axon. The compartmentalized nature of neurons requires active mechanisms of transport to distribute organelles to localized regions of demand. With most of the essential proteins and organelles required for pre and postsynaptic function being synthesized in the soma, molecular motors underly the mechanism by which these components get properly localized to the segments of the neuron where they are required (Hirokawa et al., 2010). Neuronal function is dependent on axonal transport and many neurodevelopmental and neurodegenerative diseases are attributed to mutations in axonal transport machinery including Charcot-Marie-Tooth disease and hereditary spastic paraplegia (Maday et al., 2014). Neuronal components can be transported at fast or slow speeds and may need to travel from the soma (anterograde), to the soma (retrograde), or bi-directionally (Hirokawa and Takemura, 2005). Anterograde transport supplies the distal axon terminals with newly synthesized synaptic proteins and organelles that are necessary to maintain presynaptic activity. Retrograde transport maintains homeostasis by removing ageing proteins and organelles from the distal axon for degradation and recycling of their components.

1.3.1 Axonal Transport Mechanisms

Longitudinally orientated microtubules provide the highway along which molecular motors to carry their cargo (Kreutzberg, 1969). Microtubules are long, hollow cylinders composed

of α- and β-tubulins which possess an intrinsic polarity. The direction in which microtubule is polarized plays a critical role in transport directionality (Griffin et al., 1976). In neurons, microtubules have a unipolar orientation in the axons and distal dendrites, with the "plus-end" pointing away from the soma (Burton and Paige, 1981; Stepanova et al., 2003). Interestingly, the proximal dendrites possess microtubules of mixed polarity (Baas et al., 1988; Kwan et al., 2008; Kleele et al., 2014). Although microtubules are rather dynamic structures, their stability and distribution in neurons are tightly controlled by microtubule-associated proteins (MAPs) (Kelliher et al., 2019). MAPs promote microtubule polymerization and stability and are highly expressed in neurons, allowing for microtubules to be generally more stable than other cells (Maday et al., 2014).

The motors of the kinesin superfamily proteins, known as KIFs, are largely responsible for the selective plus-end anterograde transport of molecules from the cell body to the axons (Hirokawa, 1998). There are 45 KIF genes organized into 14 subfamilies, with 38 of those genes expressed in the brain (Miki et al., 2001). All KIFs have a globular motor domain with both a microtubule-binding sequence and an ATP-binding sequence, which is highly homologous between all KIFs (Hirokawa and Takemura, 2005). Axonal transport is an energetically costly process. The molecular motor kinesin-1, for example, hydrolyzes 1 ATP molecule to carry out a single 8 nm step along the microtubule (Hackney, 1994). Outside the motor domain, the cargo domains of each KIF have a unique sequence (Hirokawa and Takemura, 2005). Such diversity contributes to the ability of KIFs to specifically transport a variety of different cargos. Adding to the diversity, different classes of KIFs form homodimers, heterodimers, or function as monomeric motors.

Kinesin-1, kinesin-2, and kinesin-3 subfamilies all contribute to anterograde axonal transport (Maday et al., 2014). Kinesin-1 family members transport a wide range of cargos including vesicles, organelles (including mitochondria), proteins, and RNA particles. Activated motors form a complex from a dimer of kinesin heavy chains (mammalian genes: KIF5A, KIF5B, and KIF5C) and kinesin light chains (KLC). Although the KLC dimer is not always part of the complex, it contributes to the autoinhibitory mechanism of the motor. Kinesin-2 members can assemble into either homodimeric or heterodimeric motors (Scholey, 2013). Kinesin-2 motors drive the transport of fodrin-positive plasma membrane precursors (Takeda et al., 2000), N-cadherin and β-catenin (Teng et al., 2005), choline acetyltransferase (Ray et al., 1999), and Rab7-positive late endosome-lysome compartments (Hendricks et al., 2010; Castle et al., 2014). Kinesin-3 members undergo cargo-mediated dimerization, generating highly functional motors when bound to intracellular organelles (Soppina et al., 2009). Kinesin-3 motors transport synaptic vesicle precursors (SVPs) and dense core vesicles (DCVs) to the axon terminal (Hall and Hedgecock, 1991; Okada et al., 1995; Lo et al., 2011).

Retrograde transport of cargo to the cell body is mediated primarily by the minus-end directed molecular motors of the dynein superfamily. Cytoplasmic dynein is the major retrograde motor in neurons. Unlike the kinesin family, the motor subunit of cytoplasmic dynein, dynein heavy chain (DHC), is encoded by a single gene (Roberts et al., 2013). However, there are multiple genes that encode the other non-motor subunits of the dynein complex, dynein intermediate chain and dynein light intermediate chain (Kuta et al., 2010). Two DHCs dimerize together by their N-terminal tail, followed by the addition of other dynein complex subunits to the DHC tail, forming a cargo binding domain.

1.3.2 Selective Transport of Synaptic Proteins and Synaptic Vesicle Precursors by Kinesin-3

SVPs packed with neuropeptides (including synaptic vesicle proteins such as synaptobrevin, synaptotagmin, synaptophysin, and Rab-3) make up a large fraction of the vesicular organelles in the axon destined to the active zone (Maday et al., 2014). Anterograde transport of SVPs is driven by motors from the kinesin-3 family, KIF1A, KIF1β or KIF1C. Several neurodevelopmental and neurodegenerative disorders have been associated with mutations in kinesin-3 genes (Zhao et al., 2001; Erlich et al., 2011; Hamdan et al., 2011; Rivière et al., 2011; Klebe et al., 2012; Dor et al., 2014; Novarino et al., 2014). Mammalian KIF1A has been of particular interest and was first identified as Unc-104 (Uncoordinated-104) in *C. elegans* (Hall and Hedgecock, 1991; Okada et al., 1995). *Unc-104* mutant worms displayed slow and "uncoordinated" (hence the name) movement, as well as synaptic vesicles mis-localized to the axon terminal, suggesting an impairment in SV transport. Similarly, the neurons of KIF1A knockout mice fail to develop normal synapses and accumulate synaptic precursor proteins in the soma, while overexpression of KIF1A promotes presynaptic bouton formation (Kondo et al., 2012).

KIF1A is thought to be in an autoinhibited state when unbound to cargo by intramolecular interactions involving the neck and tail regions holding it in a monomeric, inactive state (Siddiqui and Straube, 2017). Upon activation or binding of cargo, the motors dimerize with their neck coil and tail regions, undergoing intermolecular interactions. In support of this, four mutations in the stalk region and the motor domain of Unc-104/KIF1A were shown to specifically disrupt autoinhibition and cause excessive activation of Unc-104 (Niwa et al., 2016). *In vivo*, these mutations lead to decreased synaptic density, smaller synapses, and ectopic localization of SVs to

the dendrites. Consistent with what is observed in *C. elegans*, it was also shown that the synaptic vesicle-bound small GTPase Arl-8 activates Unc-104 by unlocking the autoinhibition (Klassen et al., 2010; Wu et al., 2013). These results provide *in vivo* evidence of how the Unc-104 autoinhibitory mechanisms regulate the distribution of synapse-destined cargoes and synaptic development (Niwa et al., 2016).

While some motors bind their cargo directly, often cargo adapter proteins are required to mediate motor activation and cargo recruitment. Interestingly in *C. elegans*, several adaptor proteins associated with the AZ are thought to be involved in Unc-104 motor cargo loading. Binding of Syd-2 (Liprin-α) to Unc-104 results in its translocation to different subcellular compartments in neuronal cells, suggesting that adapter proteins can steer motors and recruit them to their cargo (Wagner et al., 2009; Hsu et al., 2011). Furthermore, binding of Lin-2 (CASK) and Syd-2 (Liprin-α) positively regulates the Unc-104 motor by increasing its velocity, and in the case of Lin-2 increases its run lengths. Additionally, transport of the synaptic vesicle-associated protein, synaptobrevin-1, was reduced in the neurons of *Lin-2* knockout worms, suggesting Lin-2 may be an activator of Unc-104 motor activity (Wu et al., 2016).

In *Drosophila*, the homolog for KIF1A was first identified as the gene *immaculate connections* (*imac*) (Pack-Chung et al., 2007). *imac* mutants were identified in an Electroretinogram (ERG) screen by their lack of on-off transients, suggesting impairments in photoreceptor neurotransmission. At the larval NMJ, *imac* mutants showed a failure in synaptic bouton formation and an absence of synaptic vesicles in motor neuron nerve endings. Another study found that a hypomorphic allele, *unc-104*^{bris}, disrupts the morphogenesis of synaptic terminals at the larval NMJ (Kern et al., 2013). In particular, the reliable apposition of the AZ and PSD was disrupted, possibly by control of the site-specific delivery of AZ cargo. This same *unc-*

104^{bris} allele was later shown to have impairments in AZ maturation and neurotransmission (Zhang et al., 2017a). In the R8 photoreceptor axon terminals, Imac/Unc-104 (potentially activated by the divergent canonical Wnt pathway) was shown to be important in the reversible remodelling of AZ proteins during prolonged exposure to natural ambient light (Sugie et al., 2015). These results suggested a potential role for Imac in the regulation of active zone composition in response to changes in environmental conditions. Interestingly, Imac has recently been demonstrated to promote dendritic pruning in *Drosophila* sensory neurons during metamorphosis (Zong et al., 2018). Imac mediates this action by functioning in a pathway with Pruning Defect 1 (Prd1) and α-Adaptin to down-regulate the cell-adhesion molecule, Neuroglian, by facilitating lysosome-dependent protein degradation.

1.4 The *Drosophila* Visual System

1.4.1 The *Drosophila* Visual System as a Model

Drosophila melanogaster, or more commonly referred to as the fruit fly, has been a workhorse in the fields of genetics and developmental biology for the last century (Morgan, 1910; Tolwinski, 2017) The short lifespan and relative simplicity of the organism compared to mammals allows researchers to follow developmental processes of many different systems throughout the lifespan of the animal. From embryogenesis to adulthood, every stage of the fruit fly's life provides an abundance of knowledge which can be translated to mammalian systems. In its 10-day life cycle, the fly goes through a series of dramatic and stereotyped metamorphic changes from the time of egg fertilization, through the larval and pupal stages, and finally after eclosure becoming an adult fly. Each stage of the life cycle provides a biological model that has added to our

understanding of the contributions of cell lineage and genetic expression to tissue development and function.

The power of the fruit fly in understanding these processes stems from the genetic tools that are available for genetic manipulation. The human and fly genomes share roughly 35% homology, and just under 75% of the genes known to be associated with a disease in humans have a *Drosophila* homolog that can be characterized and studied (Fortini et al., 2000). Beyond simply generating mutations, transgenic RNAi constructs can be stably expressed generating tissue-specific knockdowns of genes (Perkins et al., 2015). Conversely, transgenes can be used to perform cell-type-specific rescue experiments or express a tagged protein (i.e. with GFP) to track the intracellular localization of specific proteins or organelles. The short life cycle and rapid reproduction of the fly is also of large benefit in these circumstances, as it allows for researchers to perform large scale forward and reverse genetics screens to identify potential genes involved in specific biological processes (Bellen et al., 2004, 2011; Mohr, 2014; Mohr et al., 2014). In addition, binary expression systems such as the GAL4/UAS system have become a staple in the drosophilist's tool kit (Duffy, 2002). Such systems allow for the tissue-specific expression of the aforementioned RNAi lines, rescue constructs, and markers.

The *Drosophila* visual system provides an excellent model to study the processes of neuronal circuit development and function (Sanes and Zipursky, 2010; Nériec and Desplan, 2016). The overall structure of the fly visual system is homologous to that of the mammalian retina in both anatomy and connectivity. Ramon y Cajal was one of the first people to recognize this similarity, noting that the cell-types and connectivity of neurons in the fly and mammalian visual system shared striking similarities (Cajal and Sanchez, 1915; Meinertzhagen, 1993). Nearly a century later, using advanced genetic and physiological techniques, the similarities in circuitry and

cell-types Cajal initially observed have been confirmed (Sanes and Zipursky, 2010). For these reasons, the *Drosophila* visual system provides an excellent model to build a greater understanding of the genes and processes underlying visual system circuitry development and function.

1.4.2 The *Drosophila* Retina

Each adult *Drosophila* compound eye is made up of roughly 800 single eye units called ommatidia. The ommatidia reside in the most distal portion of the visual system, called the retina. Each ommatidium is composed of 8 light-sensitive photoreceptors (R-cells), with the motion-sensitive outer R1-R6 cells forming a stereotypical horseshoe shape around the colour-sensitive inner R7-R8 cells. The R7 cell body is more distal (on top) of the R8 cell body (deeper) (Fig. 1.6A). Therefore, due to the curvature of the fruit fly eye, R7 and R8 cells in the same ommatidia "see" light in the same visual field, while the R1-R6 cells in the same ommatidia do not. The R1-R6 cells are responsible for motion detection and express rhodopsin(Rh)-1 which detects light in a broad spectrum (Montell, 2012; Behnia and Desplan, 2015). The R7 and R8 photoreceptors are responsible for colour vision and express Rh3 or Rh4 and Rh5 or Rh6, respectively (Rister and Heisenberg, 2006; Morante and Desplan, 2008).

The R7 and R8 photoreceptors each can be further differentiated into either short-wavelength pale (p) or long-wavelength yellow (y) subtypes depending on the rhodopsin they express. R7y and R7p express Rh-3 and Rh-4 respectively and detect light in the UV-spectrum, while R8y and R8p express Rh-5 and Rh-6 respectively and detect blue and green light, respectively (Morante and Desplan, 2008). Interestingly, the R7 and R8 photoreceptor in a single ommatidium will always be of the same pale or yellow subtype. Therefore, an R7y expressing Rh4 will always be in the same ommatidia as an R8y expressing Rh6 and vice versa for the R7p and R8p subtypes. This specificity of the ommatidia to either a yellow or pale fate is not evenly

distributed, with ~70% of the ommatidia containing the yellow (long-wave UV and green) and ~30% containing the pale (short-wave UV and blue) (Yamaguchi et al., 2010; Montell, 2012). All R-cells have their cell bodies within the retina but project their axons into the optic lobe where they form synaptic connections with their respective targets (Fischbach and Dittrich, 1989).

1.4.3 The *Drosophila* Optic Lobe

Beyond the retina, the *Drosophila* optic lobe is composed of ~60,000 neurons organized in parallel, retinotopically arranged columns within 4 consecutive neuropil regions: the lamina, the medulla, the lobula, and the lobula plate (Varija Raghu et al., 2011). The lamina is the most superficial of the four regions and receives inputs from the motion-sensitive R1-R6 photoreceptor axons, while the colour sensitive R7 and R8 axons pass through the lamina to their targets in the medulla (Fischbach and Dittrich, 1989). The lobular complexes are innervated by projection neurons from the medulla with the lobula plate containing neurons that are strongly responsive to motion (Farrow et al., 2003; Haag and Borst, 2008; Joesch et al., 2008; Jagadish et al., 2014), while neurons sensitive to looming stimuli (generated by objects on a direct collision course with the fly) have been identified in the lobula plate (de Vries and Clandinin, 2012).

All R-cells are histaminergic, meaning that they release the neurotransmitter histamine (Xu et al., 2015). There exists a retinotopic pattern by which the neurons in the retina and the other optic lobes are organized. R-cells that “observe” light from the same specific point in the visual field converge onto a common set of target cells, forming structures called “cartridges” in the lamina and “columns” in the medulla (Takemura et al., 2008; Millard and Pecot, 2018). Because of this organization, the number of modules within each neuropil of the optic lobe matches the number of ommatidia in the retina, with each neighbouring columnar circuit processing inputs from neighbouring points in the visual field, therefore, establishing the retinotopic map. Each

individual laminal cartridge or medullar column possesses a consistent cellular makeup. However, there exists substantially more cellular complexity in the medulla than the lamina, with more than 60 cell types innervating the medulla compared to 18 cell types in the lamina (Millard and Pecot, 2018). Two major types of neurons can be identified within the optic lobes: "Interneurons" whose cell bodies and projections remain within the optic lobe, and "projection" neurons, which connect the optic lobe to the central brain (Hofbauer and Campos-Ortega, 1990; Nériec and Desplan, 2016).

1.4.4 R-cells in the Lamina

The motion-sensitive achromatic R1-R6 photoreceptors are the main innervation to the lamina. Given the curvature of the eye, R1-R6 cells in the same ommatidia "see" different locations in the visual field. Therefore, during development, the R1-R6 axons from a single ommatidium defasciculate from one another and join up with R1-R6 axons from the neighbouring ommatidia that "see" the same location in the visual field, forming laminal cartridges (Clandinin and Zipursky, 2000). This complex connectivity pattern which reconstructs visual space in the lamina is called "neural superposition" (Langen et al., 2015). Neural superposition of R1-R6 photoreceptors to the correct laminal cartridge is highly stereotyped and appears to be genetically hardwired. Clandinin and Zipursky describe the process of R1-R6 neural superpositioning as "the most extraordinary examples of connection specificity known" (Clandinin and Zipursky, 2000).

The protocadherin, Flamingo (Fmi), was identified to be responsible for R1-R6 axons separating from the ommatidial bundle to target the appropriate cartridge (Lee et al., 2003). Fmi is required in the R-cell axons and is thought to mediate its function through repulsive homophilic interactions between neighbouring afferents (Chen and Clandinin, 2008). Additionally, N-cadherin and the receptor tyrosine phosphatase LAR have also been implicated in R1-R6 neural superposition (Clandinin et al., 2001; Lee et al., 2001). In *N-cadherin* mutants, R1-R6

photoreceptors do not separate. Experiments identified that N-cadherin is required in both the photoreceptor axons and the target neurons in the lamina cartridge, while LAR is only required in the afferent photoreceptor axons. More recent studies have shown that LAR interacts with N-cadherin to mediate the afferent-target interaction between the R1-R6 axon terminals and their synaptic targets (Prakash et al., 2009).

Each cartridge is composed of a central core of L1 and L2 neurons that are surrounded by six R-cell (R1-R6) axons, with the main neurites of L3, L4, and L5 neurons situated in the periphery (Fig. 1.6B). R1-R6 cells form roughly 50 synapses per axon terminal (300 per cartridge) in an *en passant* manner along the length of the cartridge (Meinertzhagen and O'Neil, 1991; Rivera-Alba et al., 2011). These synapses are referred to as tetrad synapses because the postsynaptic terminal is comprised of 4 distinct elements: two invariable lamina cells L1 and L2, and two other variable contributions from either a local amacrine cell, an L3 cell and/or epithelial glial cell (Prokop and Meinertzhagen, 2006). Lamina neurons L4 and L5 do not receive synaptic input from R-cells. L1 and L2 neurons have distinct roles in the motion detection circuitry, therefore motion vision might be dependent on equal R-cell inputs onto both these neurons (Silies et al., 2014). L1-L2 pairing at a single synapse is achieved by repulsion forces between processes of the same cell. This process which prevents postsynaptic pairings of two elements from the same cell is called "synaptic exclusion" (Millard et al., 2010). Interestingly, synaptic exclusion at the *Drosophila* tetrad synapse in the lamina cartridge has been shown to be dependent on the transmembrane immunoglobulin superfamily proteins, Dscam1 and Dscam2. Alternative splicing of these two genes results in isoform-specific homophilic binding, which induces repulsion between the same cells and same cell-types (Millard and Pecot, 2018).

1.4.5 R-cells in the Medulla

The medulla receives inputs from both the colour and motion-sensing pathways, then processes and relays that information to the downstream lobula and lobula plate, where it undergoes further integration (Morante and Desplan, 2008). Unlike the laminal cartridges, with identical afferents onto the same targets, each column in the medulla is innervated by different afferent neurons onto many different types of target cells. For example, the medulla receives direct inputs from the colour-sensitive R7 and R8 photoreceptors and indirect inputs from the motion-sensitive R1-R6 photoreceptors through lamina neurons L1-L3. Pioneering work by Fischbach and Dittrich utilizing Golgi impregnation identified more than 60 cell types that innervated the medulla (Fischbach and Dittrich, 1989). Additionally, based on the characteristic depths of the neurites of neurons of the same type, they defined ten parallel layers in the medulla. These ten layers are labelled M1-M10 and are divided into the outer "distal medulla" (M1-M6) and inner "proximal medulla" (M8-M10) (Fischbach and Dittrich, 1989; Morante and Desplan, 2008; Takemura et al., 2008). Electron microscopy (EM) analysis in the years since have identified that the depth at which the axons a specific cell-type terminates, or dendrites initially arborize is largely predictive of where synapses form.

The inner R7 and R8 cells from the same ommatidia (carrying input from the same location in the visual field) project and terminate their axons into the same column within the medulla. Therefore, the topographic organization of the columns maintains retinotopic order (Clandinin and Zipursky, 2002; Sanes and Zipursky, 2010). Although quite intimate with each other within the column, R7 and R8 axon terminals differ in two distinct ways. First, they terminate in different layers with the R8 axon stopping at the M3 layer and R7s projecting deeper to the M6 layer. Secondly, they form their synapses in different layers with R8s forming 35-50 synapses between

the M1 and M3 layers, while the R7s form 20-26 synapses between the M4-M6 layers (Takemura et al., 2008, 2015; Rivera-Alba et al., 2011; Chen et al., 2014). Interestingly, over 70% of the R7 presynaptic sites are located at their terminal boutons and stem, while in R8s the presynaptic sites are distributed fairly evenly along the axon terminal (Melnattur and Lee, 2011). Given the level of complexity, it has been difficult to determine the entire connectome of the medulla from EM reconstruction, but for the most part, the initial connections of the R-cells within the lamina have been identified.

Work from Chi-Hon Lee and colleagues has been instrumental in determining the chromatic circuitry in the *Drosophila* optic lobe. The R7 and R8 photoreceptors are the first step in the colour vision pathway and provide inputs for the amacrine neuron Dm8 and the transmedulla neurons Tm5a/b/c, Tm9 and Tm20 (Melnattur et al., 2014). The medulla projection (Tm) neurons, analogous to vertebrate retinal ganglion cells, relay photoreceptor information to higher visual centers in the lobula while the distal medulla (Dm) neurons connect photoreceptors to Tm neurons. More specifically the R8s form synaptic connections with the first-order interneurons Tm9, Tm20 and Tm5c, while the R7s innervate Tm5a and Tm5b. Multiple R7s also provide input onto the amacrine neuron Dm8, which innervate the Tm5a/b/c neurons (Gao et al., 2008; Lin et al., 2016). More recently a technique developed called “Tango-Trace” identified four potentially novel subtype-specific postsynaptic targets for R-cells which they aptly named, Rh3TmY, Rh4TmY, Rh5TmY and Rh6TmY (Jagadish et al., 2014). These complex transmedullary Y neurons (TmY) were shown to have axon projections directly to the proximal medulla, the lobula, and the lobula plate. In addition to the four TmY cells, the “Tango-Trace” technique identified connections with two interneurons, Dm8 and Mia, that were postsynaptic to the inner R7 and R8 photoreceptors. However, the findings of this technique still need to be verified on the ultrastructure level.

1.4.6 R7 and R8 Photoreceptor Layer Selection and Targeting

Much work has been done in understanding the development of R7 and R8 cells, especially how they target the appropriate layer and are restricted within their columnar space in the medulla. In a developing ommatidium, the R8 is the first photoreceptor born, followed sequentially by R2 and R5, R3 and R4, R1 and R6, and finally R7 (Kumar, 2012). The R1–R7 axons from the same ommatidium follow the pioneer R8 axon trajectory until they reach the lamina (Hakeda-Suzuki and Suzuki, 2014). The axons of all eight R-cells in a single ommatidium will fasciculate together as a single bundle into the optic lobe. As mentioned previously, R1-R6 will defasciculate and terminate their axons in the lamina, while the R7 and R8 axons continue through the lamina until they reach the medulla. The genetic mechanisms underlying the ability of the inner photoreceptors to target the proper layer and column have been studied in great detail (Millard and Pecot, 2018).

As visual circuitry develops, the R8 axon terminals initially terminate near the superficial (distal) surface of the medulla in a temporary layer (Nern et al., 2008; Pecot et al., 2013). The R7 axon terminals then overtake the paused R8s and enter the medulla to pause in their own temporary layer. Both R8 and R7 axons will then proceed to innervate their final layers during midpupal development (Ting et al., 2005). Lamina neurons L1-L5 also grow at this time and establish stereotyped arborizations in medulla layers, causing the medulla to expand and thereby increasing the distance between the R7 and R8 temporary layers (Millard and Pecot, 2018). At approximately 50 hours after puparium formation (h APF), the second stage of medulla targeting begins once all the axons of R7, R8, and lamina neurons reach their respective temporal layers. The R8 axons start to extend thin filopodia towards their final M3 target layer and by 70 h APF, both R7 and R8 axon terminals will reach their final target layers (Chen et al., 2014; Akin and Zipursky, 2016). Once at

the final target layer the axon terminals will mature, beginning the process of synaptogenesis and forming synaptic connections with their targets.

1.4.7 R8 Layer Selection and Targeting

Flamingo (Fmi) and Golden goal (Gogo) are two cell surface molecules whose interactions are critical in R8 axon layer targeting. The seven-pass transmembrane Cadherin, Fmi, is primarily expressed in the target regions of photoreceptor axons (Senti et al., 2003; Hakeda-Suzuki et al., 2011). Gogo is Fmi's putative receptor, and is mainly detectable in the photoreceptor axons (Tomasi et al., 2008; Hakeda-Suzuki et al., 2011; Mann et al., 2012). Eye-specific *gogo* and *fmi* mutants show a phenotype where the R8 axons cannot extend filopodia toward the M3 target layer at 50 h APF (Hakeda-Suzuki et al., 2011; Hakeda-Suzuki and Suzuki, 2014). Therefore, a majority of the R8 axons stay at the temporary layer and fail to innervate the medulla. Interestingly, the cytoplasmic domain of Fmi is dispensable in R8 targeting, while the cytoplasm is necessary for the functionality of Gogo. This suggests that Fmi mediates axon-target interactions through the adhesive properties of its extracellular domain and Gogo requires its intracellular signalling capability for relaying axon pathfinding information to the growth cone.

The secreted chemotropic guidance molecule, Netrin (Net), and its receptor, Frazzled (Fra, i.e. a homolog of DCC), have also been implicated in R8 targeting to the M3 layer. Both *net* and *fra* expression begin at 42 h APF, with *fra* being expressed in both the R8 axon and M3 layer target neurons, while *net* expression is isolated to the emerging M3 layer (Timofeev et al., 2012). Disruption of Netrin or Frazzled causes R8 growth cones to stall at the temporary layer or inappropriately terminate at the superficial M1 or M2 layers. *In vivo* time-lapse imaging revealed that R8 growth cones with impaired Netrin/Frazzled signalling properly extend and target to the M3 layer normally but cannot maintain their position in the M3 layer and retract (Akin and

Zipursky, 2016). Interestingly, it was revealed that expression of Netrin in the neurites of L3 neurons (which are restricted to the M3 layer and make contact but do not synapse with R8s), was able to direct R8 axons to the proper M3 layer (Timofeev et al., 2012; Millard and Pecot, 2018).

Lastly, a homophilic transmembrane protein with leucine-rich repeats, Capricious (Caps), has also been shown to be critical for R8 axon targeting (Shinza-Kameda et al., 2006). In the adult visual system, *caps* is expressed specifically in the R8 axons and multiple layers within the medulla, including M3. *caps* mutants display an axon mistargeting phenotype, where the R8 axons terminate too superficially or overshoot the M3 layer altogether. In addition, these terminals also show tiling defects with some R8 axons extending into neighbouring columns. Ectopic expression of *caps* in R7 axons, which normally terminate in the M6 layer, causes them to mistarget to the M3 layer. Intriguingly, it was later shown that the mistargeting of R7 axon terminals to the M3 layer induced by *caps* overexpression does not require Caps in the target region (Berger-Müller et al., 2013). These recent insights suggest that Caps in visual circuit development may not rely on its homophilic R8-target interactions, but possibly via heterophilic interactions with another unknown ligand (Hakeda-Suzuki and Suzuki, 2014).

1.4.8 R7 Layer Selection and Targeting

Similar to R8s, R7s arrest at a temporary layer before they extend growth cones out to their destined layers. Initial genetic screens based on visual behaviours and histology identified three surface receptors, N-cadherin, the receptor tyrosine phosphatases LAR, and PTP69D, that are required for R7 layer selection (Newsome et al., 2000; Clandinin et al., 2001; Lee et al., 2001; Maurel-Zaffran et al., 2001). N-cadherin, the homophilic transmembrane molecule, is required in the first stage for R7 growth cones to reach and remain in the R7-temporary layer (Ting et al., 2005), as well as in the second stage where R7 axons lacking N-cadherin mistarget to the R8

recipient layer (Lee et al., 2001). While LAR has a role in R1-R6 neural superposition, it is also required cell-autonomously in R7 layer target selection. Similar to *N-cadherin* mutants, *LAR* mutant R7 axons ectopically terminate in the M3 R8 recipient layer (Clandinin et al., 2001). Further observation of the mechanism revealed that *LAR* mutant R7 axons properly target to the M6 R7 recipient layer initially, but later retract to the M3 layer. The absence of PTP69D in R7 axons also causes a mistargeting of the axon terminal to the M3 layer (Newsome et al., 2000). It is suggested that LAR and PTP69D have a permissive role in synaptic-layer selection, perhaps by downregulating the adhesion of R1-R6 and R7 growth cones to the pioneer R8 axon so that they can respond independently to their specific targeting cues (Millard and Pecot, 2018). In support of this, recent work from our lab has shown that the Ig-super family member transmembrane adhesion molecule, *borderless*, is negatively regulated by LAR in controlling synaptic-layer selection of R7 axons (Cameron et al., 2013).

1.4.9 Colour Vision in the *Drosophila*

Colour vision requires the ability to distinguish light of distinct spectral composition (i.e. different wavelengths) independent of intensity (Morante and Desplan, 2008). As mentioned previously, the R7 and R8 cells are responsible for detecting coloured light in the *Drosophila* visual system. A vast complexity of richly arborizing intrinsic neurons and projection neurons in the medulla has made it difficult to identify all of the postsynaptic partners of R7 and R8 neurons (Takemura et al., 2008; Melnattur and Lee, 2011). In addition, the stacked configuration of the R7 and R8 cell bodies in the retina, as well as the complexity of their connections within the medulla, have made it difficult to record these neurons with electrophysiological techniques (Hardie, 1979). However, recent studies using EM, genetic-labelling, behaviour, and calcium-sensing techniques

have shed light on the mechanisms underlying how the fruit fly sees colour (Yamaguchi et al., 2010; Takemura et al., 2015; Weir et al., 2016; Schnaitmann et al., 2018).

Because the medulla receives direct input from the R7 and R8 photoreceptors, it is the first step in the colour-vision pathway. The medulla is the largest and most complex structure in the *Drosophila* visual system, containing about 40,000 of the 60,000 total cells in the optic lobe (Hofbauer and Campos-Ortega, 1990). Within the medulla, there are ~800 columns, each containing a single R7 and R8 axon from the same ommatidium that see the same point in space. Each column can be considered a functional unit made up of a fixed number of columnar and noncolumnar neurons that can innervate or be innervated by the inner photoreceptors.

Although the earliest screens to identify some of the most integral genes in synaptic function were identified with the ERGs (Dolph et al., 2011), electrophysiology in the fly visual system is quite difficult because of the size and complexity within the neuropils. Phototactic T-maze behavioural experiments by Yamaguchi and colleagues confirmed the contribution of individual photoreceptor subtypes in detecting different wavelengths of colour (Yamaguchi et al., 2010). Recent experiments by Schnaitmann and colleagues took those experiments to the next level by using two-photon calcium imaging to look at the presynaptic responses of individual R7 and R8 axon terminals within the medulla when a fly observes different wavelengths of light (Schnaitmann et al., 2018). Interestingly, they observed evidence of colour opponency where R7 and R8 photoreceptors from the same ommatidia mutually inhibit one another. They further identified that this inhibition is mediated by both direct inhibitions between R7 and R8 axons onto each other via histamine release onto HisCl1 histamine receptors and by indirect mechanisms through feedback loops from local neurons, but via another histamine receptor, Ort.

Genetic mosaic analysis continues to identify more and more individual cell types within the colour vision circuitry of the medulla. As the techniques become more advanced we will continue to identify the innervations and circuits within the medulla and the lobula complexes. Ultimately, the daunting task of complete EM reconstruction of the visual system will be the gold standard to confirm these findings, however, the full EM dataset of the entire *Drosophila* brain is now available for this pursuit (Zheng et al., 2018). In conjunction with behavioural and physiological techniques, we will have a better appreciation for the circuitry underlying colour vision in the fly.

1.5 Rationale and Objectives for This Study

Recent work from our lab has demonstrated that the conserved IgSF9 subfamily member of the Ig superfamily, Borderless (Bdl), functions as a cell adhesion molecule, and is capable of mediating both homophilic and heterophilic binding (Cameron et al., 2013, 2016; Hansen and Walmod, 2013; Chen et al., 2017). Recent studies on the mammalian homologs of Bdl, IgSF9a and IgSF9b, show that IgSF9a and IgSF9b function as trans-synaptic adhesion molecules by mediating homophilic binding (Hansen and Walmod, 2013; Woo et al., 2013). Interestingly, IgSF9b has been shown *in vitro* to form a complex with the postsynaptic adhesion molecule Neuroligin-2 (Nlg2) via the scaffolding molecule, S-SCAM (Woo et al., 2013). In the developing *Drosophila* visual system of third-instar larvae, Bdl is exclusively expressed in wrapping glia and is required for mediating axon-glia recognition (Cameron et al., 2016). However, in the adult fly, Bdl is also expressed in R-cell axons and its overexpression induces R7 axon terminal layer selection and tiling defects (Cameron et al., 2013). Interestingly, it appears that *bdl* is negatively regulated by another Ig transmembrane protein, Turtle (Tutl), and the receptor tyrosine

phosphatase, LAR, to ensure proper R7 axon tiling and layer selection, respectively (Cameron et al., 2013). However, as *bdl* mutants show no apparent photoreceptor layer selection or targeting defects, the role of Bdl in R-cell axons remains unknown.

Given the roles of IgSF9a and IgSF9b homophilic binding in synaptic development in mammals and the expression of Bdl in R-cell axons, I investigated the role of Borderless (Bdl) in R-cell synaptic function in the *Drosophila* visual system. The *Drosophila* visual system has proven to be an excellent model to study the mechanisms controlling neuronal circuit development and function (Sanes and Zipursky, 2010; Nériec and Desplan, 2016). In experiments I identified that R8 cells in *bdl* mutants display a mis-localization of SVP to the R8 proximal axon, suggesting in the absence of Bdl the transport of synaptic proteins is impaired. Whether and how synaptogenic adhesion at axo-dendritic contact sites regulates axonal transport of presynaptic components remains unknown. For the above-stated reasons, I carried out the present study with the aims to (1) determine whether R8 synaptic function and SVP localization are dependent on Bdl homo- or heterophilic interactions between pre- and postsynaptic targets; (2) elucidate the intracellular mechanisms downstream of Bdl that underly the SVP mis-localization phenotype in the R8 axon terminals of *bdl* mutants; (3) determine any other genes that Bdl interacts with genetically and/or physically at axo-dendritic contacts to mediate the proper recruitment of SVPs to R8 axon terminals.

As this thesis is manuscript based, Chapter 2 addresses my first two aims and describes my published work in the *Journal of Neuroscience* where I elucidate the mechanisms underlying Bdl-mediated transport of SVP to the R8 axon terminal (Shaw et al., 2019). In Chapter 3, I will address the final aim and describe a manuscript that is in preparation studying the physical and genetic

interactions between Bdl and Dnlg2, and how they contribute to R8 SVP localization. In Chapter 4, I discuss my conclusions and future directions.

Figure 1.1

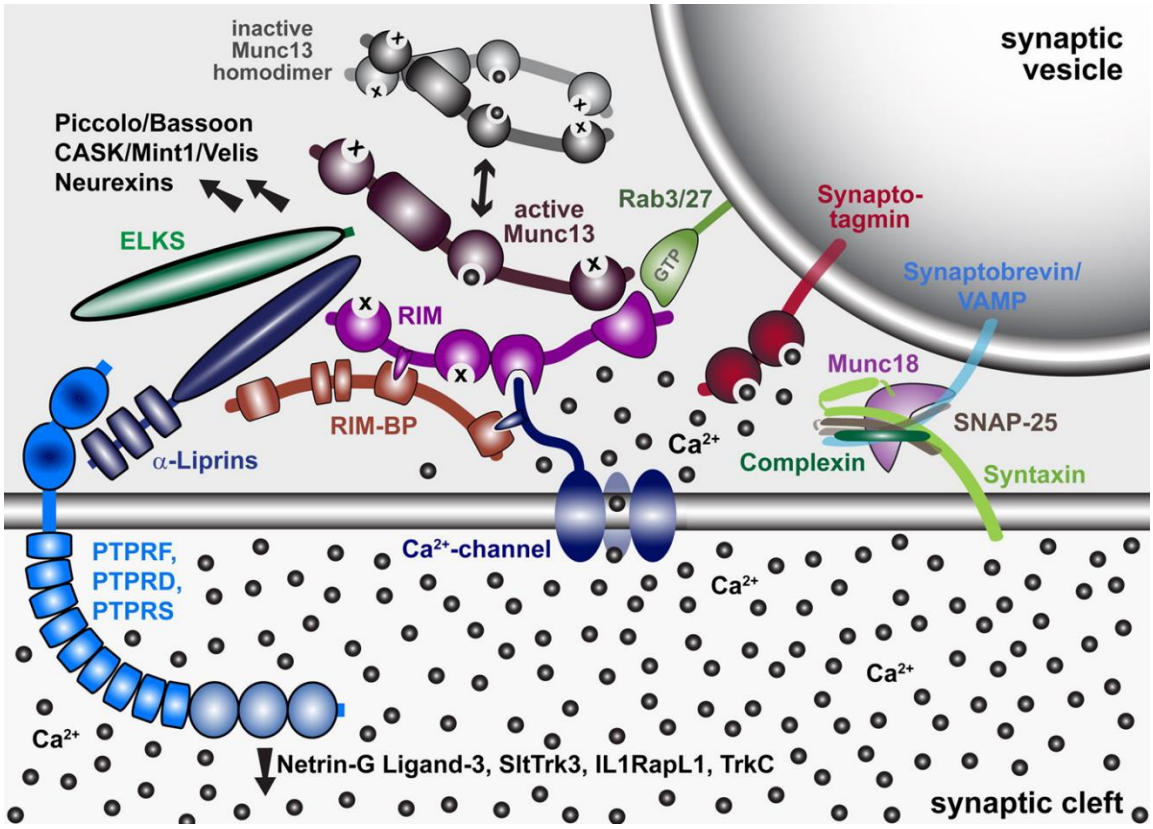
inactive
Munc13
homodimer
synaptic
vesicle
Piccolo/Bassoon
CASK/Mint1/Velis
Neurexins
active
Munc13
Rab3/27
GTP
Synapto-
tagmin
ELKS
RIM
Synaptobrevin/
VAMP
Munc18
RIM-BP
SNAP-25
Ca2+
α-Liprins
Complexin
Syntaxin
PTPRF,
PTPRD,
PTPRS
Ca2+-channel
Ca2+
Ca2+
Ca2+
Netrin-G Ligand-3, SltTrk3, IL1RapL1, TrkC
synaptic cleft

Figure 1.1. Molecular model of the active zone. Molecular model of the active zone protein complex and its relation to the synaptic vesicle fusion machinery, Ca^{2+} channels, and synaptic cell-adhesion molecules. Adapted from *Südhof TC (2012) The Presynaptic Active Zone. Neuron 75:11–25.*

Figure 1.2

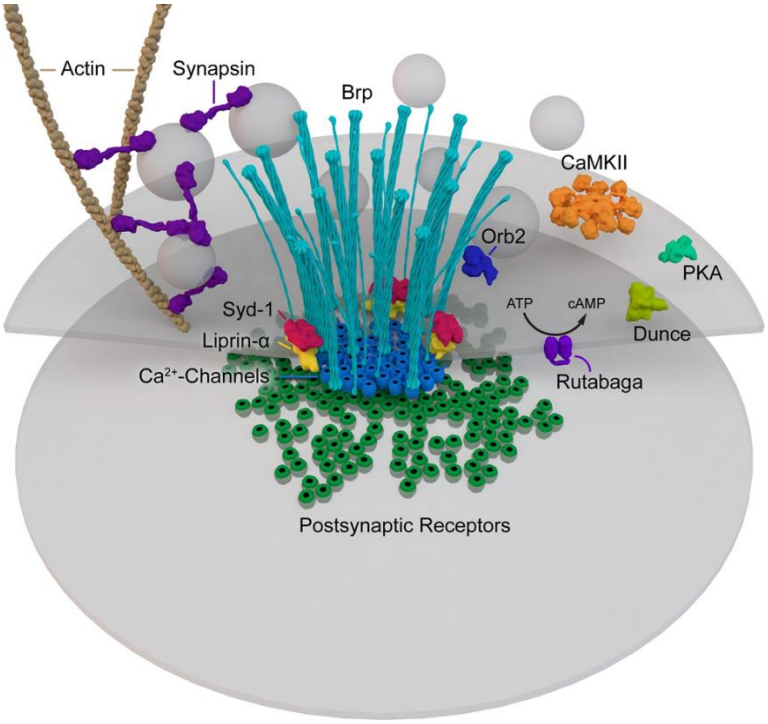
Actin
Synapsin
Brp
CaMKII
Orb2
PKA
ATP
cAMP
Dunce
Syd-1
Liprin-α
Ca²⁺-Channels
Rutabaga
Postsynaptic Receptors

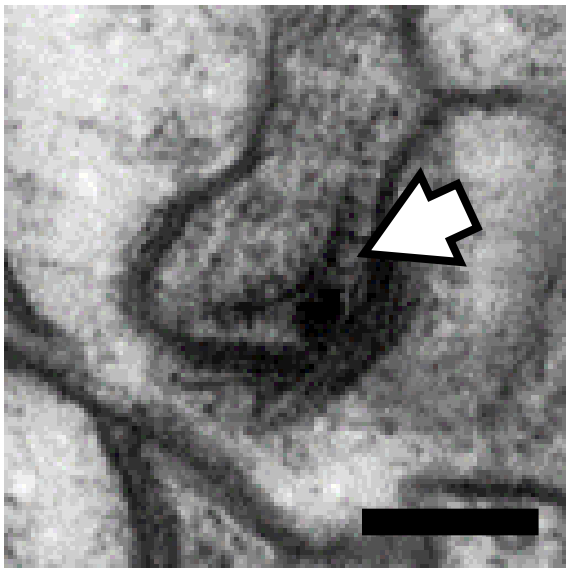

Figure 1.2. Molecular components of the active zone in the *Drosophila* CNS. (Above) Shown are presynaptic molecules that comprise the T-bar ribbon of central AZs. Adapted from *Ehmann N, Owald D, Kittel RJ (2018) Drosophila active zones: From molecules to behaviour. Neurosci Res 127:14–24.* (Below) Electron micrograph of a presynaptic T-bar ribbon (indicated by arrow) in the *Drosophila* lamina. Scale bar = 0.2 µm.

Figure 1.3

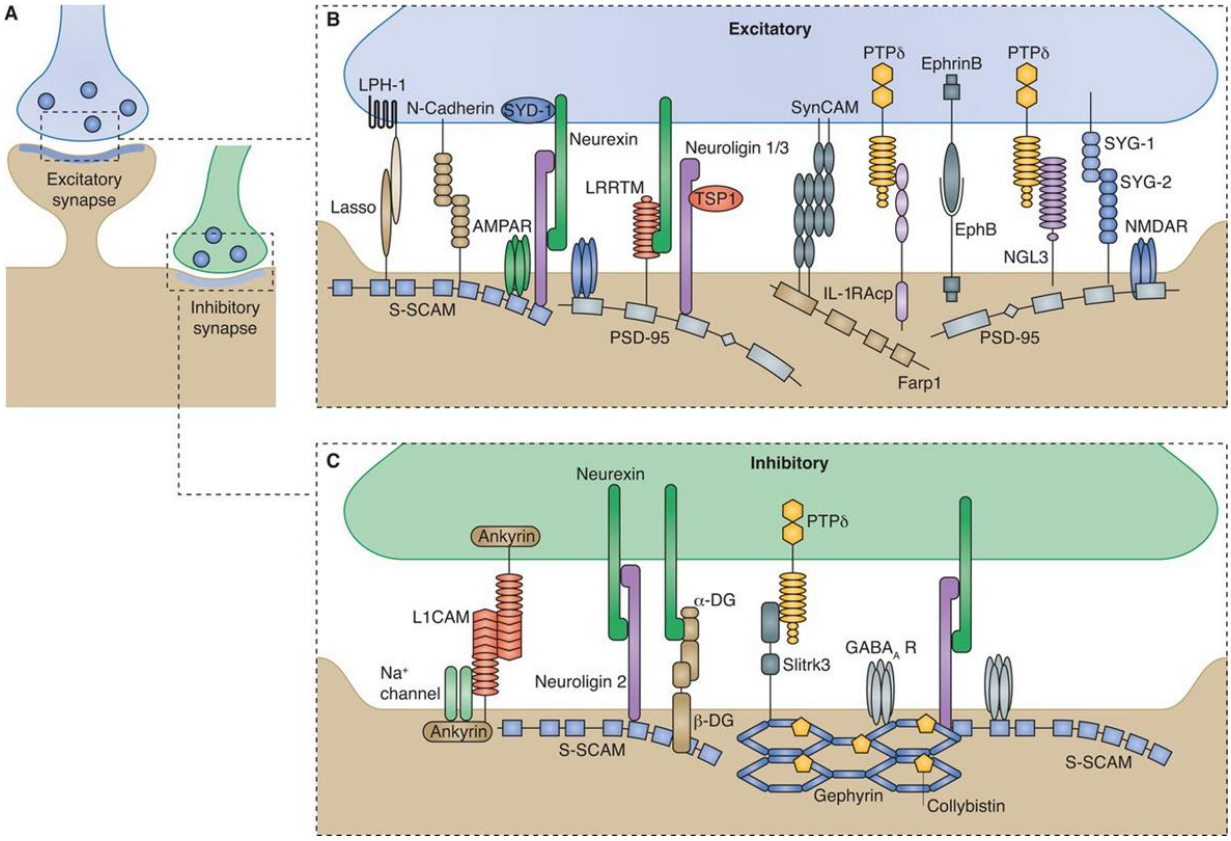
A
Excitatory synapse
Inhibitory synapse
B
Excitatory
LPH-1
N-Cadherin
SYD-1
Neurexin
Neuroligin 1/3
SynCAM
PTPδ
EphrinB
PTPδ
SYG-1
SYG-2
NMDAR
Lasso
AMPAR
LRRTM
TSP1
EphB
NGL3
S-SCAM
PSD-95
IL-1RAcp
PSD-95
Farp1
C
Inhibitory
Neurexin
PTPδ
Ankyrin
L1CAM
α-DG
Na+ channel
Neuroligin 2
Slitrk3
GABAA R
Ankyrin
β-DG
S-SCAM
S-SCAM
Gephyrin
Collybistin

Figure 1.3. Trans-synaptic adhesion molecules and scaffolding proteins. Adhesive trans-synaptic signalling orchestrates excitatory and inhibitory synaptic assembly and function. Multiple pairs of trans-synaptic adhesion molecules organize synaptic differentiation and function on both pre- and postsynaptic sites. Scaffolding molecules anchor trans-synaptic adhesion molecules through protein-protein interactions. Different adhesion molecules and scaffolding molecules are used at excitatory and inhibitory synapses. Adapted from *Chia PH, Li P, Shen K (2013) Cellular and molecular mechanisms underlying presynapse formation. J Cell Biol 203:11–22.*

Figure 1.4

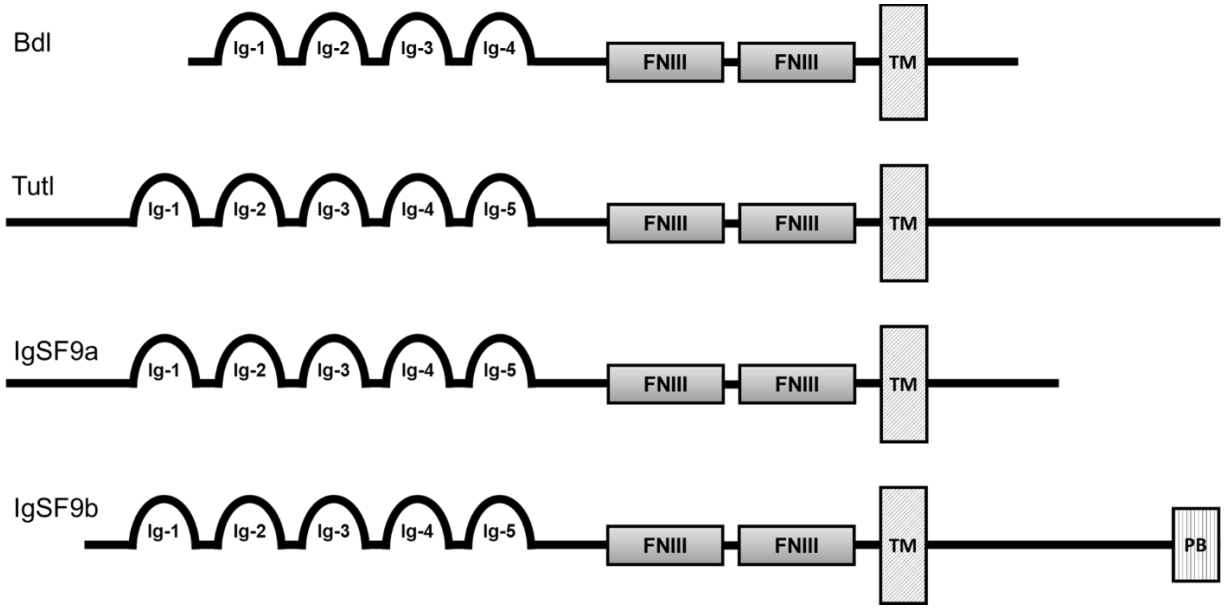
Bdl
Ig-1
Ig-2
Ig-3
Ig-4
FNIII
FNIII
TM
Tutl
Ig-1
Ig-2
Ig-3
Ig-4
Ig-5
FNIII
FNIII
TM
IgSF9a
Ig-1
Ig-2
Ig-3
Ig-4
Ig-5
FNIII
FNIII
TM
IgSF9b
Ig-1
Ig-2
Ig-3
Ig-4
Ig-5
FNIII
FNIII
TM
PB

Figure 1.4. IgSF9 family of molecules in *Drosophila* and mammals. *Drosophila* Bdl and Tutl are comprised of four and five Immunoglobulin (Ig)-domains, respectively, two fibronectin type III domains (FNIII), a transmembrane domain (TM), and a short cytoplasmic tail. Mammalian IgSF9a and IgSF9b are comprised of five Immunoglobulin (Ig)-domains, two fibronectin type III domains (FNIII), a transmembrane domain (TM), and a short cytoplasmic tail. Additionally, a protein binding (PB) domain in the cytoplasmic tail of IgSF9b has been identified. Note: figures are intended to demonstrate similarities in overall protein structure and are therefore not necessarily to scale.

Figure 1.5

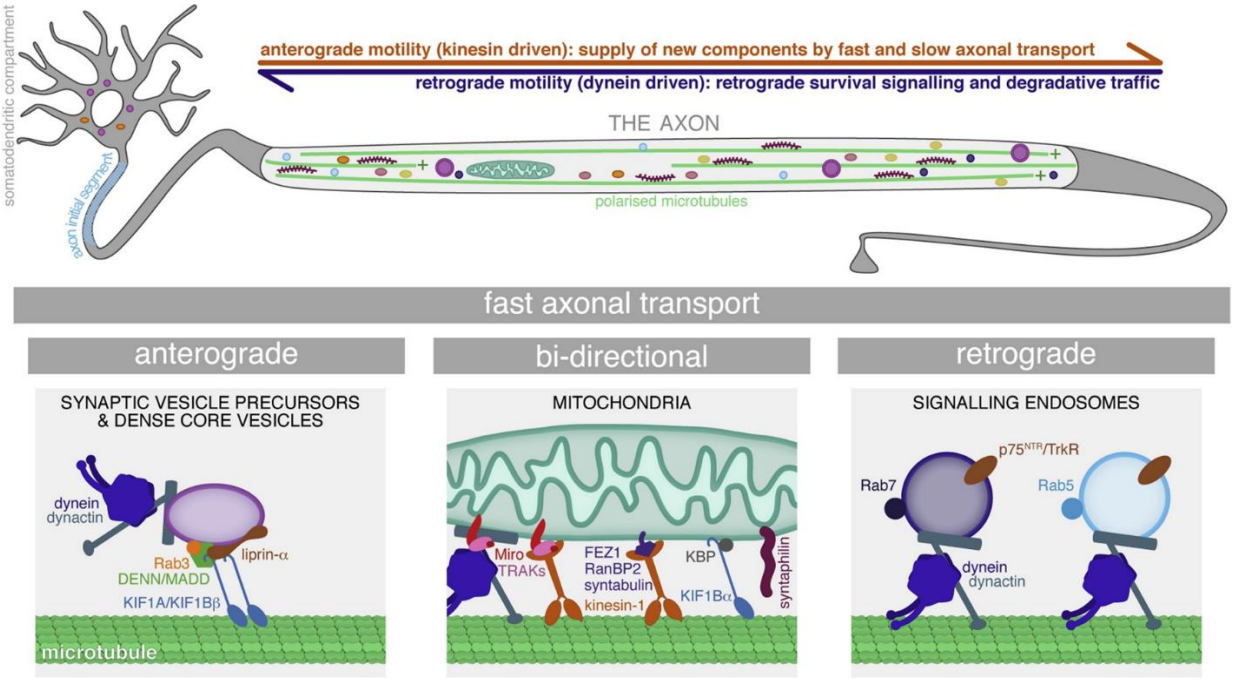
somatodendritic compartment
axon initial segment
anterograde motility (kinesin driven): supply of new components by fast and slow axonal transport
retrograde motility (dynein driven): retrograde survival signalling and degradative traffic
THE AXON
polarised microtubules
fast axonal transport
anterograde
bi-directional
retrograde
SYNAPTIC VESICLE PRECURSORS & DENSE CORE VESICLES
dynein dynactin
Rab3 DENN/MADD
liprin-α
KIF1A/KIF1Bβ
microtubule
MITOCHONDRIA
Miro TRAKs
FEZ1 RanBP2 syntabulin kinesin-1
KBP
KIF1Bα
syntaphilin
SIGNALLING ENDOSOMES
p75NTR/TrkR
Rab7
Rab5
dynein dynactin

Figure 1.5. Microtubule motor proteins in axonal transport. Microtubule motor proteins kinesin and dynein drive the movement of organelles, vesicles, RNA granules, and proteins along the axon. Kinesins drive anterograde transport outward from the soma, and dynein drives retrograde transport back from the distal axon. Anterograde transport of synaptic vesicle precursors and dense core vesicles is mediated by kinesin-3 motors (i.e. KIF1A and KIF1Bβ). Adapted from *Maday S, Twelvetrees AE, Moughamian AJ, Holzbaur ELF (2014) Axonal transport: cargo-specific mechanisms of motility and regulation. Neuron 84:292–309.*

Figure 1.6

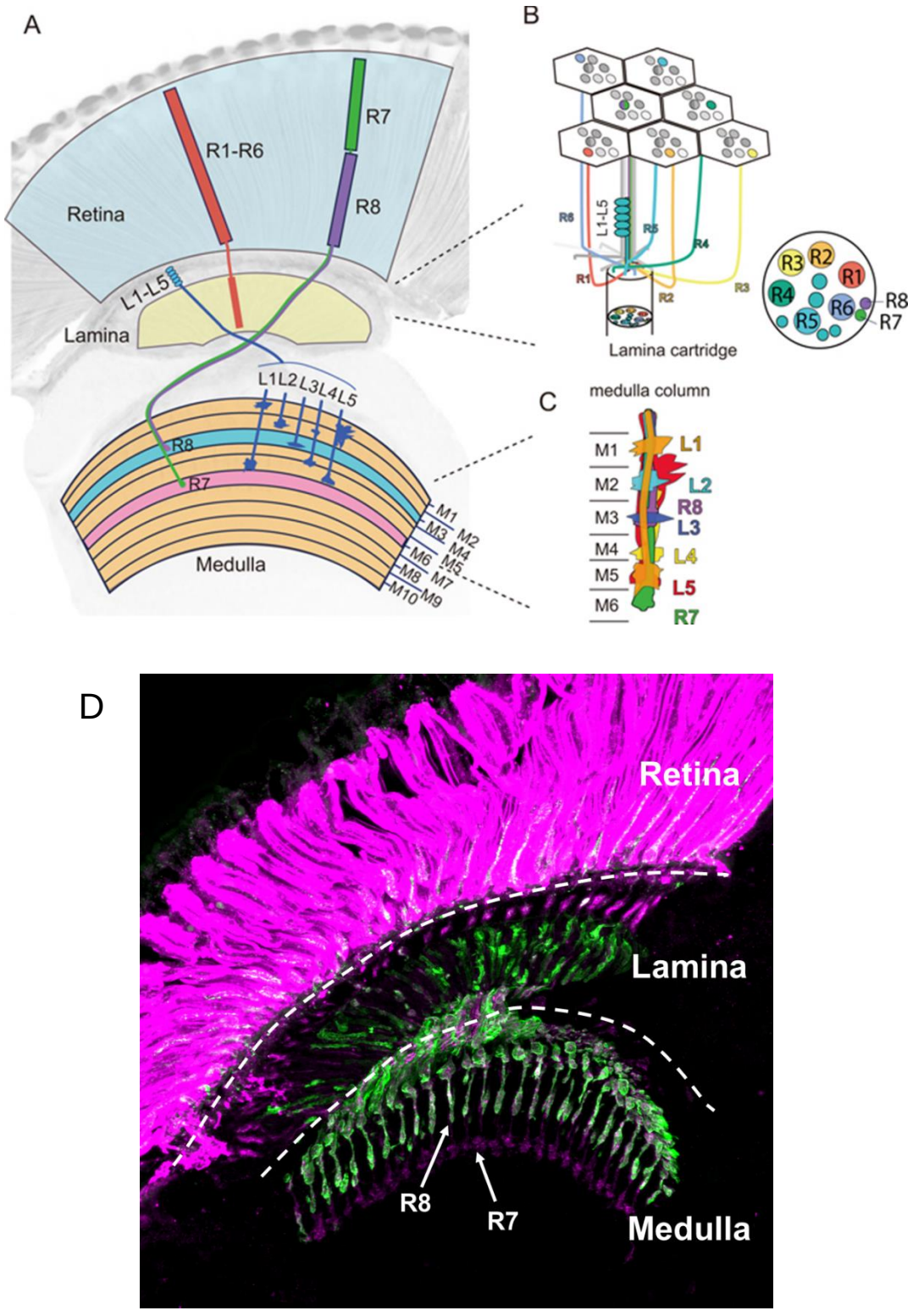
A
R7
R1-R6
R8
Retina
L1-L5
Lamina
L1L2L3L4L5
R8
R7
M1
M2
M3
M4
M6
M5
M7
M8
M10
M9
Medulla
B
R8
L1-L5
R5
R4
R1
R2
R3
Lamina cartridge
R3
R2
R1
R4
R6
R8
R5
R7
C
medulla column
M1
M2
M3
M4
M5
M6
L1
L2
R8
L3
L4
L5
R7
D
Retina
Lamina
R8
R7
Medulla

Figure 1.6. The adult *Drosophila* optic lobe. (A) The axons from the outer photoreceptors R1–R6 (red) innervate the lamina, whereas the inner photoreceptors R7 (green) and R8 (purple) extend into the medulla. The medulla is divided into ten layers, and R7 and R8 target the M6 (pink) and M3 (blue) layers, respectively. (B) R1–R6 projection pattern to a cartridge in the lamina. The R7/R8 axons extend towards the medulla through the lamina cartridge directly below. The axons from the R1–R6 of six surrounding ommatidia, which "see" the same point as R7/R8 of the central ommatidium, converge onto the same cartridge with R7/R8. (C) The R7 and R8 axons from the same ommatidium and axons of lamina neurons L1–L5 from its corresponding cartridges project into a single column in the medulla. Each cell-type in the medulla target a distinct layer, at which they form synaptic connections. Adapted from *Hakeda-Suzuki S, Suzuki T (2014) Cell surface control of the layer specific targeting in the Drosophila visual system. Genes Genet Syst 89:9–15.* (D) Cross-sectional image of the *Drosophila* visual system. Dashed lines delineate the borders between the retina, lamina, and medulla. Arrows indicate R8 axons (green) terminating at the M3 layer and R7 axons (magenta) terminating at the M6 layer.

Chapter 2: The conserved IgSF9 protein Borderless regulates axonal transport of presynaptic components and colour vision in *Drosophila*[1]

[1] This chapter has been published in the journal: *Journal of Neuroscience* 24 June 2019, 0075-19;

DOI: 10.1523/JNEUROSCI.0075-19.2019

Hunter S. Shaw, Scott A. Cameron, Wen-Tzu Chang, Yong Rao

2.1 Abstract

Normal brain function requires proper targeting of synaptic vesicle (SV) and active zone (AZ) components for presynaptic assembly and function. Whether and how synaptogenic signals (e.g. adhesion) at axo-dendritic contact sites promote axonal transport of presynaptic components for synapse formation, however, remain unclear. In this study, we show that Borderless (Bdl), a member of the conserved IgSF9-family trans-synaptic cell adhesion molecules, plays a novel and specific role in regulating axonal transport of SV components. Loss of *bdl* disrupts axonal transport of SV components in photoreceptor R8 axons, but does not affect the transport of mitochondria. Genetic mosaic analysis, transgene rescue and cell-type-specific knockdown indicate that Bdl is required both pre- and postsynaptically for delivering SV components in R8 axons. Consistent with a role for Bdl in R8 axons, loss of *bdl* causes a failure of R8-dependent phototaxis response to green light. *bdl* interacts genetically with *imac* encoding for a member of the Unc-104/Imac/KIF1A-family motor proteins, and is required for proper localization of Imac in R8 presynaptic terminals. Our results support a model in which Bdl mediates specific axo-dendritic interactions in a homophilic manner, which up-regulates the Imac motor in promoting axonal transport of SV components for R8 presynaptic assembly and function.

2.2 Introduction

After initial axon-dendrite contact, cellular morphogenetic events occur at both sides of the contact, which eventually leads to the formation of chemical synapses. Each synapse consists of specialized presynaptic and postsynaptic structures that allow proper neuronal communications. The assembly and function of presynaptic structures requires proper delivery of active zone (AZ) and synaptic vesicle (SV) components from soma to nerve terminals. For instance, axonal transport of Piccolo-bassoon Transport Vesicles (PTVs) and Synaptic Vesicle Precursors (SVPs) is required for the assembly of AZs and the accumulation of SVs for synapse formation and maintenance (Goldstein et al., 2008; Maeder et al., 2014). Whereas axonal transport of mitochondria is crucial for meeting energy demands at presynaptic terminals (Goldstein et al., 2008; Maeder et al., 2014).

Synapse formation involves rapid recruitment of SV and AZ components at the sites of axo-dendritic contact (McAllister, 2007; Chia et al., 2013). Accumulated evidence supports a key role for the kinesin-3 family motor Unc-104/Imac/KIF1A in regulating axonal transport of SVPs and PTVs (Hall and Hedgecock, 1991; Otsuka et al., 1991; Okada et al., 1995; Zhao et al., 2001; Pack-Chung et al., 2007; Barkus et al., 2008; Niwa et al., 2008). In the absence of Unc-104/Imac/KIF1A, most SVPs are unable to move from soma into axons. Recent studies also show that Unc-104/Imac/KIF1A is activated by the SVP-localized small arf-like GTPase ARL-8 (Klassen et al., 2010; Niwa et al., 2017), and can also be modulated by the JNK MAP kinase pathway (Byrd et al., 2001; Wu et al., 2013). While it is clear that synaptogenic signals such as trans-synaptic adhesion modulate local recruitments of SV components at the presynaptic terminals for the control of synaptic plasticity (Bury and Sabo, 2016), a recent *in vitro* study shows that Neuroligin-Neurexin-mediated trans-synaptic adhesion does not significantly affect axonal transport of SV components in cultured cortical neurons (Bury and Sabo, 2014). It remains

unknown whether and how synaptogenic adhesion at axo-dendritic contact sites regulates axonal transport of SV components to sites of presynaptic assembly *in vivo*.

In this study, we investigate the role of Borderless (Bdl) in the *Drosophila* visual system, which is an excellent model to study the mechanisms controlling neuronal circuit development and function (Sanes and Zipursky, 2010; Nériec and Desplan, 2016). Bdl belongs to the conserved IgSF9 subfamily of Ig superfamily (Hansen and Walmod, 2013). In our previous studies (Cameron et al., 2013; Chen et al., 2017), we show that Bdl functions as a cell adhesion molecule, and is capable of mediating both homophilic and heterophilic binding. Recent studies on IgSF9a and IgSF9b, homologs of Bdl in mammals, show that IgSF9a and IgSF9b function as trans-synaptic adhesion molecules by mediating homophilic binding (Hansen and Walmod, 2013; Woo et al., 2013). In *Drosophila*, Bdl is exclusively expressed in wrapping glia and is required for mediating axon-glia recognition at the third-instar larval stage (Cameron et al., 2016). Whereas at later stages, Bdl is expressed in R-cell axons, and negative regulation of Bdl by another Ig transmembrane protein Turtle (Tutl) is required for the tiling of R7 axonal terminals (Cameron et al., 2013). The role of Bdl in R-cell axons, however, remains unknown.

Our present study shows that loss of *bdl* disrupted axonal transport of SV components in R8 axons, and caused the accumulation of the AZ protein Bruchpilot (Brp) in R8 soma. In contrast, axonal transport of the mitochondria remained normal in *bdl* mutants. Cell-type-specific knockdown and transgene rescue support that Bdl is required both pre- and postsynaptically. Bdl interacts genetically with the Unc-104/Imac/KIF1A motor, and removing Bdl significantly decreased the levels of Imac in R8 axonal terminals. To our knowledge, our study shows for the first time that a trans-synaptic cell adhesion molecule plays a specific role in regulating axonal transport of presynaptic components, and presents an excellent starting point for dissecting the

signalling events that link synaptogenic adhesion and axonal transport of SV components for presynaptic assembly and function.

2.3 Materials and Methods

2.3.1 Genetics

imac^{170}, *FRT42D* flies were provided by T. Schwarz. *UAS-imac-RFP* flies were provided by F. Yu and T. Schwarz. *Rh5/6-GAL; UAS-nSyb-GFP* was provided by C. Lee. *Rh6-lexA::*p65 was provided by T. Suzuki. *ey-FLP*; *GMR-myr-mRFP*, *FRT40A/Cyo* (BDSC#7122), *Rh3-GAL4* (BDSC#7457), *Rh4-GAL4* (BDSC#8689 and #8690), *UAS-mito-GFP* (BDSC#8443), *UAS-imac.GFP* (BDSC#6926), *UAS-αTub84B-GFP* (BDSC#7373), *Rh5-brp.mCherry,Rh6-brp.mCherry* (BDSC#57322), *lexAop-nSyb-spGFP1-10* (BDSC#64315) and *UAS-Syt-GFP* (BDSC#8443) flies were obtained for the Bloomington *Drosophila* Stock Center (BDSC). The *UAS-bdl-RNAi* line (VDRC#4806) was obtained from the Vienna *Drosophila* Resource Center (VDRC). For eye-specific mosaic analysis of Bdl in axonal transport of SV components, genetic crosses were performed to generate flies with the genotype *ey*$^{3.5}$*-FLP; bdl*^{EX2}*, FRT40A/ GAL80, FRT40A; Rh5/Rh6-GAL4, UAS-nSyb-GFP*/+. To selectively remove *bdl* in R7 and R1/R6 axons, genetic crosses were performed to generate flies with the genotype *GMR-FLP*; *GMR-myr-mRFP*, *FRT40A*/*bdl*^{EX2}, *FRT40A; Rh5/Rh6-GAL4, UAS-nSyb-GFP*/+. To examine the effects of removing *bdl* on SV localization in R7 axons, genetic crosses were performed to generate flies with the genotype *bdl*^{EX2}*/ bdl*^{EX2}*; Rh3/Rh4-GAL4, UAS-nSyb-GFP*/+. For rescue experiments, genetic crosses were performed to generate flies with the genotype *bdl*^{EX2}*/ bdl*^{EX2}*; Rh5/Rh6-GAL4, UAS-nSyb-GFP*/*GMR-bdl*, or *bdl*^{EX2}*/ bdl*^{EX2}*; Rh5/Rh6-GAL4, UAS-nSyb-GFP*/*HS-bdl*. For detecting endogenous Brp-mCherry puncta in R8 axons, genetic crosses were performed to generate flies with the genotypes *bdl*^{EX2}*/bdl*^{EX2}*; Rh5-brp.mCherry, Rh6-brp.mCherry* /+. For examining SV localization in R8 axons in which *bdl* was knocked down in postsynaptic targets of R8, genetic crosses were performed to generate flies with the genotype *ort*$^{C1-3}$*-GAL4; lexAop-nSybspGFP1-*

10/Rh6-lexA::p65; UAS-bdl-RNAi/+. For overexpressing *imac* in R8 axons in *bdl* mutants, genetic crosses were performed to generate flies with the genotype *bdl*^{EX2}*/ bdl*^{EX2}*; Rh5/Rh6-GAL4, UAS-nSyb-GFP*/*UAS-imac-RFP*. Previous studies show that the *UAS-imac-RFP* transgene rescued the *imac* mutant phenotype (Pack-Chung et al., 2007; Zong et al., 2018).

2.3.2 Histology

Adult heads were dissected and fixed for 3 hours on ice in 3.2% paraformaldehyde (PFA) in phosphate buffer (PB) (pH 7.2). Cryostat sections of adult and pupal heads were cut on a Leica CM3050 S or Leica CM1950 microtome at a thickness of 10 μm and collected on Superfrost® Plus slides (Fisher Scientific). Prior to the addition of primary antibodies, sections were blocked with 10% normal goat serum in PB with 0.5% Triton X-100 (PBT). Sections were then incubated with primary antibodies overnight at 4°C. After washed 3x with PBT, sections were incubated with secondary antibodies for 45 minutes. After washed 3x with PBT, 80 μL of anti-fade gold was added to each slide, which was then covered with a glass coverslip and sealed with nail polish.

Antibodies were used at following dilutions: MAb24B10 (1:100; Developmental Studies Hybridoma Bank or DSHB), rabbit polyclonal anti-GFP (1:1000; Molecular Probes), rabbit polyclonal anti-Bdl (1:1000), chicken polyclonal anti-GFP for detecting spGFP1-10 (1:1000; Abcam), and chicken polyclonal anti-GFP (1:1000; Molecular Probes). Secondary antibodies: anti-mouse alexafluor647, anti-chicken alexafluor488, anti-rabbit alexafluor488, and (Molecular Probes) were used at 1:750 dilution. Epifluorescent images were analyzed by confocal microscopy (Olympus fluoview FV1000 LSM).

2.3.3 Quantification of relative fluorescence intensity

The Olympus Fluoview or ImageJ software was used to measure fluorescent intensities in the proximal portion of R8 axons in the lamina and the distal portion of R8 axons in the medulla. Relative intensity of SV components in each region was calculated by normalizing the intensity of nSyb-GFP staining to that of MAb24B10 staining within the same region. Similarly, relative intensity of Imac.GFP in R8 axonal terminals was quantified by normalizing the intensity of Imac.GFP staining to that of MAb24B10 staining within the same region.

2.3.4 Molecular Biology

For rescue experiments, the full-length *bdl* coding sequence was amplified by polymerase chain reaction (PCR) using the GH11322 EST clone as the template. 5' primer CAATCGCGGCCGCATGCCAGCGAAACGCA and 3' primer AGATCTGAGCAATCCTCAGGTGGAC were used. The resulting PCR products were subcloned into EcoRI and BglII sites of pGMR and pCaspeR-hs vectors. DNA constructs were verified by sequencing and used for generating transgenic lines.

2.3.5 Quantification of Brp-GFP puncta in R8 soma

Confocal microscopy was used to acquire 1.0 μm stacks of the samples. Brp-mCherry puncta were quantified using the FIJI ImageJ software. Particle Analyzer Tool was used to determine the size of puncta in the proximal region of R8 soma.

2.3.6 Phototactic T-Maze behavioural assay

The behavioural assay was modified from that described previously (Yamaguchi et al., 2010). Flies were reared with 12 hour light/dark cycles at constant humidity and temperature. Flies

at the age of 7-10 days after eclosion were used in the experiments. For each genotype, about 5-10 trials were performed, and ~50 flies were tested in each trial. Flies were transported to behaviour room at least 24 hours before each experiment, and thus were able to habituate to the new environment.

Two light sources were used, including UltraFire WF-501B 375NM UV Ultra Violet LED Flashlight and Ultrafire WF-501B CREE XR-E G2 150lm Green LED Flashlight. "UV vs. Green" choices were used to determine light preference. For each trial, flies were introduced into the T-Maze apparatus and allowed to habituate for 60 seconds. The lights were then turned on, and flies were introduced to the choice point for 20 seconds. Flies moved into either the Green or UV zone, or did not move out of the choice point (neutral). Flies were then anesthetized with CO_2 and counted. Light preference index (PI) was quantified as: $\left(\left(\frac{\text{number of flies in blue or green zone}-\text{Number of flies in UV zone}}{\text{number of flies in blue or green zone}+\text{Number of flies in UV zone}}\right)\times\left(1-\frac{\text{number of flies in neutral zone}}{\text{number of total flies}}\right)\right)$.

Since fly behaviours are sensitive to variations in experimental conditions, this may cause behavioural variations even within the control groups from one experiment to another experiment. To minimize the effects of variations in experimental conditions in each experiment, control and experimental flies for behavioural comparison were generated and collected at the same time period, and phototactic assays were performed on the same day.

2.3.7 Statistical Analysis

For experiments involving the comparison of two groups, statistical analysis was performed using two-tailed t-tests. For experiments involving the comparison of more than two groups, statistical analysis was performed using one-way ANOVA followed by post hoc Tukey's test. The difference is considered as significant when a p-value is <0.05.

2.4 Results

2.4.1 Loss of *bdl* disrupted axonal transport of SV components in R8 axons

In our previous study, we show that Bdl is expressed in both R7 and R8 axons, and is also present in the optic lobe (Cameron et al., 2013). However, R-cell axon guidance and layer-specific target selection remained normal in *bdl* null mutants (Cameron et al., 2013). To test if Bdl plays a role in the regulation of R-cell presynaptic assembly and function, we used an SV-specific marker neuronal synaptobrevin-GFP (nSyb-GFP) (Estes et al., 2000), to examine R7 and R8 presynaptic development. R8 photoreceptors express rhodopsin (Rh) Rh5 or Rh6, and show preference for blue and green light (Vasiliauskas et al., 2011). Whereas R7 photoreceptors express Rh3 or Rh4, and show preference for light in the UV spectrum (Vasiliauskas et al., 2011). R7 and R8 axons from a single ommatidia project through the lamina into the deeper medulla. R8 axons form synapses specifically within M1-M3 sub-layers of the medulla. R7 axons defasiculate from R8 axons at M3 and project deeper in the medulla, where they establish synapses in the M4-M6 sub-layers.

SV components in R7 and R8 axons were labelled by expression of nSyb-GFP under control of R7-specific drivers *Rh3-GAL4* and *Rh4-GAL4* (i.e. *Rh3/Rh4-GAL4*) and R8-specific drivers *Rh5-GAL4* and *Rh6-GAL4* (i.e. *Rh5/Rh6-GAL4*) (Fig.1), respectively. In wild type, SV components in both R7 and R8 axons were predominantly targeted to the presynaptic terminals within the medulla (Fig. 2.1A, 2.1B, 2.1G). Surprisingly, we found that many SV components were mislocalized to the proximal portion of R8 axons within the lamina in *bdl* mutants (Fig. 2.1C, 2.1D, 2.1E, 2.1F, 2.1I). In contrast, the localization of SV components remained normal in R7 axons in *bdl* mutants (Fig. 2.1H, 2.1J).

To further confirm the SV phenotype in R8 axons, we used a different SV marker synaptotagmin-GFP (Syt-GFP) (Zhang et al., 2002), to examine the targeting of SV components.

Consistently, we found that many Syt-GFP-positive vesicles were abnormally localized to the proximal portion of R8 axons within the lamina in *bdl* mutants (Fig. 2.1M, 2.1N, 2.1P).

2.4.2 *bdl* is required cell-autonomously in R8 axons for the targeting of SV components

Above phenotypes in *bdl* mutants may reflect a cell-autonomous role for Bdl in R8 axons, or a non-cell-autonomous role in its postsynaptic targets. To distinguish between these possibilities, we performed genetic mosaic analysis. Homozygous *bdl* mutant R-cell clones were generated in the eye by performing eye-specific mitotic recombination. We found that specific removal of *bdl* in R-cell axons, but not in the optic lobe, caused an SV mistargeting phenotype identical to that in *bdl* mutants (Fig. 2.2A, 2.2B), indicating that *bdl* is required in R-cell axons for axonal transport of SV components.

Since eye-specific mitotic recombination removed *bdl* in both R7 and R8 axons that associate with each other closely within the medulla, it remained possible that the SV phenotype in R8 axons was caused by loss of *bdl* in R7 axons. To address this possibility, mitotic recombination under control of the *GMR-FLP* was used to remove *bdl* in R7 but not in R8 axons. We found that the localization of SV components remained normal in wild-type R8 axons when *bdl* was removed in R7 axons within the same column (Fig. 2.2C, 2.2D). This result argues against a non-cell-autonomous role for Bdl in R7 axons in regulating SV targeting in R8 axons within the same column.

To further confirm that Bdl plays a cell-autonomous role in R8 axons, we performed R8-specific knockdown experiments. A *UAS-bdl*-RNAi transgene that has been shown previously to knock down *bdl* effectively (Cameron et al., 2016), was expressed specifically in R8 axons under control of the R8-specific driver *Rh5/Rh6-GAL4*. A similar SV phenotype was observed when *bdl* was specifically knocked down in R8 axons (Fig. 2.2G, 2.2H).

In summary, the above results from genetic mosaic analysis and R8-specific knockdown experiments suggest strongly that Bdl plays a cell-autonomous role in R8 axons for axonal transport of SV components.

2.4.3 *bdl* is required both pre- and postsynaptically

The above results support a necessary role for Bdl in R8 axons. To determine if the expression of Bdl in R8 axons is sufficient, we performed transgene rescue experiments. A transgene in which the complete *bdl* cDNA is located downstream of the eye-specific promoter *GMR* was introduced into *bdl* null mutants. However, we found that the SV phenotype in *bdl* mutants could not be rescued by restoring *bdl* expression in R-cell axons (Fig. 2.3A, 2.3B, 2.3E). This result raises the possibility that Bdl is required in both R8 axons and their targets in the medulla.

To test this, we examined the effects of restoring *bdl* in both R-cell axons and the optic lobe on the SV phenotype by introducing a *bdl* transgene containing the *bdl* coding sequence downstream of a heat-inducible promoter into *bdl* mutants. Interestingly, we found that expression of *bdl* in both R-cell axons and the target region completely rescued the SV phenotype in *bdl* mutants (Fig. 2.3C, 2.3D, 2.3E).

Taken together, our results suggest that Bdl is required both pre- and postsynaptically for axonal transport of SV components.

2.4.4 Loss of *bdl* caused the accumulation of the AZ protein Brp in the proximal region of R8 soma

In addition to axonal transport of SV components, presynaptic assembly and function also requires the recruitment of AZ components and mitochondria. To test if Bdl also plays a role in

axonal transport of AZ components, we examined the potential effects of *bdl* mutations on the targeting of the AZ protein Bruchpilot (Brp). Brp is a homologous to human AZ protein ELKS/CAST, and is essential for the establishment and maintenance of active zones for synapse formation and function in *Drosophila* (Wagh et al., 2006).

The distribution of Brp in R8 was visualized using the R8-specific AZ marker *Rh5/Rh6-Brp-mCherry*, which labels AZs in R8 axonal terminals and PTVs that transport AZ components in R8 (Ting et al., 2014). In wild type (Fig. 2.4A and 2.4B), Brp-mCherry punta were predominantly localized to R8 axonal terminals in the medulla region, where R8 axons form synaptic connections with their target neurons. Interestingly, we found that in all *bdl* homozygous mutants examined (n=10) (Fig. 2.4C, 2.4D, 2.4E), abnormal large Brp-mCherry particles were accumulated at the proximal region of R8 soma in the retina, which is close to the axonal initial segment. This phenotype was never observed in wild-type animals (n=6) (Compare Fig. 2.4B to 2.4D). This result suggests that Bdl may also be required for the transport of Brp from R8 soma into the axon.

2.4.5 Loss of *bdl* did not affect axonal transport of mitochondria

We then examined if loss of *bdl* affects axonal transport of mitochondria. The distribution of mitochondria in R8 axons was visualized using the mitochondria marker *UAS-Mito-GFP* under control of the R8-specific driver *Rh5/Rh6-GAL4*. However, no obvious difference in the localization of mitochondria in R8 axons between wild-type and *bdl* mutants was observed (Compare Fig. 2.4H and 2.4I to 2.4F and 2.4G).

2.4.6 Loss of *bdl* disrupted R8-dependent phototaxis response

We then performed differential phototaxis experiments to examine if loss of *bdl* affects R8 function. Among photoreceptors, R7 expresses *Rh3/Rh4* and is UV-sensitive. About 70% of R8 (i.e. R8y) express *Rh6* and are green-sensitive, while ~30% of R8 (i.e. R8p) express *Rh5* and are blue-sensitive. Previous studies show that manipulating the functions of R7 or R8 could switch fly light preference (Yamaguchi et al., 2010).

A T-maze apparatus was used to examine the ability of flies to distinguish lights at different wavelength similarly as described previously (Yamaguchi et al., 2010). Flies were given "UV vs. green" choice to test their light preference. When given "UV vs. green" choice, wild-type flies did not show a significant difference in their preference for different lights (Fig. 2.5A). However, we found that in the absence of *bdl*, flies largely ignored the green light source, and were predominantly attracted towards the UV light source (Fig. 2.5A).

We then performed cell-type-specific knockdown experiments to determine if Bdl is required cell-autonomously for R8 function. *bdl* was knocked down by expressing a *UAS-bdl-RNAi* transgene under control of pan-neuronal driver *C155-GAL4* (Fig. 2.5B), eye-specific driver $ey^{3.5}$*-GAL4* (Fig. 5C), or green-sensitive-R8-specific driver *Rh6-GAL4* (Fig. 2.5D). Compared to control flies carrying *GAL4* driver or *UAS-bdl-RNAi* only, flies carrying both *GAL4* driver and *UAS-bdl-RNAi* showed a significant decrease in the preference for the green light source (Fig. 2.5B-5D).

Taken together, the above results support an essential and cell-autonomous role for Bdl in the control of R8 function.

2.4.7 Knocking down *bdl* in postsynaptic target neurons in the optic lobe caused the mis-localization of SVs in R8 axons

The results from transgene rescue (Fig. 2.3) raise the interesting possibility that Bdl is required in both R8 and its postsynaptic target neuron for the transport of SV components in R8 axons. To further address this, we examined if reducing Bdl in postsynaptic target neurons in the optic lobe affects the localization of SV components in R8 axons.

To knock down *bdl* in postsynaptic targets of R8, *ort*$^{C1\text{-}3}$*-GAL4* (Gao et al., 2008) was used to drive the expression of *UAS-bdl-RNAi*. The *lexA/lexAop* system was used to label SV components in *bdl* knockdown flies; the SV marker *lexAop-nSyb-spGFP1-10* (Macpherson et al., 2015), was expressed under control of the green-sensitive-R8-specific driver *Rh6-lexA::p65* (Berger-Müller et al., 2013). We found that knocking down *bdl* in postsynaptic targets of R8 caused a similar SV mislocalization phenotype in all individuals examined (100%, n=4 animals) (Fig. 2.6C and 2.6D).

2.4.8 Knocking down *bdl* in postsynaptic target neurons in the optic lobe disrupted R8-dependent phototaxis response.

We then examined if knocking down *bdl* in postsynaptic target neurons affects R8-dependent phototaxis response. *bdl* was knocked down in postsynaptic targets of R8 by expressing *UAS-bdl-RNAi* under control of the *ort*$^{C1\text{-}3}$*-GAL4* driver. Flies were then given "UV vs. green" choice to examine their light preference. Compared to control flies carrying *ort*$^{C1\text{-}3}$*-GAL4* or *UAS-bdl-RNAi* only, *bdl* knockdown flies showed a significant decrease in the preference for the green light source (Fig. 6E).

2.4.9 *bdl* interacted genetically with *imac*

To further understand the action of Bdl in regulating axonal transport of SV components, we examined the potential effects of *bdl* mutations on the organization of microtubules in R8 axons. Microtubules were labelled with the marker *UAS-GFP-Tub84B* under control of the R8-specific driver *Rh6-GAL4*. Similarly as described previously (Sugie et al., 2015), we quantified the percentage of organized microtubule threads in each R8 axonal terminal. However, no obvious defect was observed (data not shown).

Previous studies show that the fly Imac motor protein and its orthologs Unc-104 in *C. elegans* and KIF1A in mammals play an essential role in regulating axonal transport of SV components (Hall and Hedgecock, 1991; Otsuka et al., 1991; Okada et al., 1995; Zhao et al., 2001; Pack-Chung et al., 2007; Barkus et al., 2008; Niwa et al., 2008). Consistently with previous reports (Pack-Chung et al., 2007), we showed that the removal of Imac in R-cell axons severely disrupted axonal transport of SV components, as the majority of SV components were localized abnormally in R8 cell bodies in the retina when *imac* was removed in R-cells by eye-specific mitotic recombination (Fig. 2.7C, 2.7D, 2.7E).

To test the potential genetic interaction between *bdl* and *imac*, we performed epistasis analysis. Most *bdl*/+ heterozygotes (~93%, n=15) (Fig. 2.7F and 2.7I) and *imac*/+ heterozygotes (~87%, n=16) (Fig. 7G and 7J) displayed normal SV localization pattern in R8 axons. Interestingly, when flies were transheterozygous for *bdl* and *imac* (i.e. *bdl*/*imac*), most individuals showed a *bdl*-like SV mis-localization phenotype (~80%, n=15) (Fig. 2.7H and 2.7K). This synergistic phenotype suggests that Bdl may regulate axonal transport of SV components by modulating Imac.

2.4.10 The levels of the Imac motor were significantly reduced in R8 presynaptic terminals

To further understand the action of Bdl in the regulation of Imac, we examined if reducing *bdl* affects the levels and distribution of Imac. The distribution of Imac in R8 axons was visualized with the Imac.GFP marker, which has been shown previously to recapitulate the localization of endogenous Imac (Barkus et al., 2008). *Rh6-GAL4* was used to drive the expression of *UAS-imac.GFP* in green-sensitive R8 axons of y-type ommatidia (Tahayato et al., 2003). In wild type, ~80% R8 axons were stained with imac.GFP (Fig. 2.8A-2.8C, 2.8G), consistent with that *Rh6* is only expressed in green-sensitive R8y photoreceptor cells (Salcedo et al., 1999; Yamaguchi et al., 2010). We then performed cell-type-specific knockdown to reduce the level of Bdl in R8 axons. Interestingly, we found that compared to that of control flies carrying *Rh6-GAL4* and *UAS-imac.GFP* (Fig. 2.8A-2.8C) or control flies carrying *Rh6-GAL4*, *UAS-imac.GFP* and *UAS-CD2.HRP* (Fig. 2.8G), *bdl* knockdown in flies carrying *Rh6-GAL4, UAS-imac.GFP* and *UAS-bdl-RNAi* significantly decreased the percentage of R8 axons in which Imac.GFP was localized to R8 terminals (Fig. 2.8D-2.8G). We also quantified relative levels of Imac.GFP in R8 axonal terminals. When *bdl* was knocked down, the levels of Imac.GFP staining in Imac.GFP-positive R8 presynaptic terminals were also significantly reduced (Fig. 2.8D-2.8F, 2.8H).

2.5 Discussion

Our present study identifies for the first time a cell adhesion molecule that plays a novel and specific role in promoting axonal transport of SV components for presynaptic assembly and function. Loss of *bdl* selectively disrupted axonal transport of SV components in R8 axons, and also caused the accumulation of the AZ protein Brp in the proximal region of R8 soma. In contrast, *bdl* mutations did not affect axonal transport of mitochondria. Genetic mosaic analysis, transgene rescue and cell-type-specific knockdown indicate that Bdl is required both pre- and postsynaptically. Removing *bdl* also disrupted R8-dependent phototaxis response, consistent with a role for Bdl in the control of R8 function. We also show that *bdl* interacted genetically with *imac*, and *bdl* knockdown significantly decreased the levels of the Imac motor in R8 axonal terminals. Our results support a model in which Bdl-Bdl homophilic binding mediates specific interactions at axo-dendritic contact sites in promoting the activity and/or localization of Imac, and thus facilities axonal transport of presynaptic components in R8 axons (Fig. 2.8I).

Unlike several other well-characterized cell adhesion molecules that control the development and function of the fly visual system (e.g. (Clandinin et al., 2001; Lee et al., 2001, Lee et al., 2003; Shinza-Kameda et al., 2006)), Bdl is neither required for R-cell axon guidance nor layer-specific R-cell axonal target selection (Fig. 2.1) (Cameron et al., 2013). In *bdl* null mutants, both R7 and R8 axons projected through the lamina into their correct target layers in the medulla, where R7 and R8 axonal terminals are organized in regularly spaced columns (Cameron et al., 2013). By comparison, loss of either *N-cadherin* or *Lar* causes R7 axons to project aberrantly into the R8 target layer (Clandinin et al., 2001; Lee et al., 2001), while mutations in the gene *capricious* encoding for an R8-specific cell adhesion molecule causes R8 targeting errors (Shinza-Kameda et al., 2006). Those studies indicate that Bdl is not involved in mediating the initial

formation and/or maintenance of the contact between R8 axons and their targets in the medulla. Instead, Bdl may mediate specific interactions at axo-dendrite contact sites in the medulla, which is required for axonal transport of SV components in R8 axons.

How does Bdl function? In our previous studies (Cameron et al., 2013; Chen et al., 2017), we show that Bdl is capable of mediating both homophilic and heterophilic binding. Bdl on R8 axonal terminal may bind to Bdl on the target in a homophilic manner, thus mediates the interactions at axo-dendritic contact sites. Alternatively, an unknown cell-surface receptor on the target may bind to Bdl on the R8 presynaptic terminal in promoting axonal transport of SV components in R8 axons. Based on the results from transgene rescue and cell-type-specific knockdown experiments, we favour the first model in which Bdl mediates specific interactions at axo-dendritic contact sites via a homophilic binding mechanism (Fig. 2.8I).

That Bdl interacts genetically with Imac, together with that the levels of the Imac motor was significantly reduced in R8 presynaptic terminals, suggest strongly that Bdl functions directly or indirectly in regulating Imac. Bdl may regulate the function of Imac in several ways. First, Bdl may promote axonal localization of Imac. Unc-104/Imac/ KIF1A-family motor proteins exist in axons as either inactive state due to autoinhibition, or active state upon cargo binding (Hammond et al., 2009; Huo et al., 2012; Yue et al., 2013; Niwa et al., 2016). While inactive KIF1A motors can diffuse on microtubules in the absence of cargo, active KIF1A motors undergo ATP-dependent processive motility in the presence of cargo (Hammond et al., 2009). Thus, the Bdl-dependent pathway may promote diffusion of inactive Imac on microtubules along R8 axons, which makes the motors available locally to respond to activating signals for delivering SV components to the presynaptic terminal (Fig. 2.8I). And second, the Bdl-dependent pathway may not only promote axonal localization of Imac, but also stimulate its activity. Consistent with this possibility, we

found that overexpression of Imac in R8 axons was not sufficient for rescuing the SV phenotype in *bdl* mutants (data not shown). A number of studies show that motor proteins can be activated by relieving the autoinhibition with cargo binding and phosphorylation (Espeut et al., 2008; Hammond et al., 2009; Niwa et al., 2016). Similarly, we speculate that Bdl may activate downstream signalling events, which may unlock the autoinhibition of Imac and thus promote the delivery of SV components to presynaptic terminals (Fig. 2.8I).

Our results also suggest a role for Bdl in regulating axonal transport of the AZ protein Brp. AZ components are transported in PTVs, which like SVPs, also rely on the kinesin-3 family motor Unc-104/Imac/KIF1A for axonal transport (Hall and Hedgecock, 1991; Otsuka et al., 1991; Okada et al., 1995; Zhao et al., 2001; Pack-Chung et al., 2007; Barkus et al., 2008; Niwa et al., 2008). Consistently, we show that loss of *bdl* also affected the trafficking of Brp in R8 axons. In *bdl* mutants, while many SV components were mis-localized to the proximal regions of R8 axons (Fig. 1), large Brp-positive aggregates accumulated abnormally in R8 soma close to the axonal initial segment (Fig. 4). That loss of *bdl* affected the trafficking of SVs and Brp differently may be due to cargo difference. PTVs carrying AZ components have cargo size at ~80 nm in diameter (Zhai et al., 2001; Tao-Cheng, 2007), while STVs are heterogeneous in size (Kraszewski et al., 1995; Ahmari et al., 2000). The difference in cargo size and/or surface properties of cargo may lead to different responses to altered motor function in *bdl* mutants.

While loss of *bdl* affected the trafficking of SV and AZ components, axonal transport of mitochondria remained normal in *bdl* mutants (Fig. 2.4). One likely explanation is that the transport of mitochondria in R8 axons utilizes a different motor system. It is reported that removal of the adapter protein Milton disrupts the transport of mitochondria, but not SVs, in *Drosophila* photoreceptor axons (Stowers et al., 2002). Milton directly interacts with the mitochondrial Rho-

like GTPase Miro to recruit mitochondria to the kinesin-1 motor protein (Glater et al., 2006). Thus, it appears highly possible that unlike Imac-mediated transport of SVs, kinesin-1-mediated transport of mitochondria is regulated by a Bdl-independent signalling pathway.

Bdl is highly homologous to IgSF9a and IgSF9b in mammals (Hansen and Walmod, 2013). Interestingly, a recent *in vitro* study shows that IgSF9b forms a *cis*-complex with Neuroligin-2 (Nlg-2) on the postsynaptic membrane, and facilitates the trans-synaptic interactions between Nlg-2 and Neurexin in mediating inhibitory synaptogenesis (Woo et al., 2013). IgSF9a knockout study shows that loss of IgSF9a causes a reduction in the number of inhibitory synapses in the hippocampus (Mishra et al., 2014). In the future, it would be of interest to determine if mammalian IgSF9 family proteins are also required for promoting axonal transport of SV components. Further molecular and genetic dissection of the Bdl-dependent pathway will provide novel and important insights into the general mechanisms underlying axonal transport of SV components for presynaptic assembly and function.

Figure 2.1

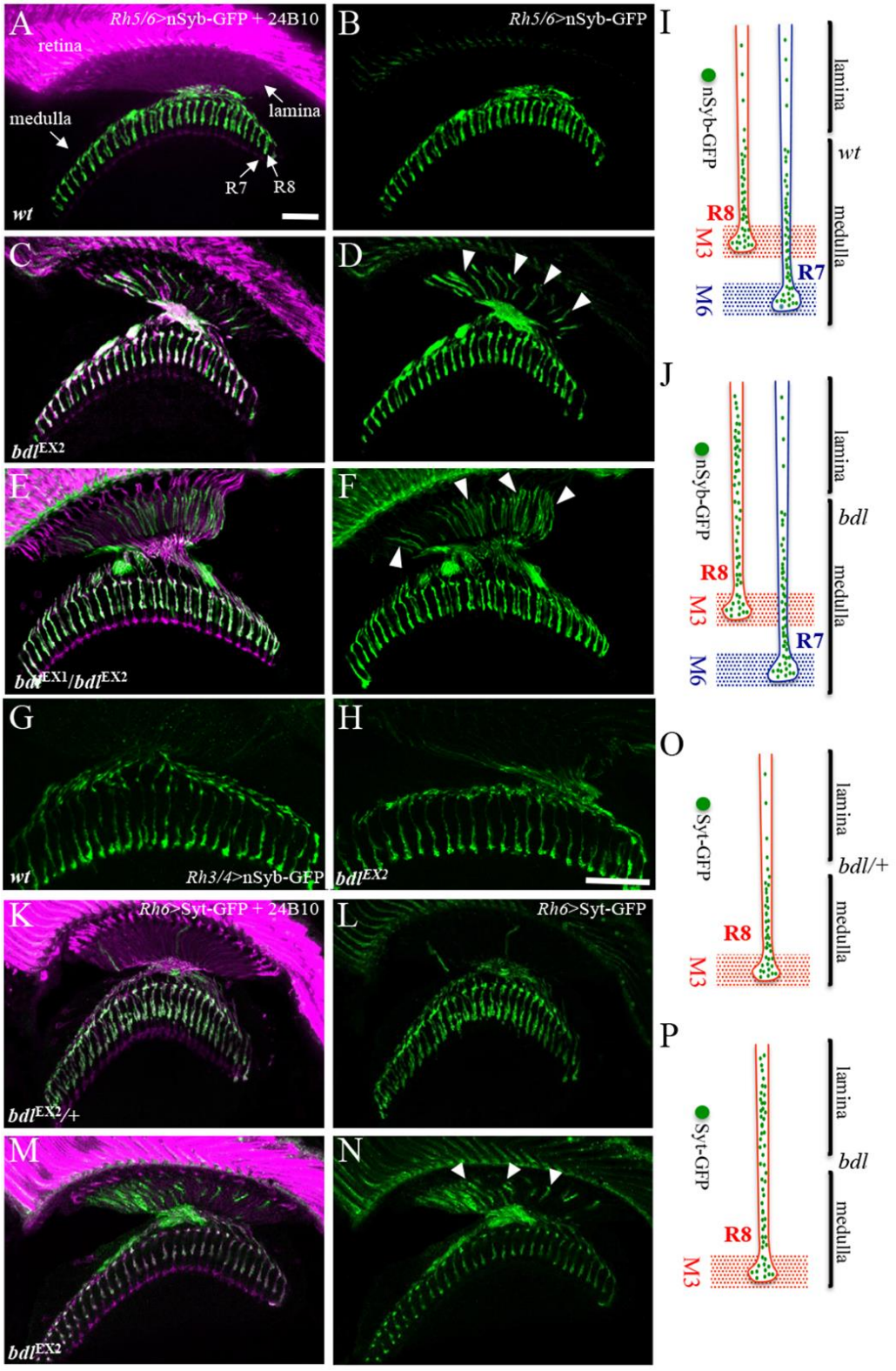
A
Rh5/6>nSyb-GFP + 24B10
retina
lamina
medulla
R7
R8
wt
B
Rh5/6>nSyb-GFP
I
nSyb-GFP
lamina
wt
medulla
R8
M3
R7
M6
C
bdlEX2
D
J
nSyb-GFP
lamina
bdl
medulla
R8
M3
R7
M6
E
bdlEX1/bdlEX2
F
G
wt
Rh3/4>nSyb-GFP
H
bdlEX2
O
Syt-GFP
lamina
bdl/+
medulla
R8
M3
K
Rho>Syt-GFP + 24B10
bdlEX2/+
L
Rh6>Syt-GFP
P
Syt-GFP
lamina
bdl
medulla
R8
M3
M
bdlEX2
N

Figure 2.1. Many SV components were mis-localized to the proximal portion of R8 axon in *bdl* mutants. (A-D) Frozen sections of adult heads expressing the SV marker *UAS-n-Synaptobrevin-GFP* (nSyb-GFP) under control of the R8-specific driver *Rh5/6-GAL4* (i.e. *Rh5/6>nSyb-GFP*), were stained with anti-GFP (green) and MAb24B10 (magenta). MAb24B10 recognizes the cell adhesion molecule Chaoptin expressed in all R-cell axons (Van Vactor et al., 1988). (A) In wild-type animals (100%, n=7), nSyb-GFP staining was predominantly localized to R8 axonal terminals in the medulla region. (B) The section in A was visualized with nSyb-GFP staining only. (C) In the majority of bdl^{EX2} homozygous mutant flies examined (6 out of 7 animals), strong n-Syb staining was also observed in the proximal portion of R8 axons in the lamina. (D) The section in C was visualized with nSyb-GFP staining only. Arrowheads indicate proximal portions of R8 axons with mis-localized nSyb-GFP. (E) In all $bdl^{EX1}bdl^{EX2}$ transheterozygotes examined (n= 6 animals), strong n-Syb staining was observed in the proximal portion of R8 axons in the lamina. (F) The section in E was visualized with nSyb-GFP staining only. (G and H) Frozen sections of adult heads expressing nSyb-GFP under control of the R7-specific driver *Rh3/4-GAL4* (i.e. *Rh3/4>nSyb-GFP*), were stained with anti-GFP. (G) In wild type (100%, n=5 animals), n-Syb staining was predominantly localized to R7 axonal terminals in the medulla region. (H) In all bdl^{EX2} homozygous flies examined (100%, n=5), n-Syb staining was still predominantly localized to R7 axonal terminals in the medulla region. (I and J) Schematic illustrations showing the distribution of SV components in R7 and R8 axons in wild-type (I) and *bdl* mutants (J). (K-N) Frozen sections of adult heads expressing another SV marker Synaptotagmin-GFP (Syt-GFP) under control of the R8-specific driver *Rh5/6-GAL4* (i.e. *Rh5/6>Syt-GFP*), were stained with anti-GFP (green) and MAb24B10 (magenta). (K) In bdl^{EX2}/+ heterozygotes (100%, n=5), Syt-GFP staining was predominantly localized to R8 axonal terminals in the medulla region. (L) The section

in K was visualized with Syt-GFP staining only. (M) In most *bdl*^{EX2} homozygous mutants (11 out of 13 animals), strong Syt-GFP staining was also observed in the proximal portion of R8 axons in the lamina. (N) The section in M was visualized with Syt-GFP staining only. Arrowheads indicate proximal portions of R8 axons with mis-localized Syt-GFP. (O and P) Schematic illustrations showing the distribution of SV components in R8 axons labelled with Syt-GFP in heterozygotes (O) and *bdl* homozygous mutants (P). Scale bar: 20 μm.

Figure 2.2

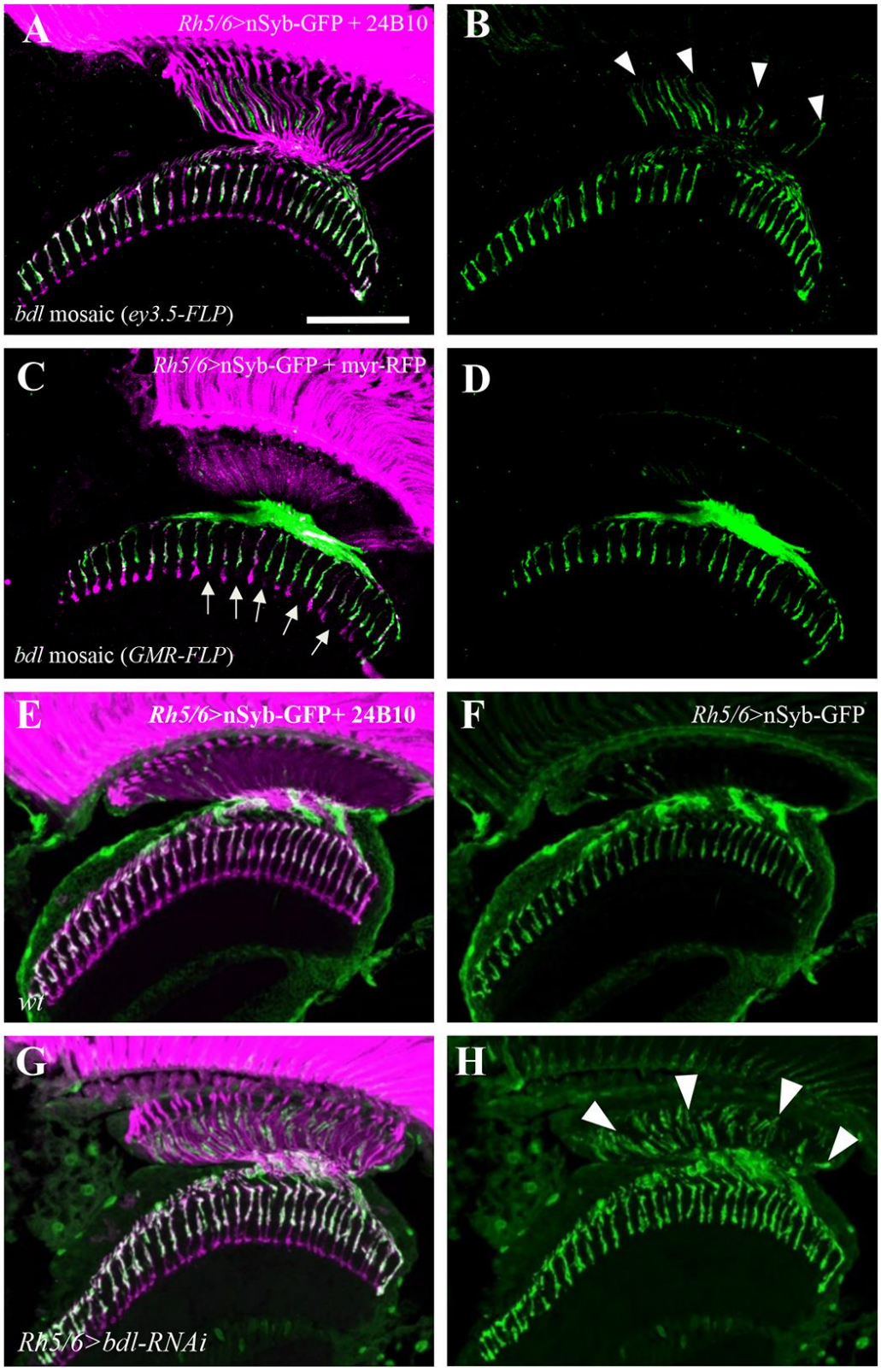
A
Rh5/6>nSyb-GFP + 24B10
bdl mosaic (ey3.5-FLP)
B
C
Rh5/6>nSyb-GFP + myr-RFP
bdl mosaic (GMR-FLP)
D
E
Rh5/6>nSyb-GFP+ 24B10
wt
F
Rh5/6>nSyb-GFP
G
Rh5/6>bdl-RNAi
H

Figure 2.2. *bdl* is required cell-autonomously in R8 axons. (A and B) Frozen sections of adult heads were stained with anti-GFP (green) and MAb24B10 (magenta). (A) In all eye-specific *bdl* mosaic animals examined (100%, n=6 animals), strong nSyb-GFP staining was observed in the proximal portion of *bdl* mutant R8 axons. (B) The section in A was visualized with nSyb-GFP staining only. Arrowheads indicate proximal portions of R8 axons with mis-localized nSyb-GFP. (C and D) Frozen sections of adult heads were stained with anti-GFP (green) and anti-RFP (magenta). Homozygous *bdl* mutant R7 axons were generated by *GMR-FLP*-induced mitotic recombination. (C) In all *GMR-FLP*-induced *bdl* mosaic animals examined (100%, n=6 animals), nSyb-GFP staining (green) was still predominantly localized to R8 axonal terminals in the medulla. Wild-type or heterozygous R-cell axons were labelled with *GMR-myr-mRFP* (magenta). Mosaic columns were identified by the absence of RFP staining in *bdl* mutant R7 axons (arrows). (D) The section in C was visualized with nSyb-GFP staining only. (E) In wild type double-stained with anti-GFP (green) and MAb24B10 (magenta), nSyb-GFP staining was predominantly localized to R8 axonal terminals in the medulla (100%, n=5 animals). (F) The section in E was visualized with nSyb-GFP staining only. (G) In flies expressing a *UAS-bdl-RNAi* transgene under control of the R8-specific driver *Rh5/6-GAL4*, strong nSyb-GFP staining was also observed in the proximal portion of R8 axons in the lamina (5 out of 6 animals). (H) The section in G was visualized with nSyb-GFP staining only. Arrowheads indicate proximal portions of R8 axons with mis-localized nSyb-GFP. Scale bar: 20 μm.

Figure 2.3

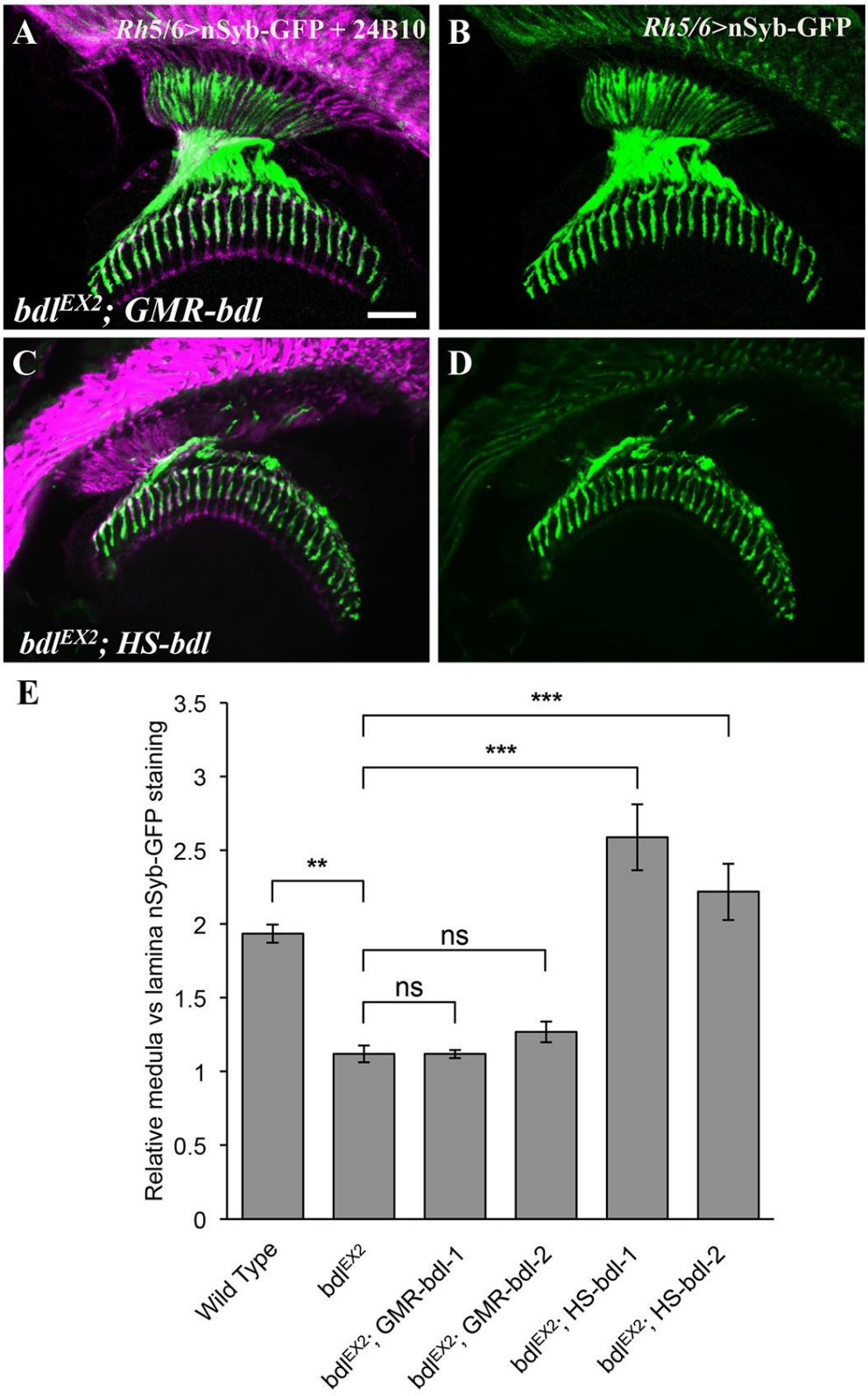
A
Rh5/6>nSyb-GFP + 24B10
bdl^EX2; GMR-bdl
B
Rh5/6>nSyb-GFP
C
bdl^EX2; HS-bdl
D
E
Relative medula vs lamina nSyb-GFP staining
3.5
3
2.5
2
1.5
1
0.5
0
***
***
**
ns
ns
Wild Type
bdl^EX2
bdl^EX2; GMR-bdl-1
bdl^EX2; GMR-bdl-2
bdl^EX2; HS-bdl-1
bdl^EX2; HS-bdl-2

Figure 2.3. Expression of *bdl* in R-cell axons was not sufficient for rescuing the SV phenotype in *bdl* mutants. (A-D) Frozen sections of adult heads expressing nSyb-GFP under control of the R8-specific driver *Rh5/6-GAL4*, were stained with anti-GFP (green) and MAb24B10 (magenta). (A) Restoring *bdl* expression in all R-cell axons under control of the eye-specific *GMR* promoter did not rescue the SV phenotype, as many SV components were still mis-localized to the proximal portion of R8 axons in the lamina. Genotype: bdl^{EX2}; *GMR-bdl/ Rh5/6-GAL4, UAS-nSyb-GFP*. Two independent *GMR-bdl* transgenic lines were used in the experiments. Eight individuals were examined in each experiment. (B) The section in A was visualized with nSyb-GFP staining only. (C) Restoring *bdl* expression in both R-cell axons and the optic lobe under control of the heat-inducible promoter completely rescued the SV phenotype. Genotype: bdl^{EX2}; *HS-bdl/ Rh5/6-GAL4, UAS-nSyb-GFP*. Two independent *HS-bdl* transgenic lines were used in the experiments. At least five individuals were examined in each experiment. (D) The section in C was visualized with nSyb-GFP staining only. (E) The ratio of medulla vs lamina relative nSyb-GFP staining intensities was quantified. One-way ANOVA followed by post hoc Tukey's test, **P<0.01; *** P<0.001; ns, P>0.05. Error Bars indicate SEM. Scale bar: 20 μm.

Figure 2.4

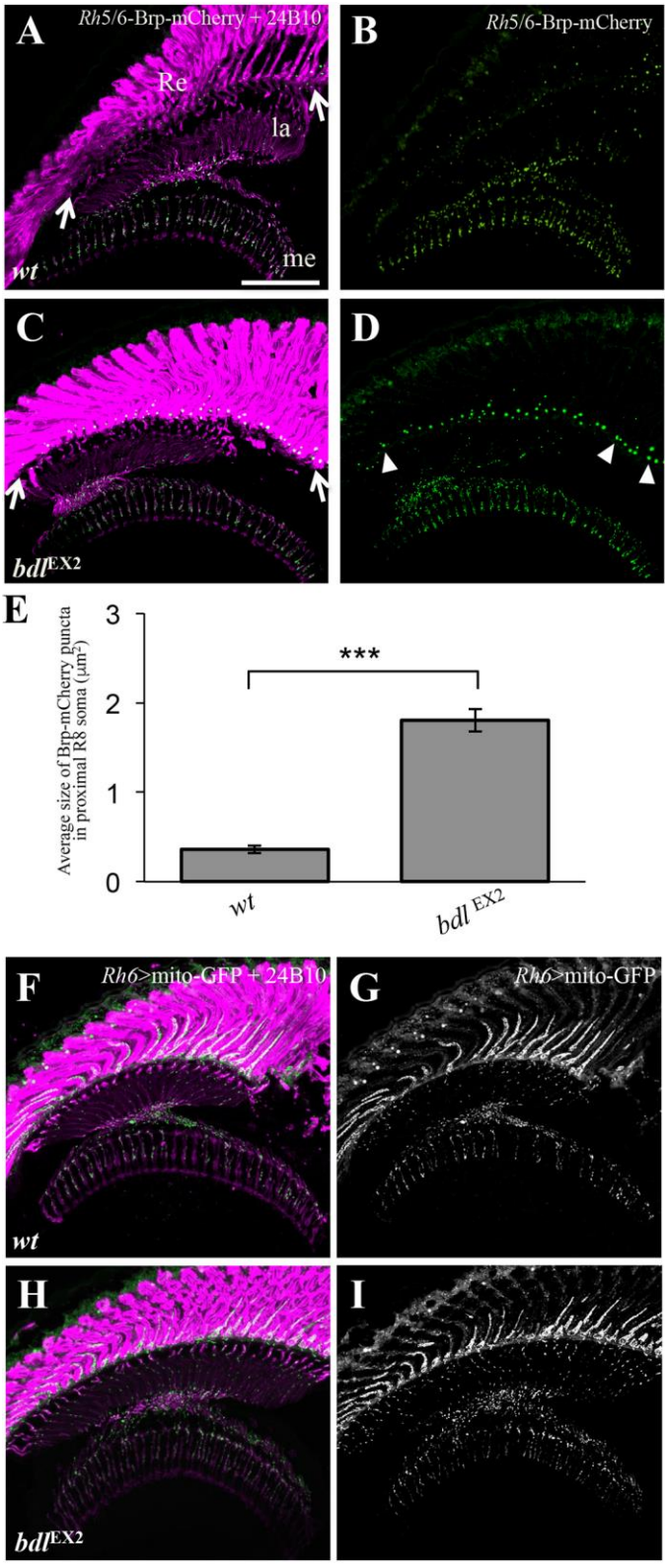
A
Rh5/6-Brp-mCherry + 24B10
Re
la
me
wt
B
Rh5/6-Brp-mCherry
C
bdlEX2
D
E
Average size of Brp-mCherry puncta in proximal R8 soma (μm²)
3
2
1
0
***
wt
bdl EX2
F
Rh6>mito-GFP + 24B10
wt
G
Rh6>mito-GFP
H
bdlEX2
I

Figure 2.4. Loss of *bdl* affected the transport of the AZ protein Brp but not the transport of mitochondria in R8 axons. (A-D) Frozen sections of adult heads carrying *Rh5/6-Brp-mCherry* were double-stained with anti-GFP (green) and MAb24B10 (magenta). (A) In wild-type animals (100%, n=6), Brp-mCherry punta was predominantly localized to R8 axonal terminals in the medulla region. (B) The section in A was visualized with Brp-mCherry staining only. (C) In bdl^{EX2} homozygous mutants (100%, n=10), abnormal large Brp-mCherry particles were accumulated at the proximal region (arrows) of R8 soma in the retina. (D) The section in C was visualized with Brp-mCherry staining only. Arrowheads indicate abnormal large Brp-mCherry particles. (E) The size of Brp-mCherry puncta in the proximal region of R8 soma was quantified. Compared to that in wild type, the size of Brp puncta in the proximal region of R8 soma in *bdl* mutants showed a significant increase. Student's t-test, ***p=4.5E-07. Error Bars indicate SEM. (F-I) Frozen sections of adult heads expressing *UAS-mito-GFP* under control of the R8-specific driver *Rh6-GAL4*, were stained with anti-GFP (green) and MAb24B10 (magenta). (F) In wild type (100%, n=7 animals), mitochondria were detected in both proximal portions of R8 axons in the lamina and R8 axonal terminals in the medulla. (G) The section in F was visualized with mito-GFP *staining only*. (H) In bdl^{EX2} mutants (100%, n=6 animals), the pattern of mitochondria distribution was similar to that in wild type. (I) The section in H was visualized with mito-GFP staining only. Scale bars: 20 μm.

Figure 2.5

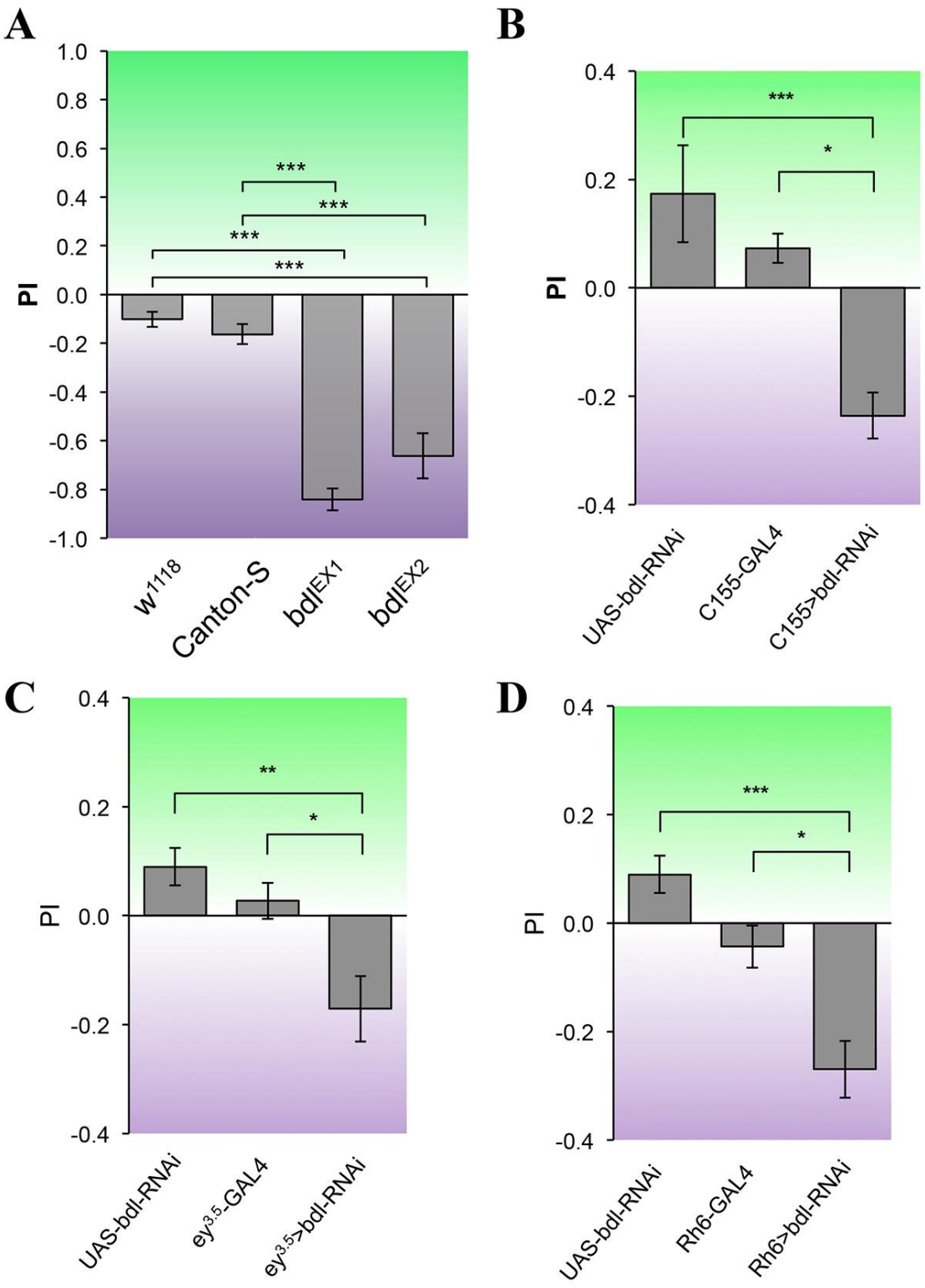
A
PI
1.0
0.8
0.6
0.4
0.2
0.0
-0.2
-0.4
-0.6
-0.8
-1.0
***
***
***
***
w1118
Canton-S
bdlEX1
bdlEX2
B
PI
0.4
0.2
0.0
-0.2
-0.4
***
*
UAS-bdl-RNAi
C155-GAL4
C155>bdl-RNAi
C
PI
0.4
0.2
0.0
-0.2
-0.4
**
*
UAS-bdl-RNAi
ey3.5-GAL4
ey3.5>bdl-RNAi
D
PI
0.4
0.2
0.0
-0.2
-0.4
***
*
UAS-bdl-RNAi
Rh6-GAL4
Rh6>bdl-RNAi

Figure 2.5. R8-dependent phototaxis response was disrupted in *bdl* mutants. Flies were given "UV vs. green" choice. Light preference index (PI) was calculated as described in Materials and Methods. (A) Canton-S wild-type and w^{1118} flies could be attracted to both UV and green light sources. However, both bdl^{EX1} and bdl^{EX2} homozygous mutant flies were predominantly attracted towards UV light source. (B) *bdl* was knocked down in flies carrying a pan-neuronal-specific driver *C155-GAL4* and a *UAS-bdl-RNAi* transgene. Compared to control flies that carried *C155-GAL4* or *UAS-bdl-RNAi* only, flies carrying both *C155-GAL4* and *UAS-bdl-RNAi* showed a much greater preference for UV light. (C) Eye-specific knockdown of *bdl* was performed by expressing *UAS-bdl-RNAi* under control of the eye-specific driver $ey^{3.5}$*-GAL4*. Reducing *bdl* in the eye significantly decreased the preference for green light. (D) *bdl* was specifically knocked down in green-sensitive R8 photoreceptors (i.e. R8y) by expressing *UAS-bdl-RNAi* under control of the R8y-specific driver *Rh6-GAL4*. Knocking down *bdl* in green-sensitive R8 decreased the preference for green light. For each genotype, about 5-10 trials were performed, and ~50 flies were tested in each trial. One-way ANOVA followed by post hoc Tukey's test, *P<0.05; **P<0.01; *** P<0.001. Error Bars indicate SEM.

Figure 2.6

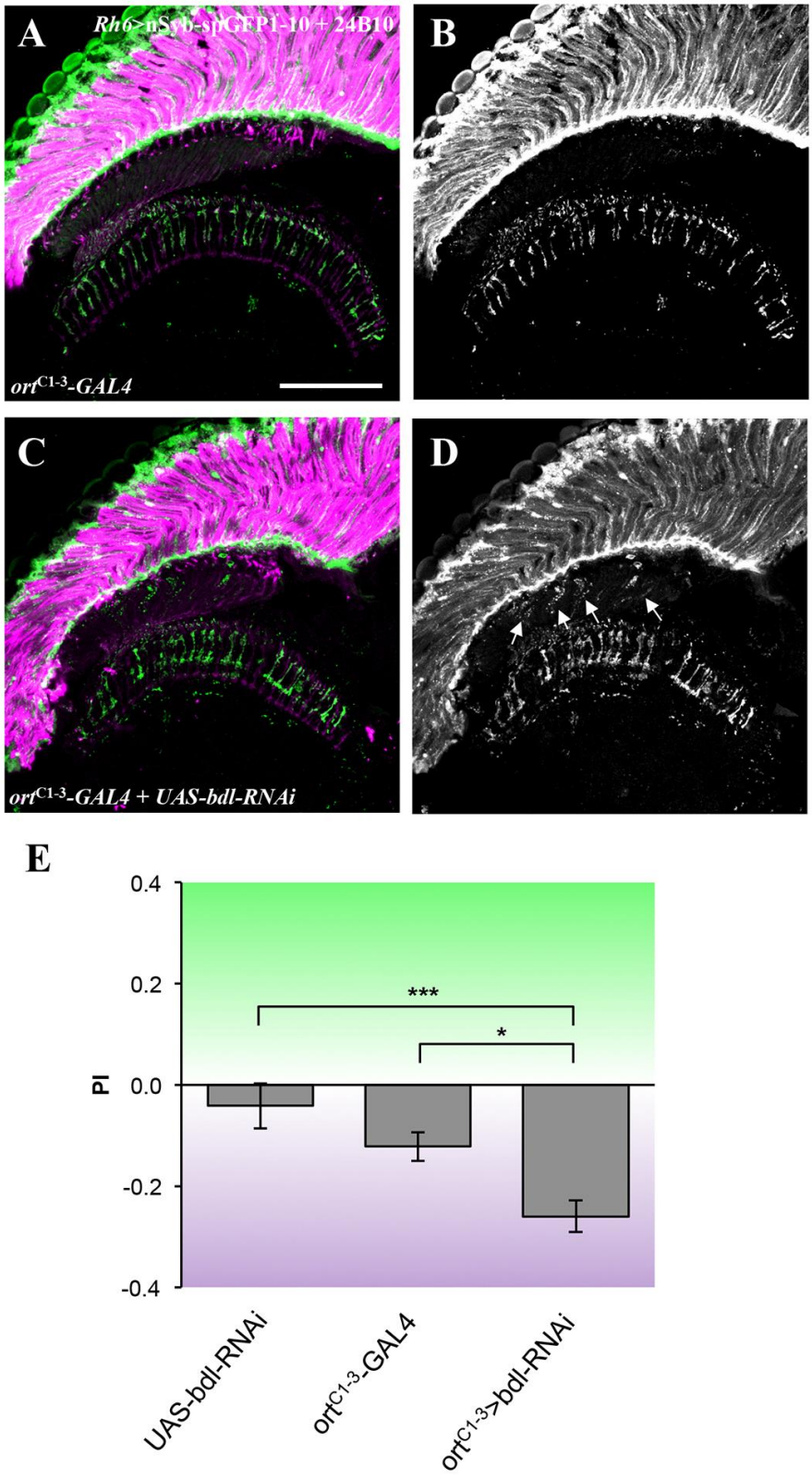
A
Rh6>nSyb-spGFP1-10 + 24B10
ortC1-3-GAL4
B
C
ortC1-3-GAL4 + UAS-bdl-RNAi
D
E
PI
0.4
0.2
0.0
-0.2
-0.4
***
*
UAS-bdl-RNAi
ortC1-3-GAL4
ortC1-3>bdl-RNAi

Figure 2.6. Knockdown of *bdl* in postsynaptic target neurons in the optic lobe disrupted the transport of SVs in R8 axons and R8-dependent phototaxis response. (A-D) Frozen sections of adult heads expressing the SV marker *lexAop-nSyb-spGFP1-10* under control of the green-sensitive-R8-specific driver *Rh6-lexA::p65,* were stained with anti-GFP (green) and MAb24B10 (magenta). (A) In most control animals carrying $ort^{C1\text{-}3}$*-GAL4* only (6 out of 7 animals), SVs labelled with nSyb-spGFP1-10 were predominantly localized to R8 axonal terminals in the medulla region. (B) The section in A was visualized with nSyb-spGFP1-10 staining only. (C) When *bdl* was knocked down in postsynaptic target neurons in the optic lobe by expressing *UAS-bdl-RNAi* under control of the $ort^{C1\text{-}3}$*-GAL4* driver, strong nSyb-spGFP1-10 staining was also observed in the proximal portion of R8 axons in the lamina (100%, n=4 animals). (D) The section in C was visualized with nSyb-spGFP1-10 staining only. Arrowheads indicate proximal portions of R8 axons with mis-localized nSyb-spGFP1-10. (E) Flies were given "UV vs. green" choice. Knocking down *bdl* in postsynaptic targets of R8 by expressing *UAS-bdl-RNAi* under control of $ort^{C1\text{-}3}$*-GAL4*, significantly decreased the preference for green light. For each genotype, about 10-13 trials were performed, and ~50 flies were tested in each trial. One-way ANOVA followed by post hoc Tukey's test, *P<0.05; *** P<0.001. Error Bars indicate SEM.

Figure 2.7

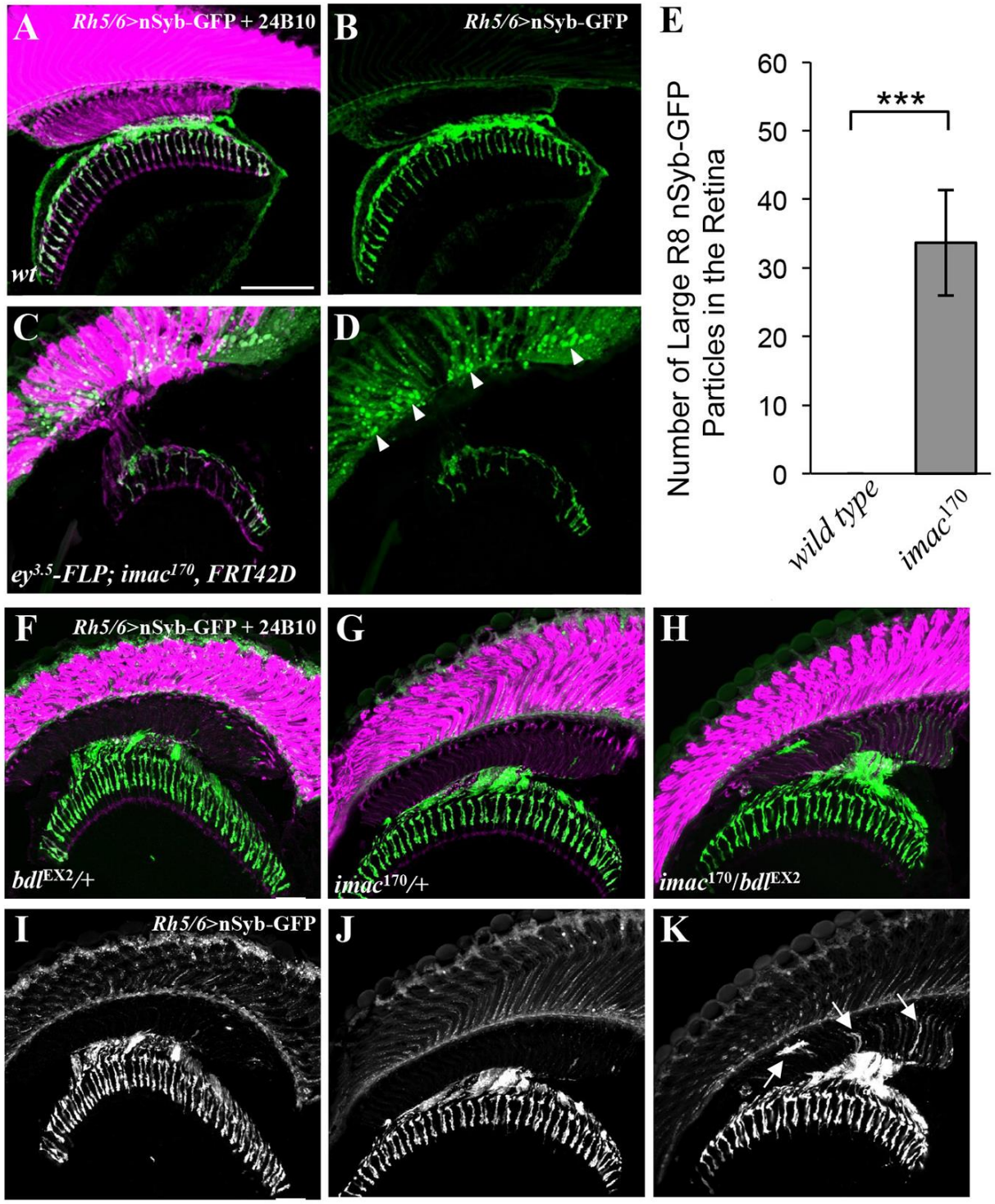
A
Rh5/6>nSyb-GFP + 24B10
wt
B
Rh5/6>nSyb-GFP
C
ey3.5-FLP; imac170, FRT42D
D
E
Number of Large R8 nSyb-GFP Particles in the Retina
60
50
40
30
20
10
0
***
wild type
imac170
F
Rh5/6>nSyb-GFP + 24B10
bdlEX2/+
G
imac170/+
H
imac170/bdlEX2
I
Rh5/6>nSyb-GFP
J
K

Figure 2.7. *bdl* interacts genetically with *imac* in the control of SV transport in R8 axons. (A-D) Loss of *imac* caused a failure of SV components to transport from R8 cell bodies into axons. Frozen sections of adult heads expressing *UAS-nSybGFP* under control of the green-sensitive-R8-specific driver *Rh6-GAL4*, were stained with anti-GFP (green) and MAb24B10 (magenta). (A) In wild type (n=6 animals), nSyb-GFP staining was predominantly localized to R8 axonal terminals in the medulla. (B) The section in A was visualized with nSyb-GFP staining only. (C) In eye-specific large $imac^{170}$ homozygous clones (n=6 animals), the levels of nSyb-GFP staining in R8 axons were greatly reduced. A large number of nSyb-GFP-positive large aggregates were observed in R8 cell bodies in the retina. (D) The section in C was visualized with nSyb-GFP staining only. (E) The number of abnormal large nSyb-GFP-positive aggregates in the retina was quantified. Loss of *imac* greatly increased the number of nSyb-GFP-positive aggregates in the retina. Student's t-test, ***p=0.0073. Error Bars indicate SEM. (F-K) Frozen sections of adult heads expressing *UAS-n-Syb-GFP* under control of the R8-specific driver *Rh5/6-GAL4*, were stained with anti-GFP (green) and MAb24B10 (magenta). In most bdl^{EX2}/+ (F and I) (14 out of 15 animals) or $imac^{170}$/+ heterozygotes (G and J) (14 out of 16 animals), nSyb-GFP staining was predominantly localized to R8 axonal terminals in the medulla region. In the majority of bdl^{EX2}/$imac^{170}$ transheterozygotes (12 out of 15 animals), however, strong n-Syb-GFP staining was also observed in the proximal portion of R8 axons in the lamina. Arrows indicate proximal portions of R8 axons with mis-localized nSyb-GFP. Scale bars: 20 μm.

Figure 2.8

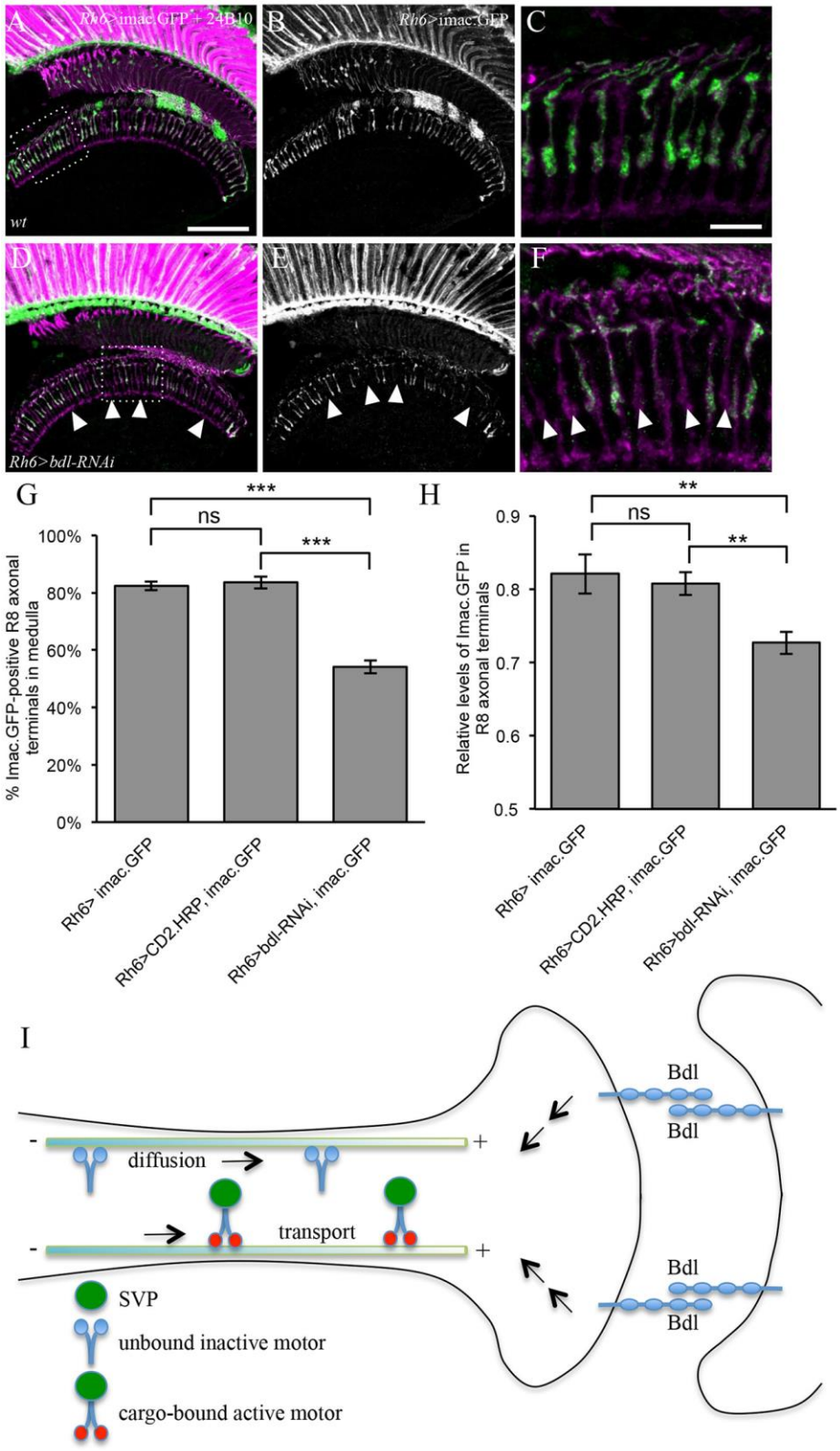
A
Rh6>imac.GFP + 24B10
wt
B
Rh6>imac.GFP
C
D
Rh6>bdl-RNAi
E
F
G
% Imac.GFP-positive R8 axonal terminals in medulla
100%
80%
60%
40%
20%
0%
ns
***
***
Rh6> imac.GFP
Rh6>CD2.HRP, imac.GFP
Rh6>bdl-RNAi, imac.GFP
H
Relative levels of Imac.GFP in R8 axonal terminals
0.9
0.8
0.7
0.6
0.5
ns
**
**
Rh6> imac.GFP
Rh6>CD2.HRP, imac.GFP
Rh6>bdl-RNAi, imac.GFP
I
Bdl
Bdl
Bdl
Bdl
-
+
diffusion
transport
-
+
SVP
unbound inactive motor
cargo-bound active motor

Figure 2.8. The levels of the Imac motor protein in R8 axonal terminals were decreased in *bdl* mutants. (A-F) Frozen sections of adult heads expressing *UAS-imac.GFP* under control of the green-sensitive-R8-specific driver *Rh6-GAL4*, were stained with anti-GFP (green) and MAb24B10 (magenta). (A) In control animals carrying *Rh6-GAL4* and *UAS-imac.GFP*, Imac.GFP staining was observed in proximal portions of R8 axons in the lamina and R8 axonal terminals in the medulla. (B) The section in A was visualized with Imac.GFP staining only. (C) The boxed area in A was enlarged. (D) In *bdl* knockdown flies carrying *Rh6-GAL4, UAS-imac.GFP* and *UAS-bdl-RNAi*, the number of R8 axonal terminals with Imac.GFP decreased. (E) The section in D was visualized with Imac-GFP staining only. (F) The boxed area in D was enlarged. Arrowheads indicate R8 axonal terminals in which Imac.GFP was absent. (G) The percentage of R8 axonal terminals with Imac.GFP staining was quantified. Compared to that in control animals carrying *Rh6-GAL4* and *UAS-imac.GFP* (n=7 animals) or control flies carrying *Rh6-GAL4, UAS-imac.GFP* and *UAS-CD2.HRP* (n=10 animals), the percentage of R8 axonal terminals with Imac.GFP was significantly reduced in *bdl* knockdown flies carrying *Rh6-GAL4, UAS-imac.GFP* and *UAS-bdl-RNAi* (n=8 animals). One-way ANOVA followed by post hoc Tukey's test, ***P<0.001; ns, P>0.05. (H) Relative intensity of Imac.GFP staining in Imac.GFP-positive R8 axonal terminals was quantified. Compared to that in control animals carrying *Rh6-GAL4* and *UAS-imac.GFP* (101 Imac.GFP-positive R8 axons, n=6 animals) or control flies carrying *Rh6-GAL4, UAS-imac.GFP* and *UAS-CD2.HRP* (189 Imac.GFP-positive R8 axons, n=6 animals), relative intensity of Imac.GFP staining was reduced in *bdl* knockdown R8 axonal terminals (131 Imac.GFP-positive R8 axons, n=7 animals). One-way ANOVA followed by post hoc Tukey's test, **P<0.01; ns, P>0.05. (I) Proposal models for the action of Bdl. Bdl-Bdl-mediated interaction between R8 and its postsynaptic target neuron may trigger downstream signalling events that promote the diffusion

of inactive Imac and/or stimulates the activity of Imac. Scale bars: A, B, D and E, 20 μm; C and F, 10 μm.

Chapter 3: The Ig transmembrane protein Borderless interacts with Neuroligin 2 in regulating axonal transport of presynaptic components in *Drosophila*

3.1 Abstract

Proper targeting of synaptic vesicle (SV) and active zone (AZ) components is critical for presynaptic assembly and function in a normal brain. The role of synaptogenic signals (e.g. adhesion) at axo-dendritic contact sites in promoting axonal transport of presynaptic components for synapse formation, however, remains unclear. Previous work from our lab reveals that Borderless (Bdl), a member of the conserved IgSF9-family of trans-synaptic cell adhesion molecules, regulates axonal transport of SV components in photoreceptor R8 axons by up-regulating the levels and/or activation of the kinesin-3 family motor, Immaculate Connections (Imac). Here we show that loss of another trans-synaptic adhesion molecule, Neuroligin-2 (Dnlg2), induces a *bdl*-like disruption in axonal transport of SV components in R8 axons. Co-immunoprecipitation and cell culture experiments suggest that Bdl and Dnlg2 physically interact in *cis* through the Bdl extracellular domain. Consistent with this observation, expression of a truncated Bdl protein lacking the cytoplasmic domain is sufficient to rescue the localization of SV components in R8 axons. Similar to *bdl*, *dnlg2* interacts genetically with *imac*, suggesting that it functions in the same pathway as Bdl to mediate Imac activation. We propose that Bdl and Dnlg2 form a cell-surface complex, which mediates trans-synaptic interactions to promote axonal transport of SV components for R8 presynaptic assembly and function.

3.2 Introduction

The formation and maintenance of a functional chemical synapse requires the precise recruitment of the appropriate pre- and postsynaptic machinery. The coordination of this process is mediated through signalling from molecules at axo-dendritic contact sites to the cell body. Maturation of a functional presynaptic terminal requires axonal transport of synaptic vesicle precursors (SVP), active zone (AZ) proteins, and organelles (such as mitochondria), from the soma to the active zone (Goldstein et al., 2008; Maday et al., 2014; Maeder et al., 2014). Previous work from our lab has demonstrated that axonal transport of synaptic cargos to the R8 axon terminal is dependent on the function of the kinesin-3 motor, Immaculate Connections (Imac), which is up-regulated by the trans-synaptic adhesion molecule Borderless (Bdl) (Shaw et al., 2019).

Bdl is a member of the conserved IgSF9 subfamily of the Ig superfamily, and possesses both homophilic and heterophilic binding activities (Cameron et al., 2013; Hansen and Walmod, 2013; Chen et al., 2017). In *bdl* null mutants, AZ and SVP are mislocalized to the soma and non-synaptic portions of the proximal axon in R8 photoreceptors (Shaw et al., 2019). Molecular and genetic analyses support a model in which the Bdl-mediated trans-synaptic adhesion between the R8 axonal terminal and its postsynaptic target neurons activates downstream events, which then promote the function of Imac motor for axonal transport of SVPs. The identity of molecular networks that link the Bdl-mediated trans-synaptic adhesion with the up-regulation of Imac, however, remains unknown. In this study, we set out to determine the underlying mechanisms by examining potential interactions between Bdl and other synaptic signalling proteins in the control of SV transport in R8 axonal terminals.

Recent studies on the mammalian homologs of Bdl (i.e. IgSF9a and IgSF9b) show that both IgSF9a and IgSF9b independently contribute to inhibitory synapse formation through trans-

synaptic homophilic adhesion (Hansen and Walmod, 2013; Woo et al., 2013; Mishra et al., 2014). IgSF9b has been shown to couple with the synaptic adhesion protein Neuroligin-2 (Nlg2) at the postsynaptic membrane of inhibitory synapses *in vitro* (Woo et al., 2013). This interaction was shown to occur indirectly through the bridging of these two molecules together via the synaptic scaffolding molecule, S-SCAM. However, the *in vivo* relevance of these interactions is still unknown.

In mammals, the trans-synaptic interaction between presynaptic Neurexins (Nrx) and postsynaptic Neuroligins (Nlg) in the control of synapse development and maturation has been studied in great detail (Yamagata et al., 2003; Araç et al., 2007; Craig and Kang, 2007; Shapiro et al., 2007; Südhof, 2008; Missler et al., 2012). At the *Drosophila* neuromuscular junction (NMJ), all four Nlg (Dnlg 1-4) have been shown to be important for synaptic development and function (Banovic et al., 2010; Sun et al., 2011; Chen et al., 2012; Xing et al., 2014; Zhang et al., 2017b). Interestingly, Dnlg1 binding to *Drosophila* Neurexin (Dnrx) is not an absolute requirement for Dnlg1 functionality, suggesting that binding of other signalling components to the extracellular or cytoplasmic domain of Dnlg1 is required to mediate its function (Banovic et al., 2010). Additionally, recent reports have demonstrated that presynaptic expression of *dnlg2* and *dnlg4* contribute to NMJ development and function (Chen et al., 2012; Zhang et al., 2017b). These findings together suggest that in *Drosophila,* the contributions of Nlgs to synaptic development and functionality may not be entirely dependent on its *trans*-interactions with presynaptic Nrx.

In this study, we examined the potential role of Dnlgs in the fly visual system. The results from transgenic RNAi and loss-of-function experiments show that loss of Dnlg2 caused a *bdl*-like SV mislocalization phenotype in R8 axons. Like *bdl*, *dnlg2* also interacts genetically with *imac* in the control of SV transport in R8 axons. Co-immunoprecipitation shows that Bdl physically

associates with Dnlg2, and this association does not require the cytoplasmic domain of Bdl. Transgene rescue indicates that the cytoplasmic domain of Bdl is dispensable for its function in regulating axonal transport of SV components in the R8 axon terminal. These results suggest that Bdl and Dnlg2 form a cell-surface complex that mediates trans-synaptic interactions between the R8 terminal and its postsynaptic target for axonal transport of presynaptic components.

3.3 Materials and Methods

3.3.1 Genetics

dnlg2^{KO70} flies were provided by X. Wie at Southeast University in China. *imac*^{170}, *FRT42D* flies were provided by T. Schwarz at Harvard. *Rh5/6-GAL; UAS-nSyb-GFP* was provided by C. Lee at NIH. UAS-TRiP RNAi lines HMS02131 (*dnlg1*, BDSC #40883), HMJ22077 (*dnlg2*, BDSC #58128), JF02966 (*dnlg2*, BDSC #28331), HMS01709 (*dnlg3*, BDSC #38264), HMJ22056 (*dnlg4*, BDSC #58119), and HMJ01710 (*dnlg4*, BDSC #38265) flies were obtained from the Bloomington *Drosophila* Stock Center (BDSC). For rescue experiments, genetic crosses were performed to generate flies with the genotype *bdl*^{EX2}*/ bdl*^{EX2}*; Rh5/Rh6-GAL4, UAS-nSyb-GFP*/*HS-bdl*Δcyto. To examine the contribution of the four Dnlgs to SV localization in R8 axons, we performed genetic crosses using TRiP RNAi lines on either the 2nd or 3rd chromosome to generate flies with the genotype *UAS-dnlg-TRiP-RNAi/+; Rh5/Rh6-GAL4, UAS-nSyb-GFP/+*, or *UAS-dnlg-TRiP-RNAi / Rh5/Rh6-GAL4, UAS-nSyb-GFP*. To examine the effects of removing *dnlg2* on SV localization in R8 axons, genetic crosses were performed to generate flies with the genotype *dnlg2*^{KO70}*/dnlg2*^{KO70}*; Rh5/Rh6-GAL4, UAS-nSyb-GFP*.

3.3.2 Histology

Adult heads were dissected and fixed for 3 hours on ice in 3.2% paraformaldehyde (PFA) in phosphate buffer (PB) (pH 7.2). Cryostat sections of adult and pupal heads were cut on a Leica CM3050 S or Leica CM1950 microtome at a thickness of 10 μm and collected on Superfrost® Plus slides (Fisher Scientific). Prior to the addition of primary antibodies, sections were blocked with 10% normal goat serum in PB with 0.5% Triton X-100 (PBT). Sections were then incubated with primary antibodies overnight at 4°C. After washed 3x with PBT, sections were incubated

with secondary antibodies for 45 minutes. After washed 3x with PBT, 80μL of anti-fade gold was added to each slide, which was then covered with a glass coverslip and sealed with nail polish.

Antibodies were used at following dilutions: MAb24B10 (1:100; Developmental Studies Hybridoma Bank or DSHB) and rabbit polyclonal anti-GFP (1:1000; Molecular Probes). Secondary antibodies: anti-mouse alexafluor647 and anti-rabbit alexafluor488 (Molecular Probes) were used at 1:750 dilution. Sections were imaged by confocal microscopy (Olympus fluoview FV1000 LSM).

3.3.3 Quantification of relative fluorescence intensity

Similarly as described previously (Shaw et al., 2019), the ImageJ software was used to measure fluorescent intensities in the proximal portion of R8 axons in the lamina and the distal portion of R8 axons in the medulla. Relative intensity of SV components in each region was calculated by normalizing the intensity of nSyb-GFP staining to that of MAb24B10 staining within the same region.

3.3.4 Cell aggregation and Co-aggregation

Cell aggregation and co-aggregation experiments were performed similarly as described previously (Cameron et al., 2013). *Drosophila* S2 cells were grown in EX-Cell 420 Serum-Free Medium for Insect Cells (Sigma) at 25˚C. Cells (1 x 10^7/10 mL) were transfected with 2 μg of total plasmid DNA (0.2 μg *actin-GAL4* and 1.8 μg either *UAS-venus, UAS-mRFP, UAS-dnlg2-venus, UAS-bdl-venus*, or *UAS-bdl-mRFP*) with Effectene (Qiagen) according to the manufacturer's instructions. At 96 hours post-transfection, cells were prepared as single-cell suspension at a concentration of 2.25 x 10^6/mL and agitated at 150 RPM for 1 hour (aggregation), or 3 hours (co-aggregation) at room temperature. 150 μl of cell mixture was then transferred onto glass slides

(Fisher Scientific). For each experiment, the total number of GFP- or RFP-positive transfected cells were counted in 10 randomly selected fields. The total number of GFP- or RFP-positive transfected cells forming cell aggregates with a size of >20 cells in each field were additionally counted to determine the percentage of transfected cells that formed large cell aggregates (i.e. defined as >20 cells). In co-aggregation experiments, a cell co-aggregate is defined as a cell aggregate (i.e. >20 cells) in which the percentage of each cell population (i.e. GFP- or RFP-positive cells) was at least 15%.

3.3.5 Molecular Biology

The deletion construct lacking the two fibronectin type-III repeats (i.e. ΔFN) was generated in our previous study (Cameron et al., 2013). For generating the deletion construct lacking the cytoplasmic domain, the fragment encoding amino-acid sequence 1-680 was amplified by PCR with 5' primer CAATCGCGGCCGCATGCCAGCGAAACGCA and 3' primer AGATCTCCTTAGGCAGCTCCGCTTC. The resulting PCR product was then subcloned into EcoRI and BglII sites of pCaspeR-hs vector. DNA constructs were verified by sequencing and used for generating transgenic lines.

For co-immunoprecipitation, 1.5 x 10^7 S2 cells transfected with 2 µg of total plasmid DNA (0.2 µg *actin-GAL4*, 0.7 µg *UAS-bdl-flag*, 1.1 µg *UAS-dnlg2-venus* or *UAS-venus*) were lysed in 1 ml lysis buffer (25mM Tris, 150mM NaCl, 1mM EDTA, 1% NP40 and 5% glycerol), followed by sonication and centrifugation. 0.5 ml of supernatant was mixed with 30 µl of anti-FLAG®M2 affinity gel (Sigma-Aldrich) at 4°C for 3 hours or 30 ul nProtein A Sepharose 4 fast flow (GE healthcare) and 1 ul of rabbit anti-GFP G10362 at 4°C overnight. The gel was then washed with lysis buffer three times. Proteins in precipitates were eluted with SDS sample buffer, followed by

SDS-PAGE and western-blot analysis with mouse anti-FLAG antibody M2 (1:1,000; Sigma-Aldrich) and rabbit anti-GFP antibody A-11122 (1:1,000; Life Technologies).

3.3.6 Statistical Analysis.

For experiments involving the comparison of two groups, statistical analysis was performed using two-tailed t-tests. For experiments involving the comparison of more than two groups, statistical analysis was performed using one-way ANOVA followed by post hoc Tukey's test. The difference is considered as significant when a p-value is <0.05.

3.4 Results

3.4.1 Presynaptic knockdown of Dnlg2 in R8s caused mislocalization of SV components in R8 axons

To identify other components of the Bdl pathway for the control of SV transport in R8 axons, we took a test-candidate approach to examine if reducing the levels of other genes causes a *bdl*-like SV phenotype. A recent *in vitro* study shows that IgSF9b, the mammalian homolog of Bdl, interacts with Neuroligin-2 through the synaptic scaffolding molecule S-SCAM in the development of inhibitory synapses in cultured cells (Woo et al., 2013), raising the interesting possibility that Dnlgs may interact with Bdl in the control of SV transport in R8 axons. To test this, we performed knockdown experiments to examine if reducing the levels of Dnlgs affects SV transport.

Similar to mammals, four Dnlgs have been identified, including Dnlg1 (CG31146), Dnlg2 (CG13772), Dnlg3 (CG34127), and Dnlg4 (CG34139) (Banovic et al., 2010). The Dnlgs share a closer homology to hNL1 than to the other three human neuroligins (Knight et al., 2011; Fig. 3.1A). However, their extracellular regions do share similarities with that of hNL2 as well (Fig. 3.1B). All four Dnlgs have been implicated in the control of neuronal development and function in the adult brain and the larval NMJ (Banovic et al., 2010; Sun et al., 2011; Chen et al., 2012; Xing et al., 2014; Zhang et al., 2017b). To test if any Dnlgs play a role in axonal transport of SV components in R8 axons, we performed knockdown experiments.

Each of the four Dnlgs was knocked down using *UAS-TRiP RNAi* lines under control of the R8-specific driver (i.e. *Rh5-GAL4*, *Rh6-GAL4*) (Perkins et al., 2015). The localization of SV components was examined using the SV marker *nSyb-GFP* transgene similarly as described in our previous study (Shaw et al., 2019). We found that reducing the levels of Dnlg2 with two different

independent RNAi lines caused a *bdl*-like SV mislocalization phenotype (Fig. 3.2). Dnlg3 and Dnlg4 knockdown also affected SV transport (Fig. 3.2E). However, since the phenotype was only observed with a single RNAi line, it is unclear if the phenotypes from Dnlg3 and Dnlg4 knockdown were due to off-target effects. Thus, we chose Dnlg2 for further molecular and genetic analysis.

3.4.2 Dnlg2 loss-of-function mutants also displayed a *bdl*-like SV mislocalization phenotype

The above knockdown experiments using two independent RNAi lines suggest a role for Dnlg2 in the control of SV transport. To further exclude the possibility that the knockdown phenotype was due to off-target effects, we performed loss-of-function analysis.

SV localization in mutant R8 axons homozygous for a *dnl2* null allele (i.e. $dnlg2^{KO70}$) (Sun et al., 2011) was examined by using the SV marker *nSyb-GFP*, and compared to that of wild-type animals. In wild-type flies, SV components are localized to the R8 axon terminals in the medulla, with no animals showing nSyb-GFP signal in the proximal portion of R8 axons in the lamina (n=7, Fig. 3.3A-B). Interestingly, we found that homozygous $dnlg2^{KO70}$ mutant flies displayed a severe *bdl*-like SV mislocalization phenotype in all the animals examined (100%, n=7, Fig. 3.3C-D). This result, together with that from knockdown experiments (Fig. 3.2), suggests strongly that like Bdl, Dnlg2 also plays a role in regulating axonal transport of SV components in R8 axons.

3.4.3 Dnlg2 interacted physically with Bdl

That loss of *dnlg2* caused a *bdl*-like SV mislocalization phenotype (Fig. 3.2), raises the interesting possibility that Bdl may interact with Dnlg2 in regulating axonal transport of SV components in R8 axons. To test this, we examined the potential physical interactions between Dnlg2 and Bdl by performing co-immunoprecipitation (Co-IP).

Bdl and Dnlg2, tagged with Flag and GFP, respectively, were expressed in cultured *Drosophila* S2 cells. Bdl and its associating proteins were precipitated from lysates prepared from transfected S2 cells. We found that Dnlg2-GFP, but not GFP control protein, was detected in Bdl precipitates pulled down by anti-Flag antibody (Fig. 3.4). This result suggests that Dnlg2 forms an *in vivo* complex with Bdl.

3.4.4 The cytoplasmic domain of Bdl was dispensable for the interaction between Dnlg2 and Bdl

To test if the association of Bdl and Dnlg2 requires the Bdl cytoplasmic domain, we generated a deletion construct (i.e. *bdl*Δ*cyto*) in which the cytoplasmic domain of Bdl is truncated. The association of BdlΔcyto and Dnlg2 was examined by performing Co-IP experiments. Surprisingly, we found that the truncated BdlΔCyto protein was still able to form a complex with Dnlg2 (Fig. 3.5). The Bdl mutant protein lacking the two fibronectin type-III repeats (FN) in the extracellular region, was also able to pull down Dnlg2 from S2 cell lysates (Fig. 3.5). These results suggest that neither the cytoplasmic domain nor the fibronectin type-III repeats are required for mediating the association of Bdl with Dnlg2.

3.4.5 Dnlg2 does not interact with Bdl in *trans*

Above results from Co-IP experiments showing that Bdl interacts physically with Dnlg2, suggest two possibilities. Bdl and Dnlg2 may be expressed in the same cell, and interact with each other in *cis* on the same cell surface. Alternatively, Bdl and Dnlg2 may interact in *trans* on opposing cell surfaces. To distinguish between the two possibilities, we performed a cell co-aggregation assay.

S2 cells transfected with Dnlg2-GFP, Bdl-GFP, Bdl-RFP, GFP or RFP expression constructs, were used in co-aggregation experiments. Cells expressing Bdl-RFP could co-aggregate with cells expressing Bdl-GFP (Fig. 3.6A), but not with cells expressing GFP (Fig. 3.6C), as Bdl possesses homophilic binding activity. However, compared to that of controls (Fig. 3.6C-E), no significant co-aggregation of cells expressing Dnlg2-GFP with cells expressing Bdl-RFP was observed (Fig. 3.6B and 3.6E). This result, together with the observation that both Bdl and Dnlg2 are required in R8 axons for SV transport (Fig. 3.2), suggests strongly that Bdl and Dnlg2 interact in *cis* in R8 axons.

3.4.6 Dnlg2 does not possess homophilic binding activity

A previous report shows that *dnlg2* expression is required both pre- and postsynaptically at the larval NMJ (Chen et al., 2012), raising the possibility that Dnlg2 may mediate the adhesion between motor axon terminal and muscle across the synaptic cleft via a homophilic binding mechanism. To test if Dnlg2, like Bdl, possesses homophilic binding activity, we performed cell-cell aggregation assay. S2 cells were transfected with Bdl-GFP, Dnlg2-GFP or GFP expression constructs. Similarly as reported previously (Cameron et al., 2013), cells expressing Bdl-GFP (Fig. 3.7B), but not GFP (Fig. 3.7B), formed large aggregates. In contrast, no large cell aggregates were formed when Dnlg2-GFP was expressed in S2 cells (Fig. 3.7C, 3.7 D). This result suggests that Dnlg2 does not possess homophilic binding activity.

3.4.7 The cytoplasmic domain of Bdl is dispensable

Since the physical association between Bdl and Dnlg2 does not require the cytoplasmic domain of Bdl, we then tested if the cytoplasmic domain of Bdl is essential for its function in the control of SV transport. An HS-*bdl*Δ*cyto* transgene in which the cytoplasmic domain is deleted

was generated and tested in rescue experiments. Surprisingly, we found that the SV phenotype in *bdl* mutants could be largely rescued by this truncated Bdl lacking the cytoplasmic domain (Fig. 3.8C-E). This result indicates that the cytoplasmic domain is dispensable for the function of Bdl in regulating axonal transport of SV components in R8 axon terminals.

3.4.8 *dnlg2* interacts genetically with *imac*

Our previous study demonstrates that *bdl* interacts genetically with *imac*, as $bdl^{EX2}/imac^{170}$ transheterozygous animals, but not $bdl^{EX2}/+$ or $imac^{170}/+$ heterozygotes, displayed a highly penetrant *bdl*-like SV phenotype (Shaw et al., 2019). If *dnlg2* indeed interacts with *bdl* in R8 axons, one may predict that *dnlg2* may also display such dosage-sensitive interactions with *imac*. To test this, we performed epistasis analysis.

In heterozygous $dnl2^{KO70}/+$ or $imac^{170}/+$ animals, like that in wild type, SV components were predominantly localized to R8 axon terminals in the medulla (Fig. 3.9A-D). Interestingly, many transheterozygous $dnlg^{KO70}/imac^{170}$ animals displayed a severe SV mislocalization phenotype, as SV components were mislocalized to the proximal portion of the R8 axon in the lamina (Fig. 3.9E-F). Thus, *dnlg2*, like *bdl*, also interacts genetically with *imac*.

3.5 Discussion

In this study, we took a test-candidate approach to identify other components of the Bdl pathway for regulating axonal transport of SV components in R8 cells. Our study presents several lines of evidence that support a novel and important role for Dnlg2 in interacting with Bdl in the control of SV transport. First, presynaptic knockdown of *dnlg2* caused a *bdl*-like SV mislocalization phenotype. Second, deletion of the *dnlg2* gene, like *dnlg2* knockdown, disrupted SV transport in R8 axons. Third, Dnlg2 interacts physically with Bdl, which is independent of the cytoplasmic domain or the FN repeats in the extracellular region. Fourth, transgene rescue reveals that the cytoplasmic domain of Bdl is dispensable for its role in the control of SV transport. Finally, epistasis experiments demonstrate that like *bdl*, *dnlg2* interacted genetically with *imac*. We propose that the homophilic binding between Bdl on the R8 terminal and Bdl on its postsynaptic targets, recruits and activates Dnlg2, which in turn up-regulates the function of the Imac motor for axonal transport of SV components (Fig. 3.10).

The association of Dnlg2 and Bdl revealed by Co-IP experiments may result from the interaction between Dnlg2 and Bdl in *cis* on R8 axonal terminals, or in *trans* between Dnlg2 on R8 terminals and Bdl on postsynaptic targets. That both *bdl* and *dnlg2* show cell-autonomous requirements in R8 axons (Fig. 3.2) (Shaw et al., 2019), together with the finding that Dnlg2-expressing cells did not co-aggregate with Bdl-expressing cells (Fig. 3.6), suggest strongly that Bdl and Dnlg2 interact with each other in *cis* on R8 axonal terminals.

The results from transgene rescue showing that Bdl mutant protein lacking the cytoplasmic domain still rescued the *bdl* SV phenotype (Fig. 3.8), argue against a model in which the Bdl-Bdl homophilic binding activates downstream signalling events through its cytoplasmic domain in R8 terminals for SV transport. This result, together with the evidence suggesting a cell-surface *cis*

interaction between Bdl and Dnlg2 that is independent of the Bdl cytoplasmic domain (Fig. 3.4-3.6), support the notion that Bdl interacts in *cis* with Dnlg2 on R8 terminals, which in turn activate downstream signalling cascades leading to the activation of the Imac motor. Several cell adhesion molecules have been shown to form such a *cis*-complex at the trans-synaptic cleft. For instance, the *cis*-binding between MDGA1 and neuroligin 2 modulates inhibitory synapse development (Lee et al., 2013). It is also worth noting that the cytoplasmic domain of neurexin is dispensable for its synaptogenic properties (Gokce and Südhof, 2013), suggesting strongly that neurexin interacts in *cis* with an unidentified partner that mediates the association of neurexin with downstream components for synaptogenesis. Furthermore, a recent study shows that replacing IgSF9a (i.e. the mammalian homolog of Bdl) with a truncated mutant lacking the cytoplasmic domain by knock-in, did not affect its function in the control of inhibitory synaptic development (Mishra et al., 2014), raising the possibility that IgSF9a also interacts in *cis* with some cell-surface proteins for activating downstream signalling proteins.

Our results from knockdown experiments show that Dnlg2 is required presynaptically for SV transport in R8 axons. Up to now, the studies on vertebrate neuroligins show that they are localized postsynaptically (Yamagata et al., 2003; Craig and Kang, 2007), and it remains unclear if neuroligins also play a role presynaptically. In *Drosophila*, however, it has been shown that both Dnlg2 and Dnlg4 are required presynaptically at the *Drosophila* larval NMJ (Chen et al., 2012; Chanda et al., 2017). In addition, Dnlg2 is also required postsynaptically at the *Drosophila* larval NMJ (Chen et al., 2012). Similarly, Dnlg2 may also be required both presynaptically in R8 terminals and postsynaptically in target neurons in the medulla. For instance, Dnlg2 may interact in *cis* with Bdl on postsynaptic target neurons, and facilitate the Bdl-Bdl homophilic binding at axo-dendrite contact sites leading to the activation of Dnlg2 on R8 terminals (Fig. 3.10).

Additionally, Dngl2 on R8 terminals may interact in *trans* with certain cell-surface receptors on postsynaptic target neurons, for instance, Dnrx (i.e. the *Drosophila* homolog of α-neurexin in mammals). Dnrx is highly expressed in the medulla (especially in the cells adjacent the R7 and R8 axon terminals) (Liu et al., 2017), and has been shown to mediate *trans* interactions with Dnlg2 at the larval NMJ (Sun et al., 2011; Chen et al., 2012; Tian et al., 2013). It will be of interest to determine if Dnrx is required in postsynaptic target neurons for interacting with Bdl/Dnlg2 on R8 terminals for axonal transport of SV components in R8 axons.

In conclusion, our present study suggests strongly that Dnlg2 functions together with Bdl in regulating axonal transport of SV components in R8 axonal terminals. Our results, together with the previous *in vitro* study showing that IgSF9b (i.e. the mammalian homolog of Bdl) associates with mammalian Nlg2 in the control of inhibitory synaptic development (Woo et al., 2013), support the evolutionary conservation of the interaction between Bdl/IgSF9b and Dnlg2/Nlg2. Future studies will be needed to determine if mammalian Nlg2 and IgSF9b play a similar role in regulating axonal transport of SV components in presynaptic terminals.

Figure 3.1

A

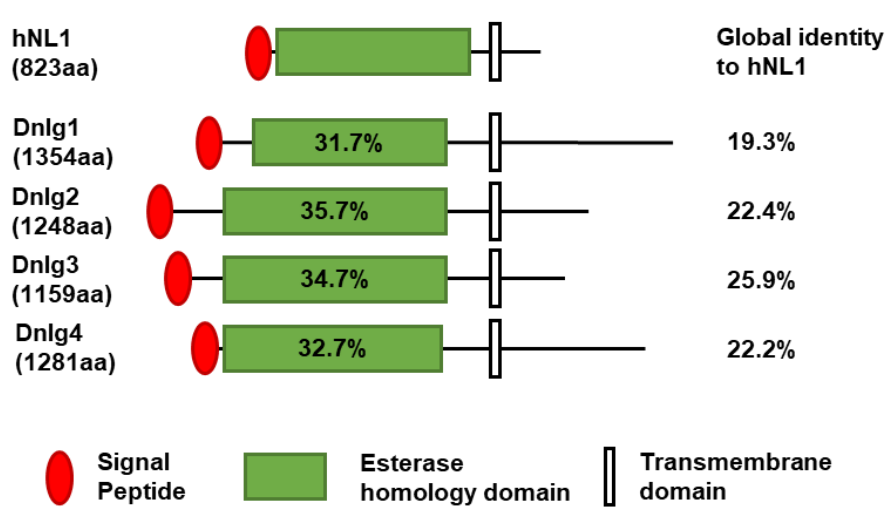

B

Neuroligin-2 (Human)
Total Length: 835 AA
Extracellular: 15-677 ;
Transmembrane: 678-698;
Cytoplasmic: 699-835

BLASTP	Range	Query Position	Subject Position	ID	Positives (+)	Gaps
neuroligin 3, isoform B [Drosophila melanogaster] (1159 AA)	#1	43 to 609	157 to 799	228/648 (35%)	340/648 (52%)	86/648 (13%)
	#2	672 to 715	908 to 945	25/44 (57%)	31/44 (70%)	6/44 (13%)
neuroligin 1, isoform D [Drosophila melanogaster] 1354 AA)	#1	44 to 606	158 to 715	202/579 (35%)	301/579 (51%)	37/579 (6%)
neuroligin 2, isoform A [Drosophila melanogaster] (1248 AA)	#1	43 to 582	184 to 726	189/565 (33%)	290/565 (51%)	47/565 (8%)
	#2	570 to 609	787 to 826	13/40 (33%)	25/40 (62%)	0/40 (0%)
neuroligin 4, isoform D [Drosophila melanogaster] (1281 AA)	#1	43 to 360	43 to 357	137/333 (41%)	187/333 (56%)	33/333 (9%)
	#2	375 to 609	427 to 689	87/268 (32%)	137/268 (51%)	38/268 (14%)
	#3	672 to 708	820 to 857	23/38 (61%)	31/38 (81%)	1/38 (2%)

Figure 3.1. Homologies between Human and *Drosophila* Neuroligins. A) The four *Drosophila* Neuroligins show higher similarity to hNL1 than to the other three Human Neuroligins. Dnlg1-4 share conserved similarities in the extracellular esterase domain with hNL1. Numbers indicated in the esterase homology domain represent percent identity. Adapted from Knight et al., 2011. B) BLASTP of hNL2 with all four *Drosophila* neuroligin amino acid sequences. The inhibitory synapse associated hNL2, which is thought to be associated with IGSF9B, the human homolog of Bdl, show similarities to Dnlg1-4 amino acid sequences in the extracellular acetylcholine esterase-like domain.

Figure 3.2

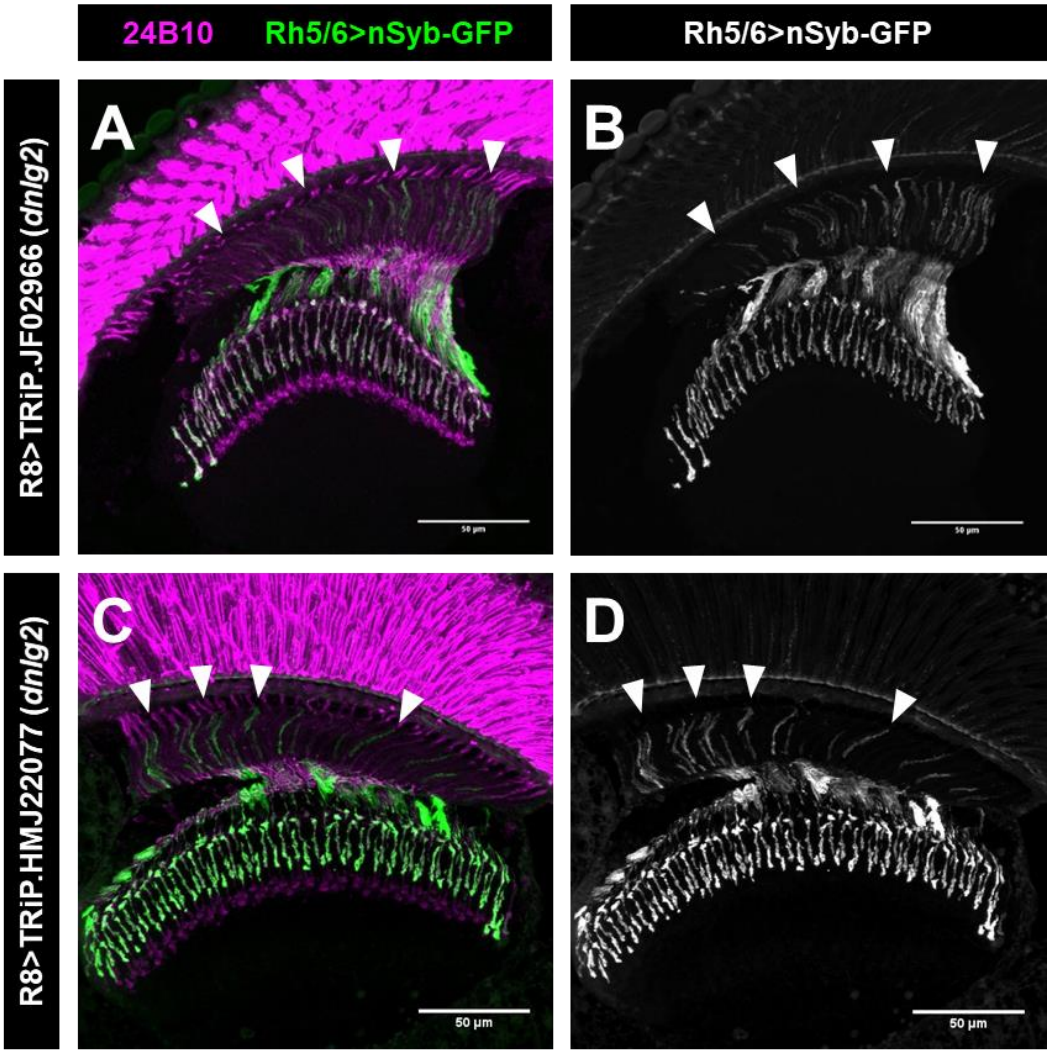

E

R8 Driven TRiP UAS-RNAi Line	Penetrance of SV mis-localization phenotype
HMS02131 (*dnlg1*)	14% (1/7)
HMJ22077 (*dnlg2*)	31% (4/13)
JF02966 (*dnlg2*)	66% (8/12)
HMS01709 (*dnlg3*)	50% (3/6)
HMJ22056 (*dnlg4*)	0% (0/8)
HMJ01710 (*dnlg4*)	43% (3/7)

Figure 3.2. Presynaptic knockdown of *Drosophila neuroligin-2* in R8s shows mislocalization of SV components. (A-D) Frozen sections of adult heads simultaneously expressing the SV marker *UAS-n-Synaptobrevin-GFP* (nSyb-GFP) and *dnlg2-TRiP-RNAi*, under control of the R8-specific driver *Rh5/6-GAL4* (i.e. *Rh5/6>nSyb-GFP*), were stained with anti-GFP (green) and MAb24B10 (magenta). MAb24B10 recognizes the cell adhesion molecule Chaoptin expressed in all R-cell axons (Van Vactor et al., 1988) (A) In the majority of *Rh5/6>TRiP.JF02966* (*dnlg2*) animals (66%, n=12), strong n-Syb staining was observed in the proximal portion of R8 axons in the lamina (arrowheads). (B) The section in A was visualized with nSyb-GFP staining only. (C) Similar SV phenotypes (31%, n=13) were also observed when *dnlg2* was knocked down using a different RNAi line (i.e. UAS-TRiP.MJ22077). (D) The section in C was visualized with nSyb-GFP staining only. (E) Table showing the penetrance of the R8 nSyb mislocalization phenotype in experiments knocking down *dnlg1, 2, 3, or 4*. Similar SV mislocalization phenotype was observed when *dnlg2* was knocked down using two different RNAi lines. Arrowheads indicate proximal portions of R8 axons with mis-localized nSyb-GFP. Scale bar: 50 μm.

Figure 3.3

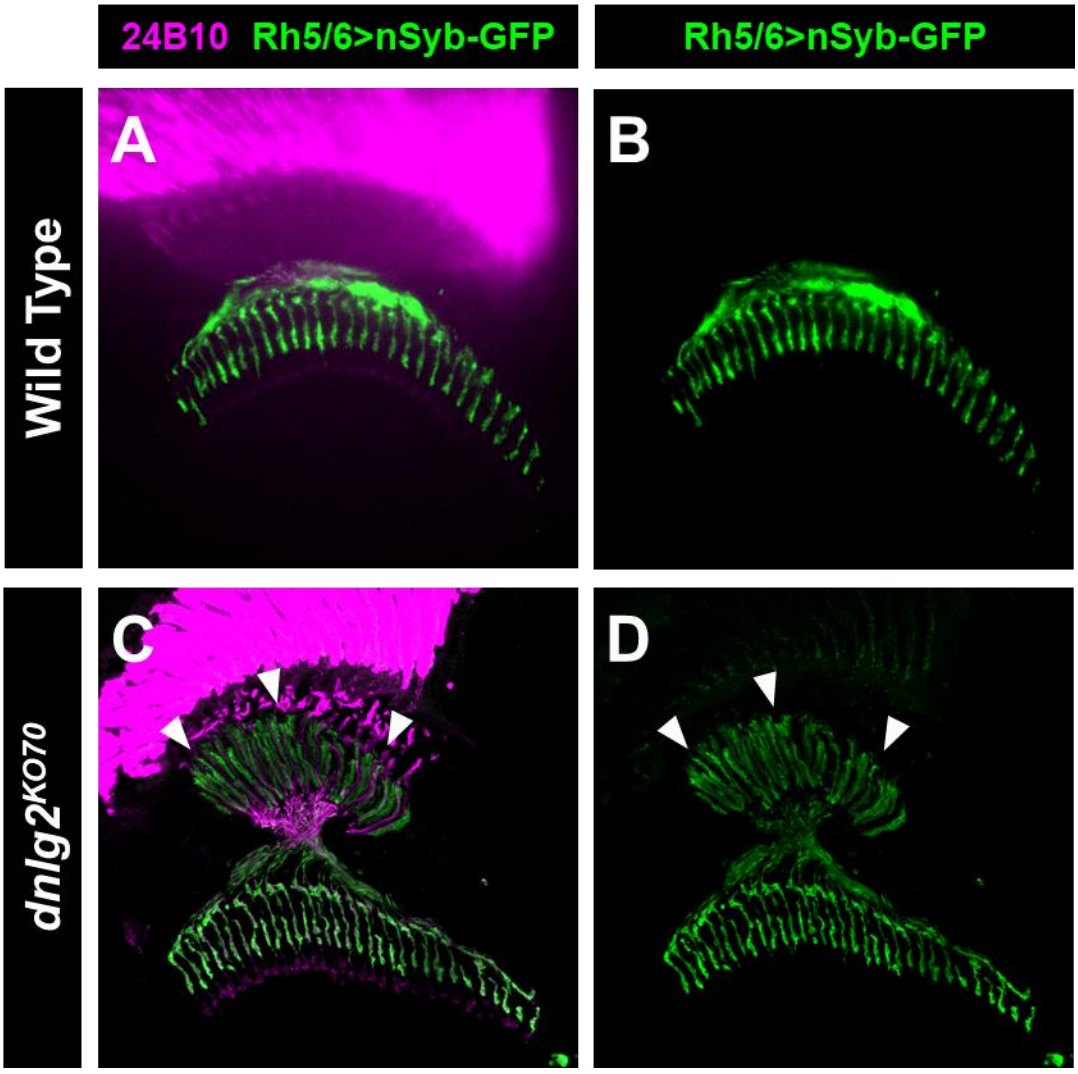

Figure 3.3. *Drosophila neuroligin-2* loss-of-function mutants display a *bdl*-like SV mislocalization phenotype in R8 axons. (A-D) Frozen sections of adult heads expressing the SV marker nSyb-GFP under control of the R8-specific driver *Rh5/6-GAL4* (i.e. *Rh5/6>nSyb-GFP*), were stained with anti-GFP (green) and MAb24B10 (magenta). (A) In wild-type animals (n=7), nSyb-GFP staining was predominantly localized to R8 axonal terminals in the medulla region. (B) The section in A was visualized with nSyb-GFP staining only. (C) In all $dnlg2^{KO70}$ homozygous mutant flies examined (n=7 animals), strong n-Syb staining was also observed in the proximal portion of R8 axons in the lamina (arrowheads). (D) The section in C was visualized with nSyb-GFP staining only. Arrowheads indicate proximal portions of R8 axons with mis-localized nSyb-GFP.

Figure 3.4

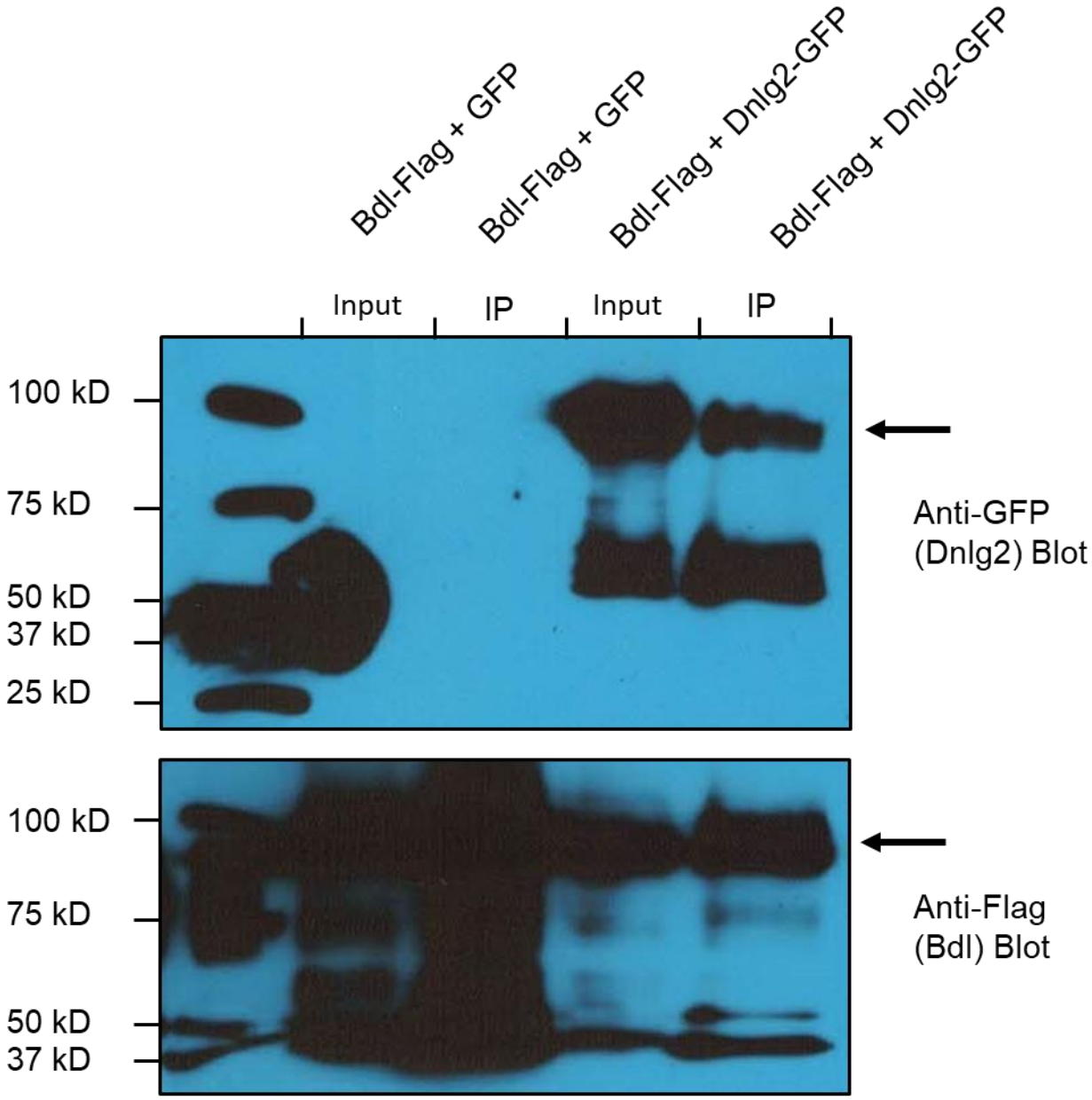
Bdl-Flag + GFP
Bdl-Flag + GFP
Bdl-Flag + Dnlg2-GFP
Bdl-Flag + Dnlg2-GFP
Input
IP
Input
IP
100 kD
75 kD
50 kD
37 kD
25 kD
Anti-GFP
(Dnlg2) Blot
100 kD
75 kD
50 kD
37 kD
Anti-Flag
(Bdl) Blot

Figure 3.4. Neuroligin-2 and Bdl interact physically. Western blot analysis of precipitates pulled down from lysates of *Drosophila* S2 cells expressing Bdl-Flag and GFP or Bdl-Flag and Dnlg2-GFP. Anti-Flag antibody was used to precipitate Bdl-Flag from S2 cells co-expressing Bdl-Flag and GFP or Bdl-Flag and Dnlg2-GFP. (Top panel) The blot was probed with anti-GFP antibody. Dnlg2-GFP was detected in Flag precipitates from lysates expressing Bdl-Flag + Dnlg2-GFP, but not from lysates expressing GFP and Bdl-Flag. Dnlg2-GFP bands were at ~100 kD (arrow). (Bottom panel) The same blot was stripped and re-probed with anti-Flag antibody. Bdl-Flag was observed at ~100 kD (arrow).

Figure 3.5

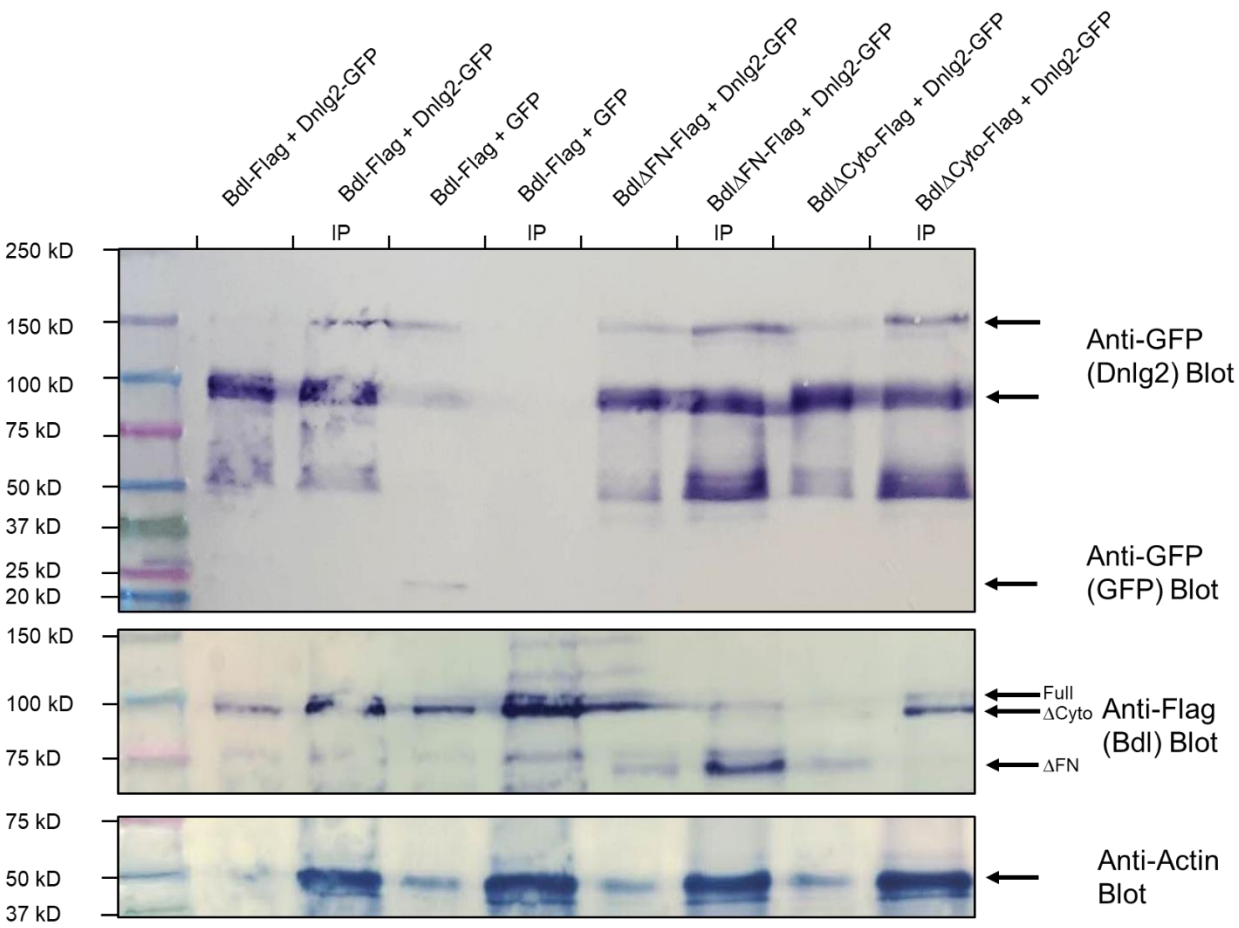
Bdl-Flag + Dnlg2-GFP
Bdl-Flag + Dnlg2-GFP
Bdl-Flag + GFP
Bdl-Flag + GFP
BdlΔFN-Flag + Dnlg2-GFP
BdlΔFN-Flag + Dnlg2-GFP
BdlΔCyto-Flag + Dnlg2-GFP
BdlΔCyto-Flag + Dnlg2-GFP
IP
IP
IP
IP
250 kD
150 kD
100 kD
75 kD
50 kD
37 kD
25 kD
20 kD
Anti-GFP (Dnlg2) Blot
Anti-GFP (GFP) Blot
150 kD
100 kD
75 kD
Full
ΔCyto
ΔFN
Anti-Flag (Bdl) Blot
75 kD
50 kD
37 kD
Anti-Actin Blot

Figure 3.5. The cytoplasmic domain of Bdl is dispensable for the association of Bdl and Dnlg2. Western blot analysis of precipitates pulled down from lysates of *Drosophila* S2 cells co-expressing Dnlg2-GFP with a Flag-tagged Bdl lacking the cytoplasmic domain (i.e. BdlΔCyto-Flag), or with a Flag-tagged Bdl lacking the fibronectin-type-III repeat (i.e. BdlΔFN-Flag). Anti-Flag antibody was used to precipitate BdlΔFN-Flag or Bdl-ΔCyto-Flag. (Top panel) The blot was probed with anti-GFP antibody. Dnlg2-GFP was detected in precipitates from lysates co-expressing Dnlg2-GFP + BdlΔCyto-Flag, and Dnlg2-GFP + BdlΔFN-Flag, but not from lysates co-expressing GFP + Bdl-Flag. The cleaved and uncleaved forms of Dnlg2-GFP were observed at ~100 kD and ~150 kD (arrows), respectively, which are consistent with previous studies (e.g. Tu et al., 2017). (Bottom panel) The same blot was stripped and re-probed with anti-Flag antibody. Bdl-Flag band was observed at ~100 kD position, BdlΔFN-Flag band was observed at ~75 kD position, and BdlΔCyto-Flag band was observed at ~100 kD position that was just below the full-length Bdl-Flag band (arrows).

Figure 3.6

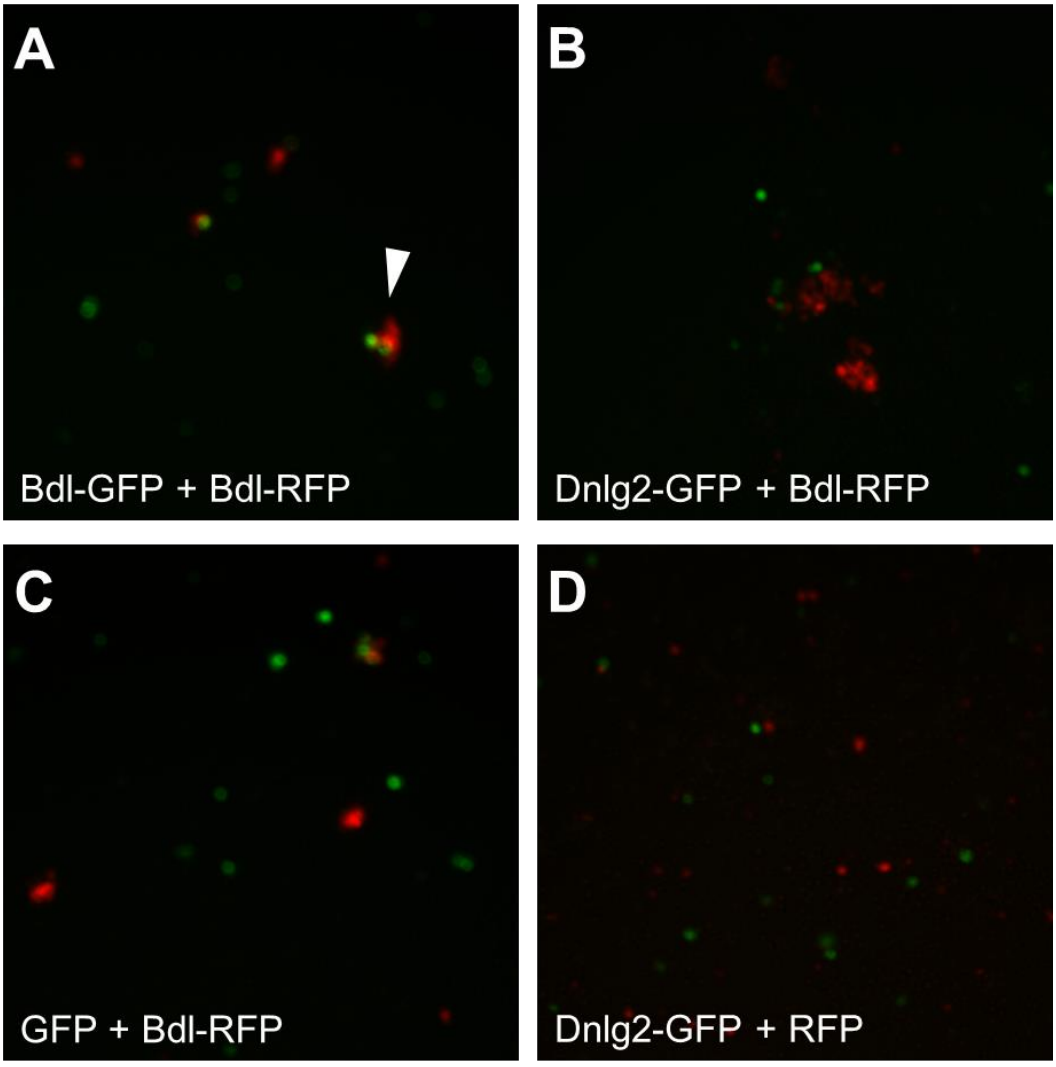
A
Bdl-GFP + Bdl-RFP
B
Dnlg2-GFP + Bdl-RFP
C
GFP + Bdl-RFP
D
Dnlg2-GFP + RFP
E
% Coaggregation with Bdl-RFP
100.0
75.0
50.0
25.0
0.0
***
ns
ns
Bdl-GFP+Bdl-RFP
Dnlg2-GFP +Bdl-RFP
GFP + Bdl-RFP
Dnlg2-GFP + RFP

Figure 3.6. Dnlg2 does not interact with Bdl in *trans* in cultured cells. (A) Co-aggregation occurs when Bdl-GFP-transfected cells were mixed with Bdl-RFP-transfected cells. (B) Dnlg2-GFP-transfected cells did not aggregate with Bdl-RFP-transfected cells. (C) GFP-transfected cells did not form co-aggregates with Bdl-RFP-transfected cells. (D) Dnlg2-GFP -transfected cells did not aggregate with RFP-transfected cells. (E) The percentage of co-aggregates was quantified. The percentage of Bdl-GFP + Bdl-RFP co-aggregates was significantly greater than that of Dnlg2-GFP + Bdl-RFP (***, $P< 0.001$). The percentage of Dnlg2-GFP and Bdl-RFP co-aggregates was not significantly different from controls (i.e. GFP + Bdl-RFP and Dnlg2 + RFP) (ns, $P>0.05$). Three independent experiments were performed. Error bars indicate SEM.

Figure 3.7

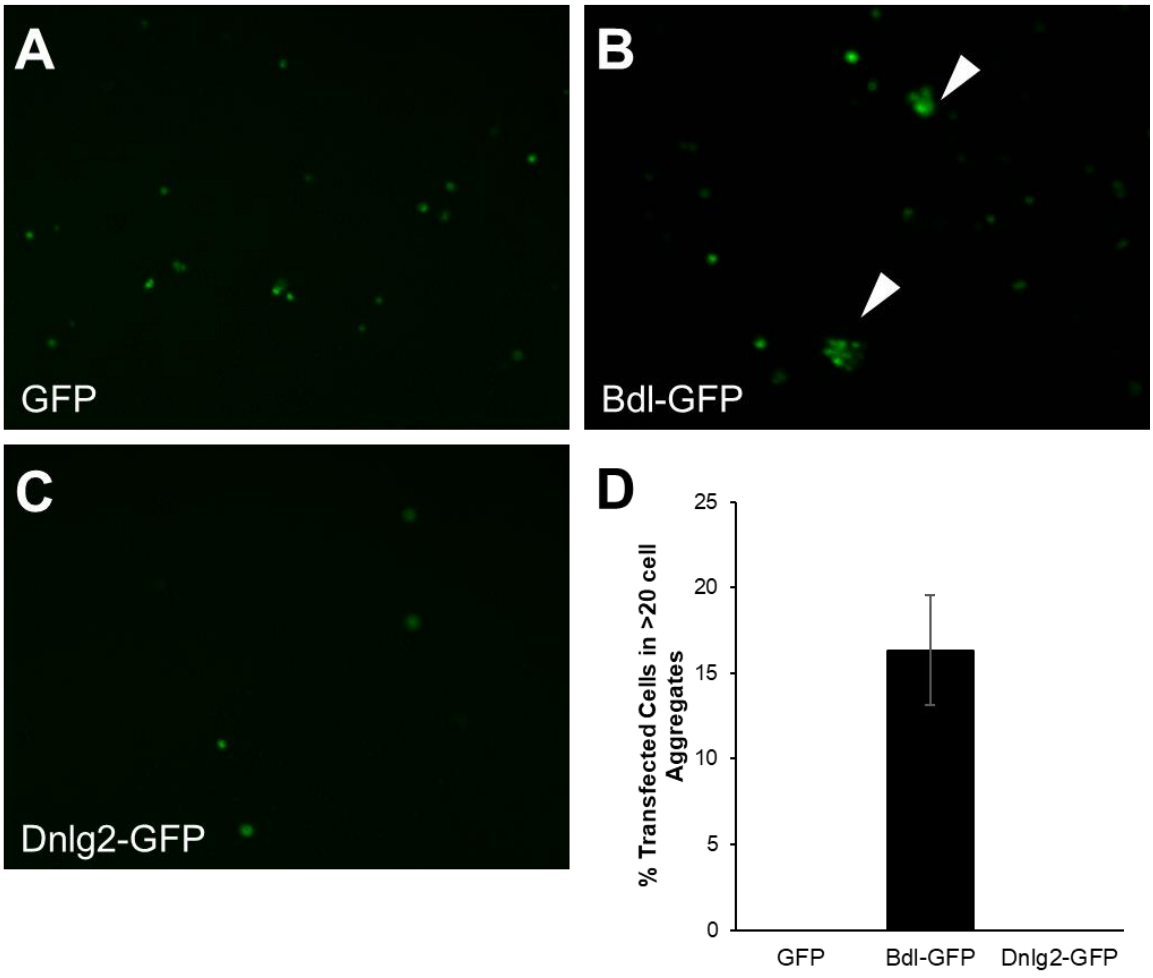
A
GFP
B
Bdl-GFP
C
Dnlg2-GFP
D
% Transfected Cells in >20 cell Aggregates
25
20
15
10
5
0
GFP
Bdl-GFP
Dnlg2-GFP

Figure 3.7. Dnlg2 does not mediate homotypic cell–cell adhesion. (A) S2 cells transfected with a GFP construct. (B) S2 cells transfected with Bdl-GFP construct formed large aggregates (arrowheads). (C) S2 cells transfected with Dnlg2-GFP construct did not form aggregates. (D) Among total transfected cells, the percentage of transfected cells that formed large aggregates (>20 cells) was quantified. No large aggregate (>20 cells) was observed for cells transfected with GFP or Dnlg2-GFP constructs. Three independent experiments were performed. Error bars indicate SEM.

Figure 3.8

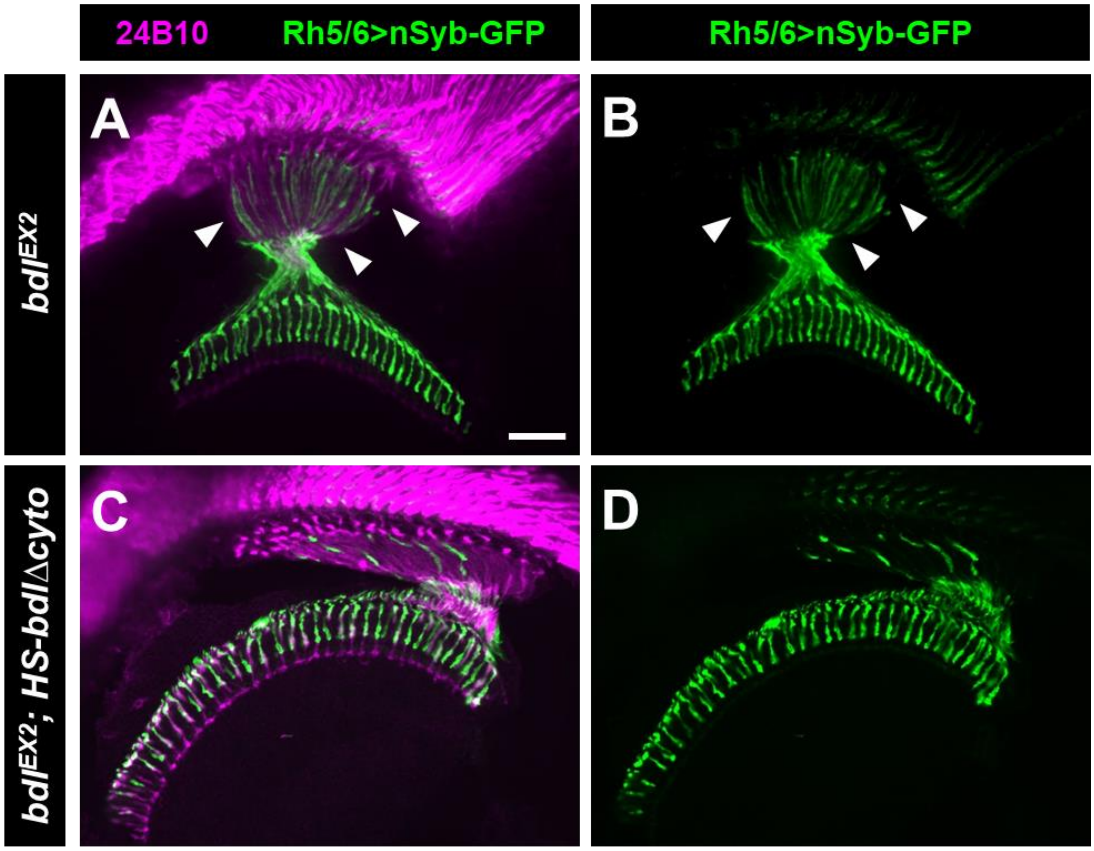
24B10
Rh5/6>nSyb-GFP
Rh5/6>nSyb-GFP
A
B
C
D
bdlEX2
bdlEX2; HS-bdlΔcyto

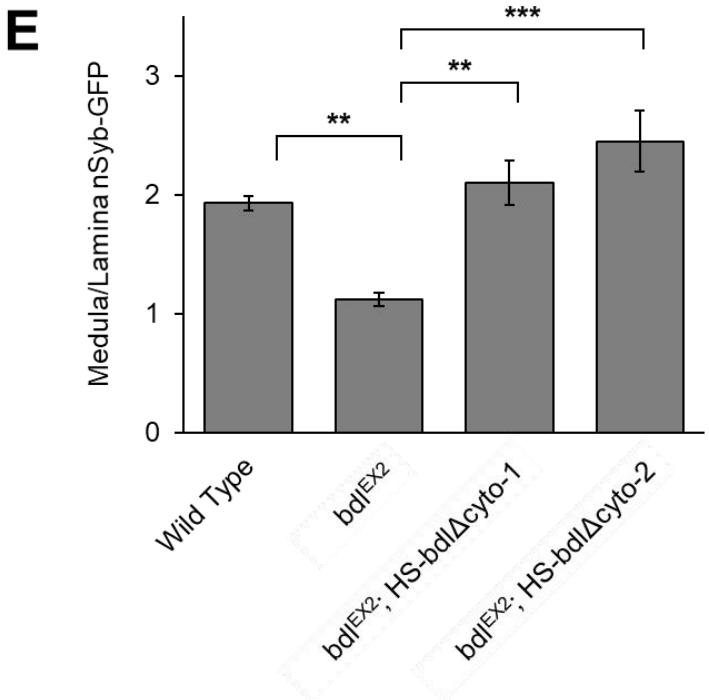
E
Medula/Lamina nSyb-GFP
0
1
2
3
**
**
***
Wild Type
bdlEX2
bdlEX2; HS-bdlΔcyto-1
bdlEX2; HS-bdlΔcyto-2

Figure 3.8. The cytoplasmic domain of Bdl is dispensable for its function in axonal transport of SV components. (A-F) Frozen sections of adult heads expressing the SV marker nSyb-GFP under control of the R8-specific driver *Rh5/6-GAL4* (i.e. *Rh5/6>nSyb-GFP*), were stained with anti-GFP (green) and MAb24B10 (magenta). (A) bdl^{EX2} homozygous mutants, strong n-Syb staining was observed in the proximal portion of R8 axons in the lamina (arrows). (B) The section in A was visualized with nSyb-GFP staining only. Arrowheads indicate proximal portions of R8 axons with mis-localized nSyb-GFP. (C) In bdl^{EX2} homozygous mutants in which a Bdl mutant protein lacking the majority of the cytoplasmic domain (i.e. BdlΔCyto) was expressed in both R-cell axons and the optic lobe, the SV phenotype was rescued. (D) The section in C was visualized with nSyb-GFP staining only. (E) The ratio of medulla vs lamina relative nSyb-GFP staining intensities was quantified. Two independent *HS-bdlΔcyto* transgenic lines were used in the experiments, with at least four individuals used in each experiment. **, $P<0.05$; ***, $P<0.005$. Error Bars indicate SEM. Scale bar: 20 μm.

Figure 3.9

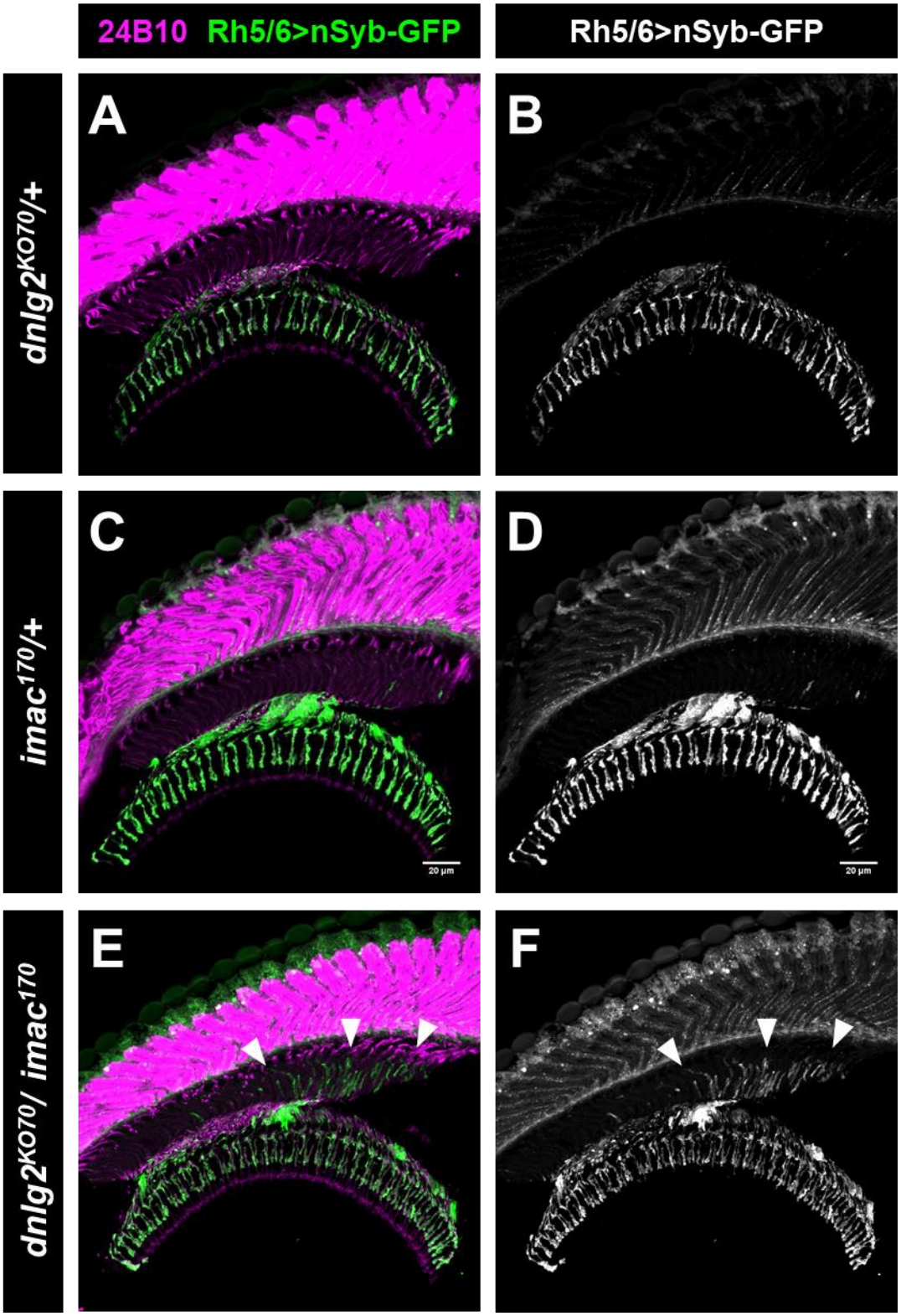
24B10 Rh5/6>nSyb-GFP
Rh5/6>nSyb-GFP
dnlg2KO70/+
imac170/+
dnlg2KO70/ imac170
A
B
C
D
E
F
20 µm
20 µm

Figure 3.9. *dnlg2* genetically interacts with *imac*. (A-G) Frozen sections of adult heads expressing the SV marker nSyb-GFP under control of the R8-specific driver *Rh5/6-GAL4* (i.e. *Rh5/6>nSyb-GFP*), were stained with anti-GFP (green) and MAb24B10 (magenta). (A) In $dnlg2^{KO70}$/+ heterozygous animals (14%, 1/7 animals), nSyb-GFP staining was predominantly localized to R8 axonal terminals in the medulla region similar to that of wild type. (B) The section in A was visualized with nSyb-GFP staining only. (C) In $imac^{170}$/+ heterozygous animals (14%, 1/7 animals), nSyb-GFP staining was predominantly localized to R8 axonal terminals in the medulla region similar to that of wild type. (D) The section in C was visualized with nSyb-GFP staining only. (E) In many the $dnlg2^{KO70}/imac^{170}$ transheterozygous animals (50%, 4/8 animals), strong n-Syb staining was also observed in the proximal portion of R8 axons in the lamina (arrowheads). (F) The section in E was visualized with nSyb-GFP staining only. Scale bar: 20 μm. Arrowheads indicate proximal portions of R8 axons with mislocalized nSyb-GFP.

Figure 3.10

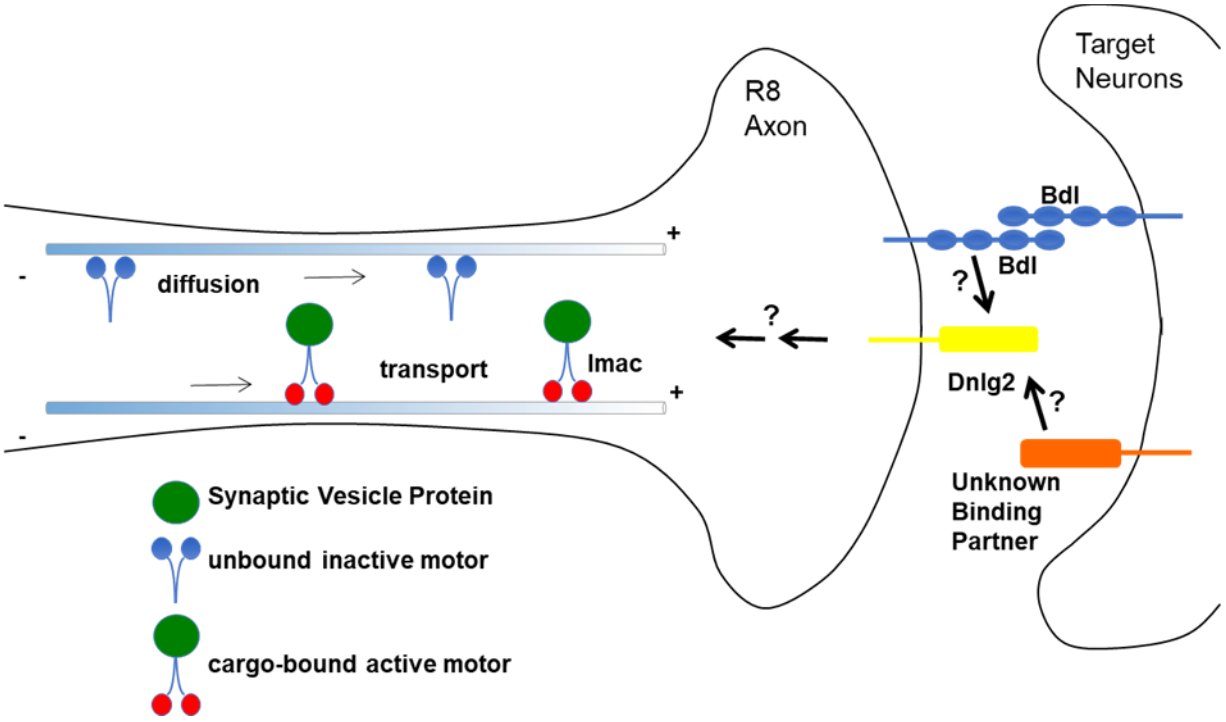
Target
Neurons
R8
Axon
Bdl
Bdl
?
diffusion
transport
Imac
?
Dnlg2
?
Unknown
Binding
Partner
+
-
+
-
Synaptic Vesicle Protein
unbound inactive motor
cargo-bound active motor

Figure 3.10. Proposed models for the action of Bdl and Dnlg2. Trans-synaptic interactions between Dnlg2 on the presynaptic R8 axon with an unknown binding partner on the R8 postsynaptic target neuron may trigger downstream signalling events that promote the diffusion of inactive Imac and/or stimulates the activity of Imac. *Cis*-interactions between Bdl and Dnlg2 in conjunction with Bdl-Bdl homophilic binding between R8 and its postsynaptic target neurons may regulate both Dnlg2 functionality and Imac-mediated transport of presynaptic components to the R8 axon terminal.

Chapter 4: Conclusions and Future Directions

4.1 Discussion

4.1.1 Homophilic Adhesion of Bdl Mediates Synaptic Protein Localization and Function

The IgSF9 family is one of the most evolutionarily ancient of the IgSF superfamily of cell adhesion molecules (CAM; Hansen and Walmod, 2013). Its members have been implicated in the outgrowth and branching of neurites, axon guidance, synapse maturation, self-avoidance, and tiling. The first of these CAMs identified was Turtle (Tutl) in *Drosophila*, gaining its name from the inability of larvae to regain an upright position when flipped on their back (Bodily et al., 2001). Until the identification of Borderless (Bdl), Tutl was thought to be the sole IgSF9 member expressed by *Drosophila* (Cameron et al., 2013). Tutl has been studied extensively and has been shown to play roles in axonal tiling, dendrite self-avoidance, neuron-glia interactions, axonal pathfinding and coordinated motor control (Bodily et al., 2001; Ferguson et al., 2009; Long et al., 2009; Cameron et al., 2013; Hansen and Walmod, 2013; Chen et al., 2017). Although demonstrated to contribute to R7 axon tiling and layer selection, the role for Bdl has been more elusive, as null mutants do not appear to have any noticeable anatomical defects.

For the mammalian homologs of Tutl and Bdl, IgSF9a and IgSF9b, evidence is mounting for the importance of homophilic interactions by both these two IgSF9 CAMs across the synaptic cleft for inhibitory synapse formation and maturation (Shi et al., 2004; Woo et al., 2013; Mishra et al., 2014; Babaev et al., 2018). Although, experiments looking at both the individual pre and postsynaptic requirements of IgSF9 molecules in mediating synaptic development and functionality are missing. Early electrophysiological evidence expressing a dominant negative form pointed to IgSF9a having a role in the later developmental stages of glutamatergic synapse development (Shi et al., 2004). Results a decade later, however, identified IgSF9a and IgSF9b actually being required at the inhibitory GABAergic and glycinergic synapses (Woo et al., 2013;

Mishra et al., 2014). *IgSF9a* null mutant hippocampal slices and postsynaptic knockdown of *IgSF9b* in cultured hippocampal interneurons showed impairments in inhibitory synaptic transmission. Although behavioural assays in *IgSF9a* null mice did show an increase in seizure susceptibility, a major limitation with these electrophysiological approaches is that they were focused on the postsynaptic requirements of IgSF9 molecules and were performed *in vitro* (Mishra et al., 2014).

It was recently reported that IgSF9b is required for presynaptic function *in vivo* (Babaev et al., 2018). *IgSF9b* null mutant mice were surprisingly shown to have a presynaptically mediated increase in inhibitory synaptic function, and an increase in vesicular inhibitory amino acid transporter (VIAAT)-positive vesicles in the presynaptic terminals of centromedial amygdala inhibitory neurons. The impaired accumulation of VIAAT, a well-characterized vesicular neurotransmitter transporter, at the presynaptic terminal is of particular interest because it resembles the SVP mislocalization phenotype I observed in histaminergic R8 axon terminals of *bdl* null mutants. However, once again the findings by Babaev et al. were limited in that they did not look at the individual contributions of IgSF9b at the pre- and postsynaptic terminals.

My findings in Chapter 2 demonstrate for the first time the *in vivo* requirements of IgSF9 family CAMs individually in both the presynaptic axon and their postsynaptic targets. By taking a combination of cell-type-specific rescue and knockdown approaches, I was able to demonstrate the requirements of Bdl in both the R8 photoreceptor presynaptic terminal and its postsynaptic targets for the proper recruitment of SV and AZ proteins to the R8 axon terminal (Fig. 2.2, 2.3, 2.6). Additionally, I was able to demonstrate the functional requirements of pre- and postsynaptic Bdl for fruit fly colour vision (Fig. 2.5). Pre- and/or postsynaptic knockdown of *bdl* significantly impaired the fly's ability to distinguish green light, suggesting an impairment in the green-sensitive

R8 photoreceptors in relaying information to the colour vision pathway in the medulla. Therefore, by using the genetic tools available in the fruit fly, I was able to identify the molecular and physiological contributions of IgSF9 CAM homophilic binding between synaptic partners, and elucidate how this evolutionarily conserved family of molecules may be functioning in mammals.

4.1.2 Bdl Mediated Activation of Imac is Required for SVP and AZ Protein Recruitment

My work identifies for the first time that a cell adhesion molecule at axo-dendritic contacts plays a novel and specific role in promoting the transport of SV components for presynaptic assembly and function. In Chapter 2, I demonstrated that in the absence of Bdl, SVP and AZ proteins are specifically mislocalized in R8 axons, while mitochondria distribution appeared to be intact (Fig. 2.1, 2.4). These results suggested that in the absence of Bdl, the activity of a specific motor was impaired, as opposed to an overall disruption in axonal transport. In accordance with this, I discovered that Bdl specifically regulates the localization and levels of the kinesin-3 motor, Imac, at the R8 axonal terminal (Fig. 2.8). The Unc-104/Imac/KIF1A- family of motors is highly conserved, and mediates anterograde transport of SVP and dense core vesicle (DCV) from the soma to the axon terminal (Pack-Chung et al., 2007; Goldstein et al., 2008; Lo et al., 2011; Maday et al., 2014). My findings suggest that Bdl promotes axonal localization of Imac, and may also stimulate the activity of Imac in SV transport. Activation of motor proteins can be mediated by relieving the autoinhibition with cargo binding or phosphorylation (Espeut et al., 2008; Hammond et al., 2009; Niwa et al., 2016). However, the signalling events downstream of Bdl which may unlock the autoinhibition of Imac and thus promote the delivery of SV components to presynaptic terminals are still yet to be determined.

In the rescue experiments I performed in Chapter 3, the Bdl cytoplasmic domain was shown to be dispensable for SVP localization (Fig. 3.8), suggesting that Bdl may not directly mediate the

downstream signalling events via its cytoplasmic domain, and likely recruits and/or activates Imac in the R8 axonal terminal by interacting with other cell-surface proteins. Furthermore, the *cis* ectodomain interactions between Bdl and Dnlg2, in conjunction with the genetic interactions between *imac* and *dnlg2*, implicate a role for Dnlg2 in the Bdl-mediated transport of SV and AZ components in R8 axons. These results suggest that the *cis* interaction between Bdl and Dnlg2 may allow Dnlg2 to initiate downstream signalling cascades leading to the recruitment and/or activation of Imac (Fig. 3.10). The Bdl/Dnlg2 complex at R8 presynaptic terminals may be activated by Bdl on postsynaptic target neurons through Bdl-Bdl homophilic binding. Alternatively or additionally, Dnlg2 at R8 presynaptic terminals may also be activated through trans-synaptic interactions with an unknown adhesion molecule (Fig. 3.10). One attractive candidate that has trans-synaptic interactions with Dnlg2 may be a member of Neurexins.

Neurexins are the most well-characterized trans-synaptic binding partner of neuroligins (Yamagata et al., 2003; Missler et al., 2012), with *in vitro* studies indicating that neuroligin-neurexin binding is required for presynaptic recruitment of synaptic vesicles (Dean et al., 2003; Missler et al., 2012). In *Drosophila*, *dnrx* mutants display impairments in SV and AZ protein transport, as ectopic synaptotagmin (Syt) and Brp staining (which are both normally localized to the NMJ presynaptic terminal) is observed within the motor axon shafts (Li et al., 2007). By comparison, my studies demonstrate the mislocalization of SV and AZ proteins in the R8 axons of *bdl* and *dnlg2* mutant animals (Fig. 2.1, 2.4, 3.3). Furthermore, Co-IP experiments using lysates from adult fly heads show that Dnlg2 and Dnrx form an *in vivo* complex (Sun et al., 2011). Together, these studies suggest that the Bdl-dependent activation and recruitment of Imac could be mediated, in part, by Dnlg2-Dnrx interactions.

Recent insights from *C. elegans* have identified that Arl-8, an Arf-like conserved small GTPase localized to the SV membrane, physically binds and activates UNC-104/KIF1A by unlocking its autoinhibition (Takamori et al., 2006; Wu et al., 2013; Niwa et al., 2016). Interestingly, a recent publication reports that *Drosophila* NMJ presynaptic assembly depends on the Arl8-dependent axonal co-transport of SV and AZ proteins (i.e. Brp) in presynaptic lysosome-related vesicles (PLVs) (Vukoja et al., 2018). This study and another recent publication went on to show that loss of Arl8 results in the accumulation of SV- and AZ-protein-containing vesicles in the neuronal cell bodies, and disruption of long-range axonal transport in *Drosophila* motor neurons (Rosa-Ferreira et al., 2018; Vukoja et al., 2018). They additionally demonstrate that Arl8 and Imac colocalize and associate with each other (Vukoja et al., 2018). These results share similarities to what I observed in the R8 axon terminals of *bdl* mutants (Fig. 2.1), suggesting that Arl8 could be another strong potential downstream candidate of Bdl-mediated Imac activation.

Finally, several adaptor proteins associated with the AZ are thought to be involved in the control of Unc-104/Imac/KIF1A motor cargo loading. In Chapter 2, I demonstrate that in *bdl* null mutant animals, large aggregates of Brp, the major component of the *Drosophila* AZ, are mislocalized to the R8 soma in the retina (Fig. 2.1). As AZ proteins have been shown to be dependent on Imac transport, the Bdl-dependent activation of Imac may be mediated by interactions with AZ proteins. One interesting candidate is Liprin-α, an AZ scaffolding molecule and cargo adaptor protein which has been demonstrated to be important in the assembly and retention of presynaptic components, and more importantly a specific and positive regulator of Unc-104/Imac/KIF1A-dependent axonal transport (Shin et al., 2003; Miller et al., 2005; Wagner et al., 2009). Previous work from our lab has demonstrated that the receptor tyrosine phosphatase LAR, down-regulates Bdl to mediate proper R7 layer selection (Cameron et al., 2013).

Intriguingly, Liprin-α is the cytoplasmic binding partner of LAR (Stryker and Johnson, 2007). It would be interesting to investigate whether Bdl interacts with LAR/ Liprin-α in R8s in mediating downstream signalling events underlying the activation of the Imac transport of SV and AZ proteins.

4.1.3 Bdl and Dnlg2 Mediated SVP transport in R8 photoreceptors

My test-candidate RNAi approach in Chapter 3 revealed Dnlg2 was identified as a strong candidate to be part of the R8 SV transport pathway (Fig. 3.2). In support of this, *dnlg2* null mutants displayed highly penetrant *bdl*-like SV mislocalization phenotypes in R8 axon terminals (Fig. 3.3). Co-IP experiments identified that Bdl and Dngl2 form a complex *in vivo* (Fig. 3.4). Surprisingly, this interaction persisted even in the absence of the Bdl cytoplasmic or fibronectin domains (Fig. 3.5), while S2 cell coaggregation experiments show that Bdl and Dnlg2 did not interact in *trans* (Fig., 3.6). Taken together, these results suggest a *cis* interaction (i.e. on the same membrane) between Bdl and Dnlg2, which may be mediated by the Ig-like domains of the Bdl ectodomain. My observation that Bdl and Dnlg2 are required on the same cell membrane is consistent with what is observed with IgSF9b and Nlg2 in mammals (Woo et al., 2013).

In mammals, homophilic adhesion of IgSF9a and IgSF9b are thought to stabilize the pre- and postsynaptic membrane to mediate neurexin-neuroligin trans-synaptic interactions (Hansen and Walmod, 2013; Woo et al., 2013; Mishra et al., 2014). My data supports this stabilizing model for Bdl and Dnlg2 in the R8 axon terminal. However, there is a significant difference between the mammalian IgSF9b/Nlg2 and *Drosophila* Bdl/Dnlg2 *cis*-interactions. IgSF9b/Nlg2 are coupled indirectly through intracellular binding of their cytoplasmic tails to S-SCAM, while Bdl/Dnlg2 appear to potentially interact directly through ectodomain interactions. This raises the possibility that Bdl could regulate Dnlg2 through extracellular interactions. Recent publications have

identified *cis*-interactions between neuroligins and MAM domain-containing glycosylphosphatidylinositol anchor (MDGA) cell-surface molecules (Elegheert et al., 2017; Gangwar et al., 2017). MDGAs regulate the formation of neuroligin-neurexin trans-synaptic bridges by sterically blocking access of neurexins to neuroligins by binding to neuroligins via Ig-domain interactions. However, my results argue against such a mechanism by which Bdl *cis*-interactions negatively regulates Dnlg2 function, as Bdl and Nlg2 appear to be working together to mediate SV transport. Nonetheless, it will be important to determine how the ectodomain interactions between Bdl and Dnlg2 contribute to the activation of Imac-mediated transport of SV to the R8 axon terminal.

An interesting observation is a presynaptic role for Dngl2 in R8 SV recruitment. Neuroligins are classically thought to be expressed only on the postsynaptic terminal, mediating their action through binding with presynaptic neurexins (Craig and Kang, 2007; Missler et al., 2012; Südhof, 2012). However, evidence for the presynaptic requirements of Dnlg2 and Dnlg4 at the *Drosophila* larval NMJ suggests that neuroligins could have novel mechanisms to mediate synaptic functionality (Chen et al., 2012; Zhang et al., 2017b). At the *Drosophila* NMJ, it was recently uncovered that Dnlg4 presynaptically regulates NMJ development through the bone morphogenetic protein (BMP) pathway (Zhang et al., 2017b). Also at the NMJ, one study demonstrates the requirements of Dnlg2 on both the presynaptic motor neuron and the postsynaptic muscle (Chen et al., 2012). It is possible that Dnlg2 may mediate its action through a homophilic or heterophilic mechanism. However, the results from my S2 cell aggregation assay in Chapter 3 demonstrate that Dnlg2 lacks homophilic binding abilities (Fig. 3.7). Different binding partners for pre- and postsynaptic neuroligins could contribute to distinct and independent roles in synapse development and function (i.e. postsynaptic Dnlg2 binds to Dnrx and presynaptic Dnlg2 binds to

another receptor). It would be interesting to determine whether the novel presynaptic requirements for Neuroligins observed in *Drosophila* is evolutionarily conserved in higher organisms such as mice or humans.

Finally, as mentioned previously a ternary complex composed of Nlg2, IgSF9b and S-SCAM was identified at inhibitory postsynaptic terminals (Woo et al., 2013). IgSF9b and Nlg2 are indirectly coupled together through the binding of their cytoplasmic tails to protein binding domains on the synaptic scaffolding molecule (S-SCAM). It would be interesting to determine if this complex observed in mammals may be conserved in *Drosophila* (Woo et al., 2013). Indeed, my results demonstrating a *cis* interaction between Bdl and Dnlg2 support this model, but whether either molecule interacts with a scaffolding molecule like S-SCAM is still to be determined.

In *Drosophila*, the sole homolog of *S-SCAM* is the member of the membrane-associated guanylate kinase inverted (MAGI) family of molecules, *magi* (Zaessinger et al., 2015). Magi is a membrane-associated guanylate kinase (MAGUK) family member, composed of multiple protein-interacting PDZ and WW domains. In mammals, S-SCAM is thought to intracellularly stabilize trans-synaptic adhesion molecules at axo-dendritic contacts. This is exemplified by its coupling of Nlg2 to IgSF9b at inhibitory postsynaptic terminals and Nlg1 to N-cadherin at excitatory postsynaptic terminals (Stan et al., 2010; Woo et al., 2013). Interestingly, Unc-104/Imac/KIF1A has an MAGUK-binding stalk domain (Schnapp et al., 2003). In a recent publication, it was shown that binding of this domain by the AZ protein Lin-2/CASK positively regulates Unc-104 transport in *C. elegans* (Wu et al., 2016). Additionally, S-SCAM was demonstrated to selectively interact with KIF1Bα, a member of the Unc-104/KIF1 family of kinesin motors, in yeast two-hybrid, pull-down, and *in vivo* Co-IP experiments in rat brains (Mok et al., 2002). Interactions with the Imac

MAGUK-binding stalk domain through Magi may be another mechanism by which Dnlg2 and Bdl regulate SV transport in the R8 axon terminal.

4.2 Conclusions

Whether and how synaptogenic adhesion at axo-dendritic contact sites regulates axonal transport of presynaptic components remains unknown. In Chapter 2, I show that the homophilic adhesion molecule, Borderless (Bdl), mediates specific interactions at axo-dendritic contact sites, which is required for up-regulating the Unc-104/Imac/KIF1A motor in promoting axonal transport of synaptic vesicle components for presynaptic assembly and function in R8 photoreceptor axon terminals. In Chapter 3, I provide evidence that interactions between the trans-synaptic adhesion molecules, Bdl and Dnlg2, function cooperatively in promoting axonal transport of synaptic vesicle components for presynaptic assembly.

My thesis work identifies for the first time that a trans-synaptic adhesion molecule mediates specific interactions at axo-dendritic contacts to specifically promote the axonal transport of SV and AZ components for presynaptic assembly and function. In addition, I have provided insights into the interacting molecules and mechanisms underlying how the evolutionarily conserved IgSF9 family of molecules contribute to synaptic function. Recent studies are providing increasing amounts of evidence implicating the Neuroligin and IgSF9 family of molecules in cooperating to coordinate synaptic functionality (Woo et al., 2013; Babaev et al., 2018). Therefore, my work on Bdl and Dngl2 in the *Drosophila* visual system would help elucidate the general mechanisms of how these trans-synaptic adhesion molecules function together in higher organisms.

4.3 Future Directions

4.3.1 What is the pathway that Bdl activates Imac through?

My work provides convincing evidence of Bdl-dependent regulation of Imac in SV localization to the R8 axon terminal. However, the underlying mechanisms and signalling pathways by which Bdl mediates this action remains unclear, with many existing possibilities. Several studies demonstrate that KIF1A is inactivated by an autoinhibitory mechanism (Al-Bassam et al., 2003; Hammond et al., 2009). My results suggest that Bdl regulates SV transport in R8 axonal terminals by relieving the autoinhibition on Imac, allowing it to freely bind and transport cargo.

The SV membrane-bound protein, Arl-8, physically binds and activates Unc-104/KIF1A by unlocking its autoinhibition in *C. elegans* (Takamori et al., 2006; Wu et al., 2013; Niwa et al., 2016). Interestingly, two recent publications have identified that loss of Arl8 disrupts axonal transport in *Drosophila* motor neurons (Rosa-Ferreira et al., 2018; Vukoja et al., 2018). Vukoja et al. demonstrated that Arl8 and Imac colocalize and associate with each other and that the absence of Arl8 results in the accumulation of SV- and AZ-protein-containing vesicles in the neuronal cell bodies (Vukoja et al., 2018). These phenotypes resemble what I observed in the R8 axonal terminals and cell bodies of *bdl* mutants (i.e. mislocalization of nSyb and Brp, respectively) (Fig. 2.1, 2.4). As *arl8* null mutants do not survive past the larval stages, genetic mosaic and tissue-specific RNAi approaches should be employed to determine the potential involvement of Arl8 in R8 SV transport. Additionally, epistasis experiments by generating *bdl/arl8* transheterozygous animals may provide insights on the potential contributions of Arl8 to the Bdl-Imac activation pathway.

In addition to Arl-8, the Unc-104/Imac/KIF1A cargo adaptor and AZ protein, Liprin-α would be of interest to investigate. Work in the *Drosophila* motor neuron has shown that Liprin-α

regulates axonal transport of synaptic material and dense-core vesicles by directly increasing kinesin processivity (Miller et al., 2005; Holbrook et al., 2012). Loss of *liprin-α* and *imac* in R7 photoreceptors both induce a similar R7 layer mistargeting phenotype, with R7s terminating in the R8 target layer (Holbrook et al., 2012). While the layer termination and overall structure of R8 axon terminals appear to be normal in *liprin-α* homozygous mutant eyes, it remains unknown if the loss of *liprin-α* affects SV transport in R8 axons. In the future, it would be of great interest to determine if Liprin-α is a component of the Bdl-dependent pathway that translates the trans-synaptic signal into the activation of Imac for SV transport in R8 axons.

4.3.2 What are the pre- and postsynaptic requirements of neuroligins and neurexins in photoreceptor R8 synaptic vesicle transport?

My work demonstrates the involvement of Dnlg2 in the transport of SV components to the R8 axon terminal. *dnlg2* presynaptic knockdown and null mutant animals display a mislocalization of SVP to the proximal segment of the R8 axon (Fig. 3.2, 3.3). The presynaptic requirement of Dnlg2 is surprising, considering mammalian neuroligins are thought to be restricted to postsynaptic cells (Missler et al., 2012). However, this is not unprecedented with *Drosophila* neuroligins as both Dnlg2 and Dnlg4 have been shown to function in presynaptic motor neurons at the larval NMJ (Chen et al., 2012; Zhang et al., 2017b). In fact, evidence suggests that Dnlg2 is required in both the presynaptic motor neuron and postsynaptic muscles for synaptic functionality (Chen et al., 2012). This raises the possibility that Dnlg2 is required both in the R8 photoreceptor and its postsynaptic targets in the *Drosophila* optic lobes. To address this, future studies would be performed to examine if knocking down *dnlg2* in R8 postsynaptic target neurons in the medulla using the $Ort^{C1\text{-}3}$*-GAL4* driver similarly as described in Chapter 2 (Fig. 2.6), disrupts SV transport in R8 axons. Additionally, transgene rescue experiments can also be performed to examine if

restoring the expression of *dnlg2* in R8 axons and/or postsynaptic targets in *dnlg2* null mutants, rescues the SV phenotype in *dnlg2* mutants.

My results in Chapter 3 demonstrate that Dnlg2 is required in the R8 axon for SV transport, and does not appear to bind trans-synaptically in a homophilic manner to itself or a heterophilic manner to Bdl on postsynaptic target neurons (Fig. 3.2, 3.6, 3.7). I speculate that Dnlg2 on R8 axonal terminals may bind to an unknown cell surface protein on postsynaptic target neurons in the medulla, and thus mediates SV transport in R8 axons (Fig. 3.10). A strong candidate is the classical neuroligin trans-synaptic binding partner, Neurexin (Nrx). *Drosophila* neurexin (*dnrx*) has been implicated in synapse formation in the central nervous system of the adult fly, as well as in synaptic transmission at the larval NMJ (Li et al., 2007; Zeng et al., 2007). Additionally, *dnrx* is highly expressed in cells adjacent to the R7 and R8 axonal terminals, and Co-IP experiments using lysates from adult fly heads demonstrate that Dnl2 and Dnrx interact physically *in vivo* (Sun et al., 2011; Liu et al., 2017). Therefore, it will be important to examine if the loss of Dnrx affects the localization of SV in R8 axonal terminals. Additionally, tissue-specific knockdown approaches can also be used to determine the pre and postsynaptic requirements of Dnrx.

Another avenue of interest to study would be the involvement of other neuroligins. Although Dnlg2 showed up as the strongest hit in our test-candidate approach of all the *Drosophila* neuroligins in Chapter 3 (Fig. 3.2), low-penetrant R8 SV mislocalization phenotypes were observed when *dnlg3* and *dnlg4* were knocked down. It would be of interest to perform loss-of-function analysis to examine if the complete loss of *dnlg3* or *dnlg4* causes a *dnlg2*-like SV phenotype. Additionally, this test-candidate knockdown approach only examined the presynaptic requirements of neuroligins. It will be important to perform postsynaptic knockdown experiments

using the *Ort*$^{C1\text{-}3}$*-GAL4* driver, which may reveal the contributions of Dnlg3 and Dnlg4 in the postsynaptic targets to SV transport in R8 axons.

Finally, in mammals, multiple neuroligins can function together at a single synapse by forming physiologically relevant homodimers and heterodimers (Chanda et al., 2017). Such functional redundancy may make it difficult to reveal the requirements of individual Dnlg in SV transport *in vivo*. Thus, future studies using double or triple knockdown and/or knockout may be necessary to determine if Dnlg2 functions together with Dnlg1, 3 or 4 in mediating SV transport.

4.3.3 What is the nature of the physical interactions between Bdl and Dnlg2 for the control of SV transport in R8 axons?

As discussed previously, the dispensability of the Bdl cytoplasmic tail argues that Bdl may need to interact with other cell-surface proteins, which in turn trigger downstream signalling events leading to the activation and recruitment of Imac in R8 axons for SV transport. My work also suggests that *cis*-interactions between the extracellular domain of Bdl and Dnlg2 is important in the transport of SVs to the R8 axon terminal (Fig. 3.10). Interestingly, it is reported that IgSF9b (i.e. mammalian homolog of Bdl) associates with mammalian Nlg2 in *cis* on the postsynaptic side of inhibitory synapses (Woo et al., 2013). However, the formation of this Nlg2 and IgSF9b complex is not mediated by direct binding between Nlg2 and IgSF9b, and instead, Nlg2 and IgSF9b are coupled together by the synaptic scaffolding molecule S-SCAM (Woo et al., 2013).

While my results in Chapter 3 suggest strongly that Bdl and Dnlg2 interact physically and genetically in regulating SV transport in R8 axons, it remains unknown if Bdl binds directly to Dnlg2, or indirectly by binding to a Dnlg2-interacting intermediate protein. In the future, it will be necessary to perform biochemical analysis to examine if Bdl binds to Dnlg2 directly. Molecular

and genetic experiments should be performed to determine the domain requirements for the binding between Bdl and Dnlg2 and their function in SV transport.

If the association of Bdl and Dnlg2 is not mediated by direct Bdl-Dnlg2 binding, it will be important to determine the identity of the intermediate protein that directly couples Bdl and Dnlg2 in the complex. Since the cytoplasmic domain of Bdl is dispensable for its association with Dnlg2, the likely intermediate protein would be a Dnlg2-interacting cell-surface protein that binds directly to the ectodomain of Bdl. Future biochemical and molecular studies (e.g. Co-IP, yeast two-hybrid) will help identify the intermediate protein that directly couples Bdl and Dnlg2 in the complex.

While in mammals, Nlg2 and IgSF9b have been shown to form a complex with the cytoplasmic synaptic scaffolding molecule S-SCAM *in vitro* (Woo et al., 2013), it remains unknown if Magi, the sole homolog of mammalian S-SCAM in *Drosophila*, also forms a complex with Dnlg2 and Bdl in R8 axons. The S-SCAM/MAGI family of molecules have been demonstrated to bind and stabilize several trans-synaptic adhesion molecules through their cytoplasmic tail, such as neuroligins (Stan et al., 2010; Woo et al., 2013). The *Drosophila* homolog of S-SCAM, Magi, is a molecular scaffold with one WW and four PDZ protein-protein interaction domains, and has recently been demonstrated to regulate E-Cadherin-based adherens junctions in the developing eye (Zaessinger et al., 2015). It would, therefore, be of great interest to perform knockdown and loss-of-function experiments to examine if Magi is required for SV transport in R8 axons. If so, further biochemical, molecular and genetic studies will be performed to determine if Magi functions in the Bdl-Dnlg2 pathway for axonal transport of SV components in R8 axons.

Reference List

Ackermann F, Waites CL, Garner CC (2015) Presynaptic active zones in invertebrates and vertebrates. EMBO Rep 16:923–938.

Ackley BD, Harrington RJ, Hudson ML, Williams L, Kenyon CJ, Chisholm AD, Jin Y (2005) The Two Isoforms of the Caenorhabditis elegans Leukocyte-Common Antigen Related Receptor Tyrosine Phosphatase PTP-3 Function Independently in Axon Guidance and Synapse Formation. J Neurosci 25:7517–7528.

Ahmari SE, Buchanan J, Smith SJ (2000) Assembly of presynaptic active zones from cytoplasmic transport packets. Nat Neurosci 3:445–451.

Akin O, Zipursky SL (2016) Frazzled promotes growth cone attachment at the source of a Netrin gradient in the Drosophila visual system. Elife 5.

Al-Bassam J, Cui Y, Klopfenstein D, Carragher BO, Vale RD, Milligan RA (2003) Distinct conformations of the kinesin Unc104 neck regulate a monomer to dimer motor transition. J Cell Biol 163:743–753.

Altrock WD et al. (2003) Functional inactivation of a fraction of excitatory synapses in mice deficient for the active zone protein bassoon. Neuron 37:787–800.

Araç D, Boucard AA, Özkan E, Strop P, Newell E, Südhof TC, Brunger AT (2007) Structures of Neuroligin-1 and the Neuroligin-1/Neurexin-1β Complex Reveal Specific Protein-Protein and Protein-Ca2+ Interactions. Neuron 56:992–1003.

Aravamudan B, Fergestad T, Davis WS, Rodesch CK, Broadie K (1999) Drosophila Unc-13 is essential for synaptic transmission. Nat Neurosci 2:965–971.

Augustin I, Rosenmund C, Südhof TC, Brose N (1999) Munc13-1 is essential for fusion competence of glutamatergic synaptic vesicles. Nature 400:457–461.

Augustine GJ, Charlton MP, Smith SJ (1987) Calcium Action in Synaptic Transmitter Release. Annu Rev Neurosci 10:633–693.

Baas PW, Deitch JS, Black MM, Banker GA (1988) Polarity orientation of microtubules in hippocampal neurons: uniformity in the axon and nonuniformity in the dendrite. Proc Natl Acad Sci 85:8335–8339.

Babaev O, Cruces-Solis H, Piletti Chatain C, Hammer M, Wenger S, Ali H, Karalis N, de Hoz L, Schlüter OM, Yanagawa Y, Ehrenreich H, Taschenberger H, Brose N, Krueger-Burg D (2018) IgSF9b regulates anxiety behaviors through effects on centromedial amygdala inhibitory synapses. Nat Commun 9:5400.

Banovic D, Khorramshahi O, Owald D, Wichmann C, Riedt T, Fouquet W, Tian R, Sigrist SJ, Aberle H (2010) Drosophila Neuroligin 1 Promotes Growth and Postsynaptic Differentiation at Glutamatergic Neuromuscular Junctions. Neuron 66:724–738.

Barkus R V, Klyachko O, Horiuchi D, Dickson BJ, Saxton WM (2008) Identification of an axonal kinesin-3 motor for fast anterograde vesicle transport that facilitates retrograde

transport of neuropeptides. Linstedt A, ed. Mol Biol Cell 19:274–283.

Basu J, Shen N, Dulubova I, Lu J, Guan R, Guryev O, Grishin N V, Rosenmund C, Rizo J (2005) A minimal domain responsible for Munc13 activity. Nat Struct Mol Biol 12:1017–1018.

Behnia R, Desplan C (2015) Visual circuits in flies: beginning to see the whole picture. Curr Opin Neurobiol 34:125–132.

Bellen HJ, Levis RW, He Y, Carlson JW, Evans-Holm M, Bae E, Kim J, Metaxakis A, Savakis C, Schulze KL, Hoskins RA, Spradling AC (2011) The Drosophila gene disruption project: progress using transposons with distinctive site specificities. Genetics 188:731–743.

Bellen HJ, Levis RW, Liao G, He Y, Carlson JW, Tsang G, Evans-Holm M, Hiesinger PR, Schulze KL, Rubin GM, Hoskins RA, Spradling AC (2004) The BDGP gene disruption project: single transposon insertions associated with 40% of Drosophila genes. Genetics 167:761–781.

Bennett MK, Calakos N, Scheller RH (1992) Syntaxin: a synaptic protein implicated in docking of synaptic vesicles at presynaptic active zones. Science 257:255–259.

Benson DL, Colman DR, Huntley GW (2001) Molecules, maps and synapse specificity. Nat Rev Neurosci 2:899–909.

Berger-Müller S, Sugie A, Takahashi F, Tavosanis G, Hakeda-Suzuki S, Suzuki T (2013) Assessing the role of cell-surface molecules in central synaptogenesis in the Drosophila visual system. Chien C-T, ed. PLoS One 8:e83732.

Biederer T, Südhof TC (2000) Mints as Adaptors. J Biol Chem 275:39803–39806.

Bodily KD, Morrison CM, Renden RB, Broadie K, Stein V, Klein R (2001) A novel member of the Ig superfamily, turtle, is a CNS-specific protein required for coordinated motor control. J Neurosci 21:3113–3125.

Böhme MA, Beis C, Reddy-Alla S, Reynolds E, Mampell MM, Grasskamp AT, Lützkendorf J, Bergeron DD, Driller JH, Babikir H, Göttfert F, Robinson IM, O'Kane CJ, Hell SW, Wahl MC, Stelzl U, Loll B, Walter AM, Sigrist SJ (2016) Active zone scaffolds differentially accumulate Unc13 isoforms to tune Ca2+ channel–vesicle coupling. Nat Neurosci 19:1311–1320.

Borst A (2014) In search of the holy grail of fly motion vision. Eur J Neurosci 40:3285–3293.

Bourne JN, Harris KM (2008) Balancing Structure and Function at Hippocampal Dendritic Spines. Annu Rev Neurosci 31:47–67.

Broadie KS, Bate M (1993) Development of the embryonic neuromuscular synapse of Drosophila melanogaster. J Neurosci 13:144–166.

Brose N, Hofmann K, Hata Y, Südhof TC (1995) Mammalian Homologues of *Caenorhabditis elegans unc-13* Gene Define Novel Family of C $_2$ -domain Proteins. J Biol Chem 270:25273–25280.

Bruckner JJ, Gratz SJ, Slind JK, Geske RR, Cummings AM, Galindo SE, Donohue LK,

O'Connor-Giles KM (2012) Fife, a Drosophila Piccolo-RIM Homolog, Promotes Active Zone Organization and Neurotransmitter Release. J Neurosci 32:17048–17058.

Budreck E, Scheiffele P (2007) Neuroligin-3 is a neuronal adhesion protein at GABAergic and glutamatergic synapses. Eur J Neurosci.

Burton PR, Paige JL (1981) Polarity of axoplasmic microtubules in the olfactory nerve of the frog. Proc Natl Acad Sci 78:3269–3273.

Bury LA, Sabo SL (2014) Dynamic mechanisms of neuroligin-dependent presynaptic terminal assembly in living cortical neurons. Neural Dev 9:13.

Bury LAD, Sabo SL (2016) Building a Terminal. Neurosci 22:372–391.

Bykhovskaia M, Vasin A (2017) Electrophysiological Analysis of Synaptic Transmission in Drosophila. Wiley Interdiscip Rev Dev Biol 6.

Byrd DT, Kawasaki M, Walcoff M, Hisamoto N, Matsumoto K, Jin Y (2001) UNC-16, a JNK-signaling scaffold protein, regulates vesicle transport in C. elegans. Neuron 32:787–800.

Cajal S, Sanchez D (1915) Contribucion al conocimiento de los centros nerviosos de los insectos (Madrid: Imprenta de Hijos de Nicholas Moja).

Cameron S, Chang W-T, Chen Y, Zhou Y, Taran S, Rao Y (2013) Visual Circuit Assembly Requires Fine Tuning of the Novel Ig Transmembrane Protein Borderless. J Neurosci 33:17413–17421.

Cameron S, Chen Y, Rao Y (2016) Borderless regulates glial extension and axon ensheathment. Dev Biol 414:170–180.

Castillo PE, Schoch S, Schmitz F, Südhof TC, Malenka RC (2002) RIM1α is required for presynaptic long-term potentiation. Nature 415:327–330.

Castle MJ, Perlson E, Holzbaur EL, Wolfe JH (2014) Long-distance Axonal Transport of AAV9 Is Driven by Dynein and Kinesin-2 and Is Trafficked in a Highly Motile Rab7-positive Compartment. Mol Ther 22:554–566.

Chanda S, Hale WD, Zhang B, Wernig M, Südhof TC (2017) Unique vs. Redundant Functions of Neuroligin Genes in Shaping Excitatory and Inhibitory Synapse Properties. J Neurosci 37:0125–17.

Chen P-L, Clandinin TR (2008) The Cadherin Flamingo Mediates Level-Dependent Interactions that Guide Photoreceptor Target Choice in Drosophila. Neuron 58:26–33.

Chen X, Nelson CD, Li X, Winters CA, Azzam R, Sousa AA, Leapman RD, Gainer H, Sheng M, Reese TS (2011) PSD-95 is required to sustain the molecular organization of the postsynaptic density. J Neurosci 31:6329–6338.

Chen Y-C, Lin YQ, Banerjee S, Venken K, Li J, Ismat A, Chen K, Duraine L, Bellen HJ, Bhat MA (2012) Drosophila Neuroligin 2 is Required Presynaptically and Postsynaptically for Proper Synaptic Differentiation and Synaptic Transmission. J Neurosci 32:16018–16030.

Chen Y, Akin O, Nern A, Tsui CYKYK, Pecot MY, Zipursky SLL (2014) Cell-type-Specific

Labeling of Synapses In Vivo through Synaptic Tagging with Recombination. Neuron 81:280–293.

Chen Y, Cameron S, Chang W-T, Rao Y (2017) Turtle interacts with borderless in regulating glial extension and axon ensheathment. Mol Brain 10:17.

Chia PH, Li P, Shen K (2013) Cellular and molecular mechanisms underlying presynapse formation. J Cell Biol 203:11–22.

Chih B, Engelman H, Scheiffele P (2005) Control of Excitatory and Inhibitory Synapse Formation by Neuroligins. Science (80-) 307.

Cho KO, Hunt CA, Kennedy MB (1992) The rat brain postsynaptic density fraction contains a homolog of the Drosophila discs-large tumor suppressor protein. Neuron 9:929–942.

Choii G, Ko J (2015) Gephyrin: a central GABAergic synapse organizer. Exp Mol Med 47:e158–e158.

Clandinin TR, Lee C-HH, Herman T, Lee RC, Yang AY, Ovasapyan S, Zipursky SLL (2001) Drosophila LAR Regulates R1-R6 and R7 Target Specificity in the Visual System. Neuron 32:237–248.

Clandinin TR, Zipursky SL (2000) Afferent Growth Cone Interactions Control Synaptic Specificity in the Drosophila Visual System. Neuron 28:427–436.

Clandinin TR, Zipursky SL (2002) Making Connections in the Fly Visual System. Neuron 35:827–841.

Cooper MW, Smith SJ (1992) A real-time analysis of growth cone-target cell interactions during the formation of stable contacts between hippocampal neurons in culture. J Neurobiol 23:814–828.

Couteaux R, Pécot-Dechavassine M (1970) Synaptic vesicles and pouches at the level of “active zones” of the neuromuscular junction. C R Acad Sci Hebd Seances Acad Sci D 271:2346–2349.

Craig AM, Kang Y (2007) Neurexin–neuroligin signaling in synapse development. Curr Opin Neurobiol 17:43–52.

Dai Y, Taru H, Deken SL, Grill B, Ackley B, Nonet ML, Jin Y (2006) SYD-2 Liprin-α organizes presynaptic active zone formation through ELKS. Nat Neurosci 9:1479–1487.

de Vries SEJ, Clandinin TR (2012) Loom-Sensitive Neurons Link Computation to Action in the Drosophila Visual System. Curr Biol 22:353–362.

Dean C, Scholl FG, Choih J, DeMaria S, Berger J, Isacoff E, Scheiffele P (2003) Neurexin mediates the assembly of presynaptic terminals. Nat Neurosci 6:708–716.

del Castillo J, Katz B (1954) Quantal components of the end-plate potential. J Physiol 124:560–573.

Deng L, Kaeser PS, Xu W, Südhof TC (2011) RIM Proteins Activate Vesicle Priming by Reversing Autoinhibitory Homodimerization of Munc13. Neuron 69:317–331.

Dolph P, Nair A, Raghu P (2011) Electroretinogram Recordings of Drosophila. Cold Spring Harb Protoc 2011:pdb.prot5549.

Dor T, Cinnamon Y, Raymond L, Shaag A, Bouslam N, Bouhouche A, Gaussen M, Meyer V, Durr A, Brice A, Benomar A, Stevanin G, Schuelke M, Edvardson S (2014) *KIF1C* mutations in two families with hereditary spastic paraparesis and cerebellar dysfunction. J Med Genet 51:137–142.

Duffy JB (2002) GAL4 system indrosophila: A fly geneticist's swiss army knife. genesis 34:1–15.

Ehmann N, Owald D, Kittel RJ (2018) Drosophila active zones: From molecules to behaviour. Neurosci Res 127:14–24.

Elegheert J, Cvetkovska V, Clayton AJ, Heroven C, Vennekens KM, Smukowski SN, Regan MC, Jia W, Smith AC, Furukawa H, Savas JN, de Wit J, Begbie J, Craig AM, Aricescu AR (2017) Structural Mechanism for Modulation of Synaptic Neuroligin-Neurexin Signaling by MDGA Proteins. Neuron 95:896-913.e10.

Erlich Y, Edvardson S, Hodges E, Zenvirt S, Thekkat P, Shaag A, Dor T, Hannon GJ, Elpeleg O (2011) Exome sequencing and disease-network analysis of a single family implicate a mutation in KIF1A in hereditary spastic paraparesis. Genome Res 21:658–664.

Espeut J, Gaussen A, Bieling P, Morin V, Prieto S, Fesquet D, Surrey T, Abrieu A (2008) Phosphorylation relieves autoinhibition of the kinetochore motor Cenp-E. Mol Cell 29:637–643.

Estes PS, Ho GL, Narayanan R, Ramaswami M (2000) Synaptic localization and restricted diffusion of a Drosophila neuronal synaptobrevin--green fluorescent protein chimera in vivo. J Neurogenet 13:233–255.

Fabbri C, Serretti A (2017) Role of 108 schizophrenia-associated loci in modulating psychopathological dimensions in schizophrenia and bipolar disorder. Am J Med Genet Part B Neuropsychiatr Genet 174:757–764.

Farrow K, Haag J, Borst A (2003) Input organization of multifunctional motion-sensitive neurons in the blowfly. J Neurosci 23:9805–9811.

Fatt P, Katz B (1952) Spontaneous subthreshold activity at motor nerve endings. J Physiol 117:109–128.

Feng W, Zhang M (2009) Organization and dynamics of PDZ-domain-related supramodules in the postsynaptic density. Nat Rev Neurosci 10:87–99.

Fenster SD, Chung WJ, Zhai R, Cases-Langhoff C, Voss B, Garner AM, Kaempf U, Kindler S, Gundelfinger ED, Garner CC (2000) Piccolo, a presynaptic zinc finger protein structurally related to bassoon. Neuron 25:203–214.

Ferguson K, Long H, Cameron S, Chang W-T, Rao Y (2009) The Conserved Ig Superfamily Member Turtle Mediates Axonal Tiling in Drosophila. J Neurosci 29:14151–14159.

Fernandez I, Araç D, Ubach J, Gerber SH, Shin O, Gao Y, Anderson RG, Südhof TC, Rizo J

(2001) Three-dimensional structure of the synaptotagmin 1 C2B-domain: synaptotagmin 1 as a phospholipid binding machine. Neuron 32:1057–1069.

Fischbach K-F, Dittrich APM (1989) The optic lobe of Drosophila melanogaster. I. A Golgi analysis of wild-type structure. Cell Tissue Res 258:441–475.

Fortini ME, Skupski MP, Boguski MS, Hariharan IK (2000) A survey of human disease gene counterparts in the Drosophila genome. J Cell Biol 150:F23-30.

Fouquet W, Owald D, Wichmann C, Mertel S, Depner H, Dyba M, Hallermann S, Kittel RJ, Eimer S, Sigrist SJ (2009) Maturation of active zone assembly by Drosophila Bruchpilot. J Cell Biol 186:129–145.

Fritschy J-M, Harvey RJ, Schwarz G (2008) Gephyrin: where do we stand, where do we go? Trends Neurosci 31:257–264.

Fröhlich A, Meinertzhagen IA (1983) Quantitative features of synapse formation in the fly's visual system. I. The presynaptic photoreceptor terminal. J Neurosci 3:2336–2349.

Funke L, Dakoji S, Bredt DS (2005) Membrane-Associated Guanylate Kinases Regulate Adhesion and Plasticity at Cell Junctions. Annu Rev Biochem 74:219–245.

Gangwar SP, Zhong X, Seshadrinathan S, Chen H, Machius M, Rudenko G (2017) Molecular Mechanism of MDGA1: Regulation of Neuroligin 2:Neurexin Trans-synaptic Bridges. Neuron 94:1132-1141.e4.

Gao S, Takemura S-Y, Ting C-Y, Huang S, Lu Z, Luan H, Rister J, Thum AS, Yang M, Hong S-T, Wang JW, Odenwald WF, White BH, Meinertzhagen IA, Lee C-H (2008) The neural substrate of spectral preference in Drosophila. Neuron 60:328–342.

Garner CC, Zhai RG, Gundelfinger ED, Ziv NE (2002) Molecular mechanisms of CNS synaptogenesis. Trends Neurosci 25:243–250.

Gerber SH, Rah J-C, Min S-W, Liu X, de Wit H, Dulubova I, Meyer AC, Rizo J, Arancillo M, Hammer RE, Verhage M, Rosenmund C, Südhof TC (2008) Conformational Switch of Syntaxin-1 Controls Synaptic Vesicle Fusion. Science (80-) 321:1507–1510.

Glater EE, Megeath LJ, Stowers RS, Schwarz TL (2006) Axonal transport of mitochondria requires milton to recruit kinesin heavy chain and is light chain independent. J Cell Biol 173:545–557.

Gokce O, Südhof TC (2013) Membrane-Tethered Monomeric Neurexin LNS-Domain Triggers Synapse Formation. J Neurosci 33:14617–14628.

Goldstein AYN, Wang X, Schwarz TL (2008) Axonal transport and the delivery of pre-synaptic components. Curr Opin Neurobiol 18:495–503.

Gracheva EO, Hadwiger G, Nonet ML, Richmond JE (2008) Direct interactions between C. elegans RAB-3 and Rim provide a mechanism to target vesicles to the presynaptic density. Neurosci Lett 444:137–142.

Graf ER, Daniels RW, Burgess RW, Schwarz TL, DiAntonio A (2009) Rab3 Dynamically Controls Protein Composition at Active Zones. Neuron 64:663–677.

Graf ER, Valakh V, Wright CM, Wu C, Liu Z, Zhang YQ, DiAntonio A (2012) RIM Promotes Calcium Channel Accumulation at Active Zones of the Drosophila Neuromuscular Junction. J Neurosci 32:16586–16596.

Graf ER, Zhang X, Jin S-X, Linhoff MW, Craig AM (2004) Neurexins Induce Differentiation of GABA and Glutamate Postsynaptic Specializations via Neuroligins. Cell 119:1013–1026.

Gray E (1963) Electron microscopy of presynaptic organelles of the spinal cord. J Anat 97:101–106.

Gray EG (1959) Axo-somatic and axo-dendritic synapses of the cerebral cortex: an electron microscope study. J Anat 93:420–433.

Griffin JW, Price DL, Drachman DB, Engel WK (1976) Axonal Transport to and from the Motor Nerve Ending. Ann N Y Acad Sci 274:31–45.

Haag J, Borst A (2008) Electrical Coupling of Lobula Plate Tangential Cells to a Heterolateral Motion-Sensitive Neuron in the Fly. J Neurosci 28:14435–14442.

Hackney DD (1994) Evidence for alternating head catalysis by kinesin during microtubule-stimulated ATP hydrolysis. Proc Natl Acad Sci 91:6865–6869.

Hakeda-Suzuki S, Berger-Müller S, Tomasi T, Usui T, Horiuchi S, Uemura T, Suzuki T (2011) Golden Goal collaborates with Flamingo in conferring synaptic-layer specificity in the visual system. Nat Neurosci 14:314–323.

Hakeda-Suzuki S, Suzuki T (2014) Cell surface control of the layer specific targeting in the Drosophila visual system. Genes Genet Syst 89:9–15.

Hall DH, Hedgecock EM (1991) Kinesin-related gene unc-104 is required for axonal transport of synaptic vesicles in C. elegans. Cell 65:837–847.

Hallermann S, Fejtova A, Schmidt H, Weyhersmüller A, Silver RA, Gundelfinger ED, Eilers J (2010a) Bassoon Speeds Vesicle Reloading at a Central Excitatory Synapse. Neuron 68:710–723.

Hallermann S, Heckmann M, Kittel RJ (2010b) Mechanisms of short-term plasticity at neuromuscular active zones of *Drosophila*. HFSP J 4:72–84.

Hamdan FF et al. (2011) Excess of De Novo Deleterious Mutations in Genes Associated with Glutamatergic Systems in Nonsyndromic Intellectual Disability. Am J Hum Genet 88:306–316.

Hammond JW, Cai D, Blasius TL, Li Z, Jiang Y, Jih GT, Meyhofer E, Verhey KJ (2009) Mammalian Kinesin-3 motors are dimeric in vivo and move by processive motility upon release of autoinhibition. Schliwa M, ed. PLoS Biol 7:e72.

Han K, Kim E (2008) Synaptic adhesion molecules and PSD-95. Prog Neurobiol 84:263–283.

Han Y, Kaeser PS, Südhof TC, Schneggenburger R (2011) RIM Determines Ca2+ Channel Density and Vesicle Docking at the Presynaptic Active Zone. Neuron 69:304–316.

Hansen M, Walmod PS (2013) IGSF9 Family Proteins. Neurochem Res 38:1236–1251.

Hardie RC (1979) Electrophysiological analysis of fly retina. I: Comparative properties of R1-6 and R 7 and 8. J Comp Physiol 129:19–33.

Hata Y, Butz S, Südhof TC (1996) CASK: a novel dlg/PSD95 homolog with an N-terminal calmodulin-dependent protein kinase domain identified by interaction with neurexins. J Neurosci 16:2488–2494.

Hata Y, Slaughter CA, Südhof TC (1993) Synaptic vesicle fusion complex contains unc-18 homologue bound to syntaxin. Nature 366:347–351.

Hendricks AG, Perlson E, Ross JL, Schroeder HW, Tokito M, Holzbaur ELF (2010) Motor Coordination via a Tug-of-War Mechanism Drives Bidirectional Vesicle Transport. Curr Biol 20:697–702.

Heuser JE, Reese TS (1973) Evidence for Recycling of Synaptic Vesicle Membrane during Transmitter Release at the Frog Neuromuscular Junction. J Cell Biol 57:315–344.

Heuser JE, Reese TS, Dennis MJ, Jan Y, Jan L, Evans L (1979) Synaptic vesicle exocytosis captured by quick freezing and correlated with quantal transmitter release. J Cell Biol 81:275–300.

Hirokawa N (1998) Kinesin and dynein superfamily proteins and the mechanism of organelle transport. Science 279:519–526.

Hirokawa N, Niwa S, Tanaka Y (2010) Molecular Motors in Neurons: Transport Mechanisms and Roles in Brain Function, Development, and Disease. Neuron 68:610–638.

Hirokawa N, Takemura R (2005) Molecular motors and mechanisms of directional transport in neurons. Nat Rev Neurosci 6:201–214.

Hofbauer A, Campos-Ortega JA (1990) Proliferation pattern and early differentiation of the optic lobes in Drosophila melanogaster. Roux's Arch Dev Biol 198:264–274.

Holbrook S, Finley JK, Lyons EL, Herman TG (2012) Loss of syd-1 from R7 neurons disrupts two distinct phases of presynaptic development. J Neurosci 32:18101–18111.

Hotta Y, Benzer S (1970) Genetic dissection of the Drosophila nervous system by means of mosaics. Proc Natl Acad Sci U S A 67:1156–1163.

Hsu C-C, Moncaleano JD, Wagner OI (2011) Sub-cellular distribution of UNC-104(KIF1A) upon binding to adaptors as UNC-16(JIP3), DNC-1(DCTN1/Glued) and SYD-2(Liprin-α) in C. elegans neurons. Neuroscience 176:39–52.

Huo L, Yue Y, Ren J, Yu J, Liu J, Yu Y, Ye F, Xu T, Zhang M, Feng W (2012) The CC1-FHA Tandem as a Central Hub for Controlling the Dimerization and Activation of Kinesin-3 KIF1A. Structure 20:1550–1561.

Ichtchenko K, Hata Y, Nguyen T, Ullrich B, Missler M, Moomaw C, Südhof TC (1995) Neuroligin 1: A splice site-specific ligand for β-neurexins. Cell 81:435–443.

Irie M, Hata Y, Takeuchi M, Ichtchenko K, Toyoda A, Hirao K, Takai Y, Rosahl TW, Südhof TC (1997) Binding of neuroligins to PSD-95. Science 277:1511–1515.

Jacob TC, Moss SJ, Jurd R (2008) GABAA receptor trafficking and its role in the dynamic modulation of neuronal inhibition. Nat Rev Neurosci 9:331–343.

Jagadish S, Barnea G, Clandinin TR, Axel R (2014) Identifying Functional Connections of the Inner Photoreceptors in Drosophila using Tango-Trace. Neuron 83:630–644.

Jiao W, Masich S, Franzén O, Shupliakov O (2010) Two pools of vesicles associated with the presynaptic cytosolic projection in Drosophila neuromuscular junctions. J Struct Biol 172:389–394.

Joesch M, Plett J, Borst A, Reiff DF (2008) Response Properties of Motion-Sensitive Visual Interneurons in the Lobula Plate of Drosophila melanogaster. Curr Biol 18:368–374.

Juusola M, French AS, Uusitalo RO, Weckström M (1996) Information processing by graded-potential transmission through tonically active synapses. Trends Neurosci 19:292–297.

Kaeser PS, Deng L, Wang Y, Dulubova I, Liu X, Rizo J, Südhof TC (2011) RIM Proteins Tether Ca2+ Channels to Presynaptic Active Zones via a Direct PDZ-Domain Interaction. Cell 144:282–295.

Kaufmann N, DeProto J, Ranjan R, Wan H, Van Vactor D (2002) Drosophila Liprin-α and the Receptor Phosphatase Dlar Control Synapse Morphogenesis. Neuron 34:27–38.

Kelliher MT, Saunders HA, Wildonger J (2019) Microtubule control of functional architecture in neurons. Curr Opin Neurobiol 57:39–45.

Kern J V, Zhang Y V, Kramer S, Brenman JE, Rasse TM (2013) The kinesin-3, unc-104 regulates dendrite morphogenesis and synaptic development in Drosophila. Genetics 195:59–72.

Kerwin SK, Li JSS, Noakes PG, Shin GJ, Millard SS (2018) Regulated Alternative Splicing of *Drosophila Dscam2* Is Necessary for Attaining the Appropriate Number of Photoreceptor Synapses. Genetics 208:717–728.

Kim E, Naisbitt S, Hsueh YP, Rao A, Rothschild A, Craig AM, Sheng M (1997) GKAP, a novel synaptic protein that interacts with the guanylate kinase-like domain of the PSD-95/SAP90 family of channel clustering molecules. J Cell Biol 136:669–678.

Kim E, Sheng M (2004) PDZ domain proteins of synapses. Nat Rev Neurosci 5:771–781.

Kittel RJ, Heckmann M (2016) Synaptic Vesicle Proteins and Active Zone Plasticity. Front Synaptic Neurosci 8:8.

Kittel RJ, Wichmann C, Rasse TM, Fouquet W, Schmidt M, Schmid A, Wagh DA, Pawlu C, Kellner RR, Willig KI, Hell SW, Buchner E, Heckmann M, Sigrist SJ (2006) Bruchpilot promotes active zone assembly, Ca2+ channel clustering, and vesicle release. Science 312:1051–1054.

Klassen MP, Wu YE, Maeder CI, Nakae I, Cueva JG, Lehrman EK, Tada M, Gengyo-Ando K, Wang GJ, Goodman M, Mitani S, Kontani K, Katada T, Shen K (2010) An Arf-like Small G Protein, ARL-8, Promotes the Axonal Transport of Presynaptic Cargoes by Suppressing Vesicle Aggregation. Neuron 66:710–723.

Klebe S et al. (2012) KIF1A missense mutations in SPG30, an autosomal recessive spastic paraplegia: distinct phenotypes according to the nature of the mutations. Eur J Hum Genet 20:645–649.

Kleele T, Marinković P, Williams PR, Stern S, Weigand EE, Engerer P, Naumann R, Hartmann J, Karl RM, Bradke F, Bishop D, Herms J, Konnerth A, Kerschensteiner M, Godinho L, Misgeld T (2014) An assay to image neuronal microtubule dynamics in mice. Nat Commun 5:4827.

Knight D, Xie W, Boulianne GL (2011) Neurexins and neuroligins: recent insights from invertebrates. Mol Neurobiol 44:426–440.

Knott GW, Quairiaux C, Genoud C, Welker E (2002) Formation of dendritic spines with GABAergic synapses induced by whisker stimulation in adult mice. Neuron 34:265–273.

Koenig JH, Ikeda K (1996) Synaptic vesicles have two distinct recycling pathways. J Cell Biol 135:797–808.

Kondo M, Takei Y, Hirokawa N (2012) Motor Protein KIF1A Is Essential for Hippocampal Synaptogenesis and Learning Enhancement in an Enriched Environment. Neuron 73:743–757.

Koushika SP, Richmond JE, Hadwiger G, Weimer RM, Jorgensen EM, Nonet ML (2001) A post-docking role for active zone protein Rim. Nat Neurosci 4:997–1005.

Kraszewski K, Mundigl O, Daniell L, Verderio C, Matteoli M, De Camilli P (1995) Synaptic vesicle dynamics in living cultured hippocampal neurons visualized with CY3-conjugated antibodies directed against the lumenal domain of synaptotagmin. J Neurosci 15:4328–4342.

Kreutzberg GW (1969) Neuronal Dynamics and Axonal Flow, IV. Blockage of Intra-Axonal Enzyme Transport by Colchicine. Proc Natl Acad Sci 62:722–728.

Krueger-Burg D, Papadopoulos T, Brose N (2017) Organizers of inhibitory synapses come of age. Curr Opin Neurobiol 45:66–77.

Kumar JP (2012) Building an ommatidium one cell at a time. Dev Dyn 241:136–149.

Kursula P (2019) Shanks — multidomain molecular scaffolds of the postsynaptic density. Curr Opin Struct Biol 54:122–128.

Kuta A, Deng W, Morsi El-Kadi A, Banks GT, Hafezparast M, Pfister KK, Fisher EMC (2010) Mouse Cytoplasmic Dynein Intermediate Chains: Identification of New Isoforms, Alternative Splicing and Tissue Distribution of Transcripts Cookson MR, ed. PLoS One 5:e11682.

Kwan AC, Dombeck DA, Webb WW (2008) Polarized microtubule arrays in apical dendrites and axons. Proc Natl Acad Sci 105:11370–11375.

Lah GJ, Li JSS, Millard SS (2014) Cell-Specific Alternative Splicing of Drosophila Dscam2 Is Crucial for Proper Neuronal Wiring. Neuron 83:1376–1388.

Landgraf M, Jeffrey V, Fujioka M, Jaynes JB, Bate M (2003) Embryonic Origins of a Motor

System: Motor Dendrites Form a Myotopic Map in Drosophila Thomas M. Jessell, ed. PLoS Biol 1:e41.

Langen M, Agi E, Altschuler DJ, Wu LF, Altschuler SJ, Hiesinger PR (2015) The Developmental Rules of Neural Superposition in Drosophila. Cell 162:120–133.

Laughlin SB, de Ruyter van Steveninck RR, Anderson JC (1998) The metabolic cost of neural information. Nat Neurosci 1:36–41.

Lee C-H, Herman T, Clandinin TR, Lee R, Zipursky SLL (2001) N-Cadherin Regulates Target Specificity in the Drosophila Visual System. Neuron 30:437–450.

Lee K, Kim Y, Lee S-J, Qiang Y, Lee D, Lee HW, Kim H, Je HS, Sudhof TC, Ko J (2013) MDGAs interact selectively with neuroligin-2 but not other neuroligins to regulate inhibitory synapse development. Proc Natl Acad Sci 110:336–341.

Lee RC, Clandinin TR, Lee C-H, Chen P-L, Meinertzhagen IA, Zipursky SL (2003) The protocadherin Flamingo is required for axon target selection in the Drosophila visual system. Nat Neurosci 6:557–563.

Li J, Ashley J, Budnik V, Bhat MA (2007) Crucial Role of Drosophila Neurexin in Proper Active Zone Apposition to Postsynaptic Densities, Synaptic Growth, and Synaptic Transmission. Neuron 55:741–755.

Li Y, Zhou Z, Zhang X, Tong H, Li P, Zhang ZC, Jia Z, Xie W, Han J (2013) Drosophila neuroligin 4 regulates sleep through modulating GABA transmission. J Neurosci 33:15545–15554.

Limbach C, Laue MM, Wang X, Hu B, Thiede N, Hultqvist G, Kilimann MW (2011) Molecular in situ topology of Aczonin/Piccolo and associated proteins at the mammalian neurotransmitter release site. Proc Natl Acad Sci 108:E392–E401.

Lin T-Y, Luo J, Shinomiya K, Ting C-Y, Lu Z, Meinertzhagen IA, Lee C-H (2016) Mapping chromatic pathways in the *Drosophila* visual system. J Comp Neurol 524:213–227.

Liu KSY, Siebert M, Mertel S, Knoche E, Wegener S, Wichmann C, Matkovic T, Muhammad K, Depner H, Mettke C, Buckers J, Hell SW, Muller M, Davis GW, Schmitz D, Sigrist SJ (2011) RIM-Binding Protein, a Central Part of the Active Zone, Is Essential for Neurotransmitter Release. Science (80-) 334:1565–1569.

Liu L, Tian Y, Zhang X, Zhang X, Li T, Xie W, Han J (2017) Neurexin Restricts Axonal Branching in Columns by Promoting Ephrin Clustering. Dev Cell 41:94-106.e4.

Lo KY, Kuzmin A, Unger SM, Petersen JD, Silverman MA (2011) KIF1A is the primary anterograde motor protein required for the axonal transport of dense-core vesicles in cultured hippocampal neurons. Neurosci Lett 491:168–173.

Long H, Ou Y, Rao Y, van Meyel DJ (2009) Dendrite branching and self-avoidance are controlled by Turtle, a conserved IgSF protein in Drosophila. Development 136:3475–3484.

Lüscher B, Keller CA (2004) Regulation of GABAA receptor trafficking, channel activity, and functional plasticity of inhibitory synapses. Pharmacol Ther 102:195–221.

Ma C, Li W, Xu Y, Rizo J (2011) Munc13 mediates the transition from the closed syntaxin–Munc18 complex to the SNARE complex. Nat Struct Mol Biol 18:542–549.

Macpherson LJ, Zaharieva EE, Kearney PJ, Alpert MH, Lin T-Y, Turan Z, Lee C-H, Gallio M (2015) Dynamic labelling of neural connections in multiple colours by trans-synaptic fluorescence complementation. Nat Commun 6:10024.

Maday S, Twelvetrees AE, Moughamian AJ, Holzbaur ELF (2014) Axonal transport: cargo-specific mechanisms of motility and regulation. Neuron 84:292–309.

Maeder CI, Shen K, Hoogenraad CC (2014) Axon and dendritic trafficking. Curr Opin Neurobiol 27:165–170.

Mann K, Wang M, Luu S-H, Ohler S, Hakeda-Suzuki S, Suzuki T (2012) A putative tyrosine phosphorylation site of the cell surface receptor Golden goal is involved in synaptic layer selection in the visual system. Development 139:760–771.

Maruyama IN, Brenner S (1991) A phorbol ester/diacylglycerol-binding protein encoded by the unc-13 gene of Caenorhabditis elegans. Proc Natl Acad Sci 88:5729–5733.

Matkovic T, Siebert M, Knoche E, Depner H, Mertel S, Owald D, Schmidt M, Thomas U, Sickmann A, Kamin D, Hell SW, Bürger J, Hollmann C, Mielke T, Wichmann C, Sigrist SJ (2013) The Bruchpilot cytomatrix determines the size of the readily releasable pool of synaptic vesicles. J Cell Biol 202:667–683.

Matthews KA, Kaufman TC, Gelbart WM (2005) Research resources for Drosophila: the expanding universe. Nat Rev Genet 6:179–193.

Maurel-Zaffran C, Suzuki T, Gahmon G, Treisman JE, Dickson BJ (2001) Cell-autonomous and -nonautonomous functions of LAR in R7 photoreceptor axon targeting. Neuron 32:225–235.

McAllister AK (2007) Dynamic Aspects of CNS Synapse Formation. Annu Rev Neurosci 30:425–450.

Meinertzhagen IA (1993) Chapter 2 The synaptic populations of the fly's optic neuropil and their dynamic regulation: Parallels with the vertebrate retina. Prog Retin Res 12:13–39.

Meinertzhagen IA, O'Neil SD (1991) Synaptic organization of columnar elements in the lamina of the wild type in Drosophila melanogaster. J Comp Neurol 305:232–263.

Melnattur K V., Lee C-H (2011) Visual circuit assembly in Drosophila. Dev Neurobiol 71:1286–1296.

Melnattur K V, Pursley R, Lin T-Y, Ting C-Y, Smith PD, Pohida T, Lee C-H (2014) Multiple redundant medulla projection neurons mediate color vision in Drosophila. J Neurogenet 28:374–388.

Miki H, Setou M, Kaneshiro K, Hirokawa N (2001) All kinesin superfamily protein, KIF, genes in mouse and human. Proc Natl Acad Sci 98:7004–7011.

Millard SS, Lu Z, Zipursky SL, Meinertzhagen IA (2010) Drosophila Dscam Proteins Regulate Postsynaptic Specificity at Multiple-Contact Synapses. Neuron 67:761–768.

Millard SS, Pecot MY (2018) Strategies for assembling columns and layers in the Drosophila visual system. Neural Dev 13:11.

Miller KE, DeProto J, Kaufmann N, Patel BN, Duckworth A, Van Vactor D (2005) Direct Observation Demonstrates that Liprin-α Is Required for Trafficking of Synaptic Vesicles. Curr Biol 15:684–689.

Mishra A, Traut MH, Becker L, Klopstock T, Stein V, Klein R (2014) Genetic Evidence for the Adhesion Protein IgSF9/Dasm1 to Regulate Inhibitory Synapse Development Independent of its Intracellular Domain. J Neurosci 34:4187–4199.

Missler M, Südhof TC, Biederer T (2012) Synaptic cell adhesion. Cold Spring Harb Perspect Biol 4:a005694.

Missler M, Zhang W, Rohlmann A, Kattenstroth G, Hammer RE, Gottmann K, Südhof TC (2003) α-Neurexins couple Ca2+ channels to synaptic vesicle exocytosis. Nature 423:939–948.

Misura KMS, Scheller RH, Weis WI (2000) Three-dimensional structure of the neuronal-Sec1–syntaxin 1a complex. Nature 404:355–362.

Mohr SE (2014) RNAi screening in Drosophila cells and in vivo. Methods 68:82–88.

Mohr SE, Hu Y, Kim K, Housden BE, Perrimon N (2014) Resources for functional genomics studies in Drosophila melanogaster. Genetics 197:1–18.

Mok H, Shin H, Kim S, Lee J-R, Yoon J, Kim E (2002) Association of the kinesin superfamily motor protein KIF1Balpha with postsynaptic density-95 (PSD-95), synapse-associated protein-97, and synaptic scaffolding molecule PSD-95/discs large/zona occludens-1 proteins. J Neurosci 22:5253–5258.

Monastirioti M, Gorczyca M, Rapus J, Eckert M, White K, Budnik V (1995) Octopamine immunoreactivity in the fruit fly Drosophila melanogaster. J Comp Neurol 356:275–287.

Montell C (2012) Drosophila visual transduction. Trends Neurosci 35:356–363.

Morante J, Desplan C (2008) The Color-Vision Circuit in the Medulla of Drosophila. Curr Biol 18:553–565.

Morgan TH (1910) Sex limited inheritance in Drosophila. Science (80-) 32:120–122.

Mueller BK (1999) Growth Cone Guidance: First Steps Towards a Deeper Understanding. Annu Rev Neurosci 22:351–388.

Mukherjee K, Yang X, Gerber SH, Kwon H-B, Ho A, Castillo PE, Liu X, Sudhof TC (2010) Piccolo and bassoon maintain synaptic vesicle clustering without directly participating in vesicle exocytosis. Proc Natl Acad Sci 107:6504–6509.

Müller M, Liu KSY, Sigrist SJ, Davis GW (2012) RIM controls homeostatic plasticity through modulation of the readily-releasable vesicle pool. J Neurosci 32:16574–16585.

Munno DW, Syed NI (2003) Synaptogenesis in the CNS: an odyssey from wiring together to firing together. J Physiol 552:1–11.

Naisbitt S, Kim E, Tu JC, Xiao B, Sala C, Valtschanoff J, Weinberg RJ, Worley PF, Sheng M (1999) Shank, a novel family of postsynaptic density proteins that binds to the NMDA receptor/PSD-95/GKAP complex and cortactin. Neuron 23:569–582.

Nam CI, Chen L (2005) Postsynaptic assembly induced by neurexin-neuroligin interaction and neurotransmitter. Proc Natl Acad Sci 102:6137–6142.

Nässel DR, Winther ÅME (2010) Drosophila neuropeptides in regulation of physiology and behavior. Prog Neurobiol 92:42–104.

Nériec N, Desplan C (2016) From the Eye to the Brain: Development of the Drosophila Visual System. Curr Top Dev Biol 116:247–271.

Nern A, Zhu Y, Zipursky SL (2008) Local N-Cadherin Interactions Mediate Distinct Steps in the Targeting of Lamina Neurons. Neuron 58:34–41.

Newsome TP, Asling B, Dickson BJ (2000) Analysis of Drosophila photoreceptor axon guidance in eye-specific mosaics. Development 127:851–860.

Niwa S, Lipton DM, Morikawa M, Zhao C, Hirokawa N, Lu H, Shen K (2016) Autoinhibition of a Neuronal Kinesin UNC-104/KIF1A Regulates the Size and Density of Synapses. Cell Rep 16:2129–2141.

Niwa S, Tanaka Y, Hirokawa N (2008) KIF1Bβ- and KIF1A-mediated axonal transport of presynaptic regulator Rab3 occurs in a GTP-dependent manner through DENN/MADD. Nat Cell Biol 10:1269–1279.

Niwa S, Tao L, Lu SY, Liew GM, Feng W, Nachury M V., Shen K (2017) BORC Regulates the Axonal Transport of Synaptic Vesicle Precursors by Activating ARL-8. Curr Biol 27:2569-2578.e4.

Novarino G et al. (2014) Exome Sequencing Links Corticospinal Motor Neuron Disease to Common Neurodegenerative Disorders. Science (80-) 343:506–511.

Ohtsuka T, Takao-Rikitsu E, Inoue E, Inoue M, Takeuchi M, Matsubara K, Deguchi-Tawarada M, Satoh K, Morimoto K, Nakanishi H, Takai Y (2002) Cast. J Cell Biol 158:577–590.

Okada Y, Yamazaki H, Sekine-Aizawa Y, Hirokawa N (1995) The neuron-specific kinesin superfamily protein KIF1A is a uniqye monomeric motor for anterograde axonal transport of synaptic vesicle precursors. Cell 81:769–780.

Otsuka AJ, Jeyaprakash A, García-Añoveros J, Tang LZ, Fisk G, Hartshorne T, Franco R, Bornt T (1991) The C. elegans unc-104 4 gene encodes a putative kinesin heavy chain-like protein. Neuron 6:113–122.

Owald D, Fouquet W, Schmidt M, Wichmann C, Mertel S, Depner H, Christiansen F, Zube C, Quentin C, Körner J, Urlaub H, Mechtler K, Sigrist SJ (2010) A Syd-1 homologue regulates pre- and postsynaptic maturation in Drosophila. J Cell Biol 188:565–579.

Owald D, Khorramshahi O, Gupta VK, Banovic D, Depner H, Fouquet W, Wichmann C, Mertel S, Eimer S, Reynolds E, Holt M, Aberle H, Sigrist SJ (2012) Cooperation of Syd-1 with Neurexin synchronizes pre- with postsynaptic assembly. Nat Neurosci 15:1219–1226.

Oyler GA, Higgins GA, Hart RA, Battenberg E, Billingsley M, Bloom FE, Wilson MC (1989) The identification of a novel synaptosomal-associated protein, SNAP-25, differentially expressed by neuronal subpopulations. J Cell Biol 109:3039–3052.

Pack-Chung E, Kurshan PT, Dickman DK, Schwarz TL (2007) A Drosophila kinesin required for synaptic bouton formation and synaptic vesicle transport. Nat Neurosci 10:980–989.

Pak WL, Grossfield J, Arnold KS (1970) Mutants of the Visual Pathway of Drosophila melanogaster. Nature 227:518–520.

Palay SL (1956) Synapses in the Central Nervous System. J Cell Biol 2:193–202.

Pecot MY, Tadros W, Nern A, Bader M, Chen Y, Zipursky SL (2013) Multiple Interactions Control Synaptic Layer Specificity in the Drosophila Visual System. Neuron 77:299–310.

Perkins LA et al. (2015) The Transgenic RNAi Project at Harvard Medical School: Resources and Validation. Genetics 201:843–852.

Prakash S, McLendon HM, Dubreuil CI, Ghose A, Hwa J, Dennehy KA, Tomalty KMH, Clark KL, Van Vactor D, Clandinin TR (2009) Complex interactions amongst N-cadherin, DLAR, and Liprin-α regulate Drosophila photoreceptor axon targeting. Dev Biol 336:10–19.

Prior P, Schmitt B, Grenningloh G, Pribilla I, Multhaup G, Beyreuther K, Maulet Y, Werner P, Langosch D, Kirsch J, Betz H (1992) Primary structure and alternative splice variants of gephyrin, a putative glycine receptor-tubulin linker protein. Neuron 8:1161–1170.

Prokop A (1999) Integrating bits and pieces: synapse structure and formation in Drosophila embryos. Cell Tissue Res 297:169–186.

Prokop A, Meinertzhagen IA (2006) Development and structure of synaptic contacts in Drosophila. Semin Cell Dev Biol 17:20–30.

Ray K, Perez SE, Yang Z, Xu J, Ritchings BW, Steller H, Goldstein LSB (1999) Kinesin-II Is Required for Axonal Transport of Choline Acetyltransferase in *Drosophila*. J Cell Biol 147:507–518.

Rees RP, Bunge MB, Bunge RP (1976) Morphological changes in the neuritic growth cone and target neuron during synaptic junction development in culture. J Cell Biol 68:240–263.

Rister J, Heisenberg M (2006) Distinct functions of neuronal synaptobrevin in developing and mature fly photoreceptors. J Neurobiol 66:1271–1284.

Rivera-Alba M, Vitaladevuni SN, Mishchenko Y, Lu Z, Takemura S, Scheffer L, Meinertzhagen IA, Chklovskii DB, de Polavieja GG, de Polavieja GG (2011) Wiring Economy and Volume Exclusion Determine Neuronal Placement in the Drosophila Brain. Curr Biol 21:2000–2005.

Rivière J-B et al. (2011) KIF1A, an Axonal Transporter of Synaptic Vesicles, Is Mutated in Hereditary Sensory and Autonomic Neuropathy Type 2. Am J Hum Genet 89:219–230.

Roberts AJ, Kon T, Knight PJ, Sutoh K, Burgess SA (2013) Functions and mechanics of dynein motor proteins. Nat Rev Mol Cell Biol 14:713–726.

Rohrbough J, O'Dowd DK, Baines RA, Broadie K (2003) Cellular bases of behavioral plasticity: Establishing and modifying synaptic circuits in theDrosophila genetic system. J Neurobiol 54:254–271.

Rosa-Ferreira C, Sweeney ST, Munro S (2018) The small G protein Arl8 contributes to lysosomal function and long-range axonal transport in Drosophila. Biol Open 7:bio035964.

Salcedo E, Huber A, Henrich S, Chadwell L V, Chou WH, Paulsen R, Britt SG (1999) Blue- and green-absorbing visual pigments of Drosophila: ectopic expression and physiological characterization of the R8 photoreceptor cell-specific Rh5 and Rh6 rhodopsins. J Neurosci Off J Soc Neurosci 19:10716–10726.

Sanes JR, Yamagata M (1999) Formation of lamina-specific synaptic connections. Curr Opin Neurobiol 9:79–87.

Sanes JR, Zipursky SL (2010) Design principles of insect and vertebrate visual systems. Neuron 66:15–36.

Scheiffele P, Fan J, Choih J, Fetter R, Serafini T (2000) Neuroligin expressed in nonneuronal cells triggers presynaptic development in contacting axons. Cell 101:657–669.

Schikorski T, Stevens CF (1997) Quantitative ultrastructural analysis of hippocampal excitatory synapses. J Neurosci 17:5858–5867.

Schnaitmann C, Haikala V, Abraham E, Oberhauser V, Thestrup T, Griesbeck O, Reiff DF (2018) Color Processing in the Early Visual System of Drosophila. Cell 172:318-330.e18.

Schoch S, Castillo PE, Jo T, Mukherjee K, Geppert M, Wang Y, Schmitz F, Malenka RC, Südhof TC (2002) RIM1α forms a protein scaffold for regulating neurotransmitter release at the active zone. Nature 415:321–326.

Scholey JM (2013) Kinesin-2: A Family of Heterotrimeric and Homodimeric Motors with Diverse Intracellular Transport Functions. Annu Rev Cell Dev Biol 29:443–469.

Schwabe T, Borycz JA, Meinertzhagen IA, Clandinin TR (2014) Differential Adhesion Determines the Organization of Synaptic Fascicles in the Drosophila Visual System. Curr Biol 24:1304–1313.

Senti K-A, Usui T, Boucke K, Greber U, Uemura T, Dickson BJ (2003) Flamingo Regulates R8 Axon-Axon and Axon-Target Interactions in the Drosophila Visual System. Curr Biol 13:828–832.

Shapiro L, Love J, Colman DR (2007) Adhesion Molecules in the Nervous System: Structural Insights into Function and Diversity. Annu Rev Neurosci 30:451–474.

Shaw HS, Cameron SA, Chang W-T, Rao Y (2019) The conserved IgSF9 protein Borderless regulates axonal transport of presynaptic components and color vision in Drosophila. J Neurosci:0075–19.

Sheng M, Kim E (2011) The postsynaptic organization of synapses. Cold Spring Harb Perspect Biol 3:a005678.

Shi S-H, Cheng T, Jan LY, Jan Y-N (2004) The immunoglobulin family member dendrite

arborization and synapse maturation 1 (Dasm1) controls excitatory synapse maturation. Proc Natl Acad Sci U S A 101:13346–13351.

Shin H, Wyszynski M, Huh K-H, Valtschanoff JG, Lee J-R, Ko J, Streuli M, Weinberg RJ, Sheng M, Kim E (2003) Association of the Kinesin Motor KIF1A with the Multimodular Protein Liprin-α. J Biol Chem 278:11393–11401.

Shinza-Kameda M, Takasu E, Sakurai K, Hayashi S, Nose A (2006) Regulation of layer-specific targeting by reciprocal expression of a cell adhesion molecule, capricious. Neuron 49:205–213.

Shyn SI et al. (2011) Novel loci for major depression identified by genome-wide association study of Sequenced Treatment Alternatives to Relieve Depression and meta-analysis of three studies. Mol Psychiatry 16:202–215.

Siddiqui N, Straube A (2017) Intracellular cargo transport by kinesin-3 motors. Biochem 82:803–815.

Silies M, Gohl DM, Clandinin TR (2014) Motion-Detecting Circuits in Flies: Coming into View. Annu Rev Neurosci 37:307–327.

Smart TG, Paoletti P (2012) Synaptic neurotransmitter-gated receptors. Cold Spring Harb Perspect Biol 4:a009662.

Soppina V, Rai AK, Ramaiya AJ, Barak P, Mallik R (2009) Tug-of-war between dissimilar teams of microtubule motors regulates transport and fission of endosomes. Proc Natl Acad Sci 106:19381–19386.

Sperry RW (1963) Chemoaffinity in the Orderly Growth of Nerve Fiber Patterns and Connections. Proc Natl Acad Sci U S A 50:703–710.

St Johnston D (2002) The art and design of genetic screens: Drosophila melanogaster. Nat Rev Genet 3:176–188.

Stan A, Pielarski KN, Brigadski T, Wittenmayer N, Fedorchenko O, Gohla A, Lessmann V, Dresbach T, Gottmann K (2010) Essential cooperation of N-cadherin and neuroligin-1 in the transsynaptic control of vesicle accumulation. Proc Natl Acad Sci U S A 107:11116–11121.

Stepanova T, Slemmer J, Hoogenraad CC, Lansbergen G, Dortland B, De Zeeuw CI, Grosveld F, van Cappellen G, Akhmanova A, Galjart N (2003) Visualization of microtubule growth in cultured neurons via the use of EB3-GFP (end-binding protein 3-green fluorescent protein). J Neurosci 23:2655–2664.

Stevens DR, Wu Z-X, Matti U, Junge HJ, Schirra C, Becherer U, Wojcik SM, Brose N, Rettig J (2005) Identification of the Minimal Protein Domain Required for Priming Activity of Munc13-1. Curr Biol 15:2243–2248.

Stork T, Thomas S, Rodrigues F, Silies M, Naffin E, Wenderdel S, Klämbt C (2009) Drosophila Neurexin IV stabilizes neuron-glia interactions at the CNS midline by binding to Wrapper. Development 136:1251–1261.

Stowers RS, Megeath LJ, Górska-Andrzejak J, Meinertzhagen IA, Schwarz TL (2002) Axonal Transport of Mitochondria to Synapses Depends on Milton, a Novel Drosophila Protein. Neuron 36:1063–1077.

Strausfeld NJ, Sinakevitch I, Vilinsky I (2003) The mushroom bodies of Drosophila melanogaster: An immunocytological and golgi study of Kenyon cell organization in the calyces and lobes. Microsc Res Tech 62:151–169.

Stryker E, Johnson KG (2007) LAR, liprin alpha and the regulation of active zone morphogenesis. J Cell Sci 120:3723–3728.

Südhof TC (2004) The Synaptic Vesicle Cycle. Annu Rev Neurosci 27:509–547.

Südhof TC (2008) Neuroligins and neurexins link synaptic function to cognitive disease. Nature 455:903–911.

Südhof TC (2012) The Presynaptic Active Zone. Neuron 75:11–25.

Südhof TC, Baumert M, Perin MS, Jahn R (1989) A synaptic vesicle membrane protein is conserved from mammals to Drosophila. Neuron 2:1475–1481.

Sudhof TC, Rothman JE (2009) Membrane Fusion: Grappling with SNARE and SM Proteins. Science (80-) 323:474–477.

Sugie A, Hakeda-Suzuki S, Suzuki E, Silies M, Shimozono M, Möhl C, Suzuki T, Tavosanis G (2015) Molecular Remodeling of the Presynaptic Active Zone of Drosophila Photoreceptors via Activity-Dependent Feedback. Neuron 86:711–725.

Sumita K, Sato Y, Iida J, Kawata A, Hamano M, Hirabayashi S, Ohno K, Peles E, Hata Y (2007) Synaptic scaffolding molecule (S-SCAM) membrane-associated guanylate kinase with inverted organization (MAGI)-2 is associated with cell adhesion molecules at inhibitory synapses in rat hippocampal neurons. J Neurochem 100:154–166.

Sun M, Xing G, Yuan L, Gan G, Knight D, With SI, He C, Han J, Zeng X, Fang M, Boulianne GL, Xie W (2011) Neuroligin 2 Is Required for Synapse Development and Function at the Drosophila Neuromuscular Junction. J Neurosci 31:687–699.

Sutton RB, Davletov BA, Berghuis AM, Sudhof TC, Sprang SR (1995) Structure of the first C2 domain of synaptotagmin I: A novel Ca2+/phospholipid-binding fold. Cell 80:929–938.

Sutton RB, Fasshauer D, Jahn R, Brunger AT (1998) Crystal structure of a SNARE complex involved in synaptic exocytosis at 2.4 Å resolution. Nature 395:347–353.

Tahayato A, Sonneville R, Pichaud F, Wernet MF, Papatsenko D, Beaufils P, Cook T, Desplan C (2003) Otd/Crx, a dual regulator for the specification of ommatidia subtypes in the Drosophila retina. Dev Cell 5:391–402.

Takamori S et al. (2006) Molecular Anatomy of a Trafficking Organelle. Cell 127:831–846.

Takeda S, Yamazaki H, Seog D-H, Kanai Y, Terada S, Hirokawa N (2000) Kinesin Superfamily Protein 3 (Kif3) Motor Transports Fodrin-Associating Vesicles Important for Neurite Building. J Cell Biol 148:1255–1266.

Takemura S-Y, Lu Z, Meinertzhagen IA (2008) Synaptic circuits of the Drosophila optic lobe: the input terminals to the medulla. J Comp Neurol 509:493–513.

Takemura SSS et al. (2015) Synaptic circuits and their variations within different columns in the visual system of Drosophila. Proc Natl Acad Sci U S A 112:13711–13716.

Tao-Cheng J-H (2007) Ultrastructural localization of active zone and synaptic vesicle proteins in a preassembled multi-vesicle transport aggregate. Neuroscience 150:575–584.

Teng J, Rai T, Tanaka Y, Takei Y, Nakata T, Hirasawa M, Kulkarni AB, Hirokawa N (2005) The KIF3 motor transports N-cadherin and organizes the developing neuroepithelium. Nat Cell Biol 7:474–482.

Tian Y, Li T, Sun M, Wan D, Li Q, Li P, Zhang ZC, Han J, Xie W (2013) Neurexin regulates visual function via mediating retinoid transport to promote rhodopsin maturation. Neuron 77:311–322.

Timofeev K, Joly W, Hadjieconomou D, Salecker I (2012) Localized Netrins Act as Positional Cues to Control Layer-Specific Targeting of Photoreceptor Axons in Drosophila. Neuron 75:80–93.

Ting C-Y, McQueen PG, Pandya N, Lin T-Y, Yang M, Reddy OV, O'Connor MB, McAuliffe M, Lee C-H (2014) Photoreceptor-derived activin promotes dendritic termination and restricts the receptive fields of first-order interneurons in Drosophila. Neuron 81:830–846.

Ting C-Y, Yonekura S, Chung P, Hsu S-N, Robertson HM, Chiba A, Lee C-H (2005) Drosophila N-cadherin functions in the first stage of the two-stage layer-selection process of R7 photoreceptor afferents. Development 132:953–963.

Tolwinski NS (2017) Introduction: Drosophila—A Model System for Developmental Biology. J Dev Biol 5.

tom Dieck S, Sanmartí-Vila L, Langnaese K, Richter K, Kindler S, Soyke A, Wex H, Smalla K-H, Kämpf U, Fränzer J-T, Stumm M, Garner CC, Gundelfinger ED (1998) Bassoon, a Novel Zinc-finger CAG/Glutamine-repeat Protein Selectively Localized at the Active Zone of Presynaptic Nerve Terminals. J Cell Biol 142:499–509.

Tomasi T, Hakeda-Suzuki S, Ohler S, Schleiffer A, Suzuki T (2008) The Transmembrane Protein Golden Goal Regulates R8 Photoreceptor Axon-Axon and Axon-Target Interactions. Neuron 57:691–704.

Toni N, Buchs P-A, Nikonenko I, Bron CR, Muller D (1999) LTP promotes formation of multiple spine synapses between a single axon terminal and a dendrite. Nature 402:421–425.

Trimble WS, Cowan DM, Scheller RH (1988) VAMP-1: a synaptic vesicle-associated integral membrane protein. Proc Natl Acad Sci 85:4538–4542.

Tu JC, Xiao B, Naisbitt S, Yuan JP, Petralia RS, Brakeman P, Doan A, Aakalu VK, Lanahan AA, Sheng M, Worley PF (1999) Coupling of mGluR/Homer and PSD-95 complexes by the Shank family of postsynaptic density proteins. Neuron 23:583–592.

Tu R, Qian J, Rui M, Tao N, Sun M, Zhuang Y, Lv H, Han J, Li M, Xie W (2017) Proteolytic cleavage is required for functional neuroligin 2 maturation and trafficking in Drosophila. J Mol Cell Biol 9:231–242.

Ushkaryov Y, Petrenko A, Geppert M, Sudhof T, Toyoda A, Hirao K, Takai Y, Rosahl TW, Südhof TC (1992) Neurexins: synaptic cell surface proteins related to the alpha-latrotoxin receptor and laminin. Science (80-) 257:50–56.

Van Vactor D, Krantz DE, Reinke R, Zipursky SL (1988) Analysis of mutants in chaoptin, a photoreceptor cell-specific glycoprotein in Drosophila, reveals its role in cellular morphogenesis. Cell 52:281–290.

Varija Raghu S, Reiff DF, Borst A (2011) Neurons with cholinergic phenotype in the visual system of Drosophila. J Comp Neurol 519:162–176.

Varoqueaux F, Aramuni G, Rawson RL, Mohrmann R, Missler M, Gottmann K, Zhang W, Südhof TC, Brose N (2006) Neuroligins Determine Synapse Maturation and Function. Neuron 51:741–754.

Varoqueaux F, Jamain S, Brose N (2004) Neuroligin 2 is exclusively localized to inhibitory synapses. Eur J Cell Biol 83:449–456.

Vasiliauskas D, Mazzoni EO, Sprecher SG, Brodetskiy K, Johnston RJ, Lidder P, Vogt N, Celik A, Desplan C (2011) Feedback from Rhodopsin controls rhodopsin exclusion in Drosophila photoreceptors. Nature 479:108–112.

Vaughn JE (1989) Review: Fine structure of synaptogenesis in the vertebrate central nervous system. Synapse 3:255–285.

Vukoja A, Rey U, Petzoldt AG, Ott C, Vollweiter D, Quentin C, Puchkov D, Reynolds E, Lehmann M, Hohensee S, Rosa S, Lipowsky R, Sigrist SJ, Haucke V (2018) Presynaptic Biogenesis Requires Axonal Transport of Lysosome-Related Vesicles. Neuron 99:1216-1232.e7.

Wagh DA, Rasse TM, Asan E, Hofbauer A, Schwenkert I, Dürrbeck H, Buchner S, Dabauvalle M-C, Schmidt M, Qin G, Wichmann C, Kittel R, Sigrist SJ, Buchner E (2006) Bruchpilot, a Protein with Homology to ELKS/CAST, Is Required for Structural Integrity and Function of Synaptic Active Zones in Drosophila. Neuron 49:833–844.

Wagner OI, Esposito A, Kohler B, Chen C-W, Shen C-P, Wu G-H, Butkevich E, Mandalapu S, Wenzel D, Wouters FS, Klopfenstein DR (2009) Synaptic scaffolding protein SYD-2 clusters and activates kinesin-3 UNC-104 in C. elegans. Proc Natl Acad Sci 106:19605–19610.

Wang X, Kibschull M, Laue MM, Lichte B, Petrasch-Parwez E, Kilimann MW (1999) Aczonin, a 550-Kd Putative Scaffolding Protein of Presynaptic Active Zones, Shares Homology Regions with Rim and Bassoon and Binds Profilin. J Cell Biol 147:151–162.

Wang Y, Sugita S, Südhof TC (2000) The RIM/NIM Family of Neuronal C $_2$ Domain Proteins. J Biol Chem 275:20033–20044.

Weir PT, Henze MJ, Bleul C, Baumann-Klausener F, Labhart T, Dickinson MH (2016)

Anatomical Reconstruction and Functional Imaging Reveal an Ordered Array of Skylight Polarization Detectors in Drosophila. J Neurosci 36:5397–5404.

Wheeler SR, Banerjee S, Blauth K, Rogers SL, Bhat MA, Crews ST (2009) Neurexin IV and Wrapper interactions mediate Drosophila midline glial migration and axonal ensheathment. Development 136:1147–1157.

Wichmann C, Sigrist SJ (2010) The Active Zone T-Bar—A Plasticity Module? J Neurogenet 24:133–145.

Woo J, Kwon S-K, Nam J, Choi S, Takahashi H, Krueger D, Park J, Lee Y, Bae JY, Lee D, Ko J, Kim H, Kim M-H, Bae YC, Chang S, Craig AM, Kim E (2013) The adhesion protein IgSF9b is coupled to neuroligin 2 via S-SCAM to promote inhibitory synapse development. J Cell Biol 201:929–944.

Wu G-H, Muthaiyan Shanmugam M, Bhan P, Huang Y-H, Wagner OI (2016) Identification and Characterization of LIN-2(CASK) as a Regulator of Kinesin-3 UNC-104(KIF1A) Motility and Clustering in Neurons. Traffic 17:891–907.

Wu YE, Huo L, Maeder CI, Feng W, Shen K (2013) The Balance between Capture and Dissociation of Presynaptic Proteins Controls the Spatial Distribution of Synapses. Neuron 78:994–1011.

Xing G, Gan G, Chen D, Sun M, Yi J, Lv H, Han J, Xie W (2014) Drosophila neuroligin3 regulates neuromuscular junction development and synaptic differentiation. J Biol Chem 289:31867–31877.

Xu Y, An F, Borycz JA, Borycz J, Meinertzhagen IA, Wang T (2015) Histamine Recycling Is Mediated by CarT, a Carcinine Transporter in Drosophila Photoreceptors. PLoS Genet 11:e1005764.

Yamagata M, Sanes JR, Weiner JA (2003) Synaptic adhesion molecules. Curr Opin Cell Biol 15:621–632.

Yamaguchi S, Desplan C, Heisenberg M (2010) Contribution of photoreceptor subtypes to spectral wavelength preference in Drosophila. Proc Natl Acad Sci 107:5634–5639.

Yasuyama K, Meinertzhagen IA, Schürmann F-W (2002) Synaptic organization of the mushroom body calyx in *Drosophila melanogaster*. J Comp Neurol 445:211–226.

Yue Y, Sheng Y, Zhang H-N, Yu Y, Huo L, Feng W, Xu T (2013) The CC1-FHA dimer is essential for KIF1A-mediated axonal transport of synaptic vesicles in C. elegans. Biochem Biophys Res Commun 435:441–446.

Zaessinger S, Zhou Y, Bray SJ, Tapon N, Djiane A (2015) Drosophila MAGI interacts with RASSF8 to regulate E-Cadherin-based adherens junctions in the developing eye. Development 142:1102–1112.

Zeng X, Sun M, Liu L, Chen F, Wei L, Xie W (2007) Neurexin-1 is required for synapse formation and larvae associative learning in *Drosophila*. FEBS Lett 581:2509–2516.

Zhai RG, Bellen HJ (2004) The Architecture of the Active Zone in the Presynaptic Nerve

Terminal. Physiology 19:262–270.

Zhai RG, Vardinon-Friedman H, Cases-Langhoff C, Becker B, Gundelfinger ED, Ziv NE, Garner CC (2001) Assembling the Presynaptic Active Zone: A Characterization of an Active Zone Precursor Vesicle. Neuron 29:131–143.

Zhang Y V., Hannan SB, Kern J V., Stanchev DT, Koç B, Jahn TR, Rasse TM (2017a) The KIF1A homolog Unc-104 is important for spontaneous release, postsynaptic density maturation and perisynaptic scaffold organization. Sci Rep 7:38172.

Zhang X, Rui M, Gan G, Huang C, Yi J, Lv H, Xie W (2017b) Neuroligin 4 regulates synaptic growth via the bone morphogenetic protein (BMP) signaling pathway at the Drosophila neuromuscular junction. J Biol Chem 292:17991–18005.

Zhang Y, Luan Z, Liu A, Hu G (2001) The scaffolding protein CASK mediates the interaction between rabphilin3a and β-neurexins. FEBS Lett 497:99–102.

Zhang YQ, Rodesch CK, Broadie K (2002) Living synaptic vesicle marker: Synaptotagmin-GFP. genesis 34:142–145.

Zhao C, Takita J, Tanaka Y, Setou M, Nakagawa T, Takeda S, Yang HW, Terada S, Nakata T, Takei Y, Saito M, Tsuji S, Hayashi Y, Hirokawa N (2001) Charcot-Marie-Tooth disease type 2A caused by mutation in a microtubule motor KIF1Bbeta. Cell 105:587–597.

Zhen M, Jin Y (1999) The liprin protein SYD-2 regulates the differentiation of presynaptic termini in C. elegans. Nature 401:371–375.

Zheng Z et al. (2018) A Complete Electron Microscopy Volume of the Brain of Adult Drosophila melanogaster. Cell 174:730-743.e22.

Zong W, Wang Y, Tang Q, Zhang H, Yu F (2018) Prd1 associates with the clathrin adaptor α-Adaptin and the kinesin-3 Imac/Unc-104 to govern dendrite pruning in Drosophila Freeman M, ed. PLOS Biol 16:e2004506.